AD-A103 550 EVALUATION OF A DUAL-LIDAR METHOD FOR MEASURING AEROSOL EXTINCTION(U) NAVAL OCEAN SYSTEMS CENTER SAN DIEGO CA M R PAULSON APR 87 NOSC/TD-1075 1/1

UNCLASSIFIED F/G 7/4 NL

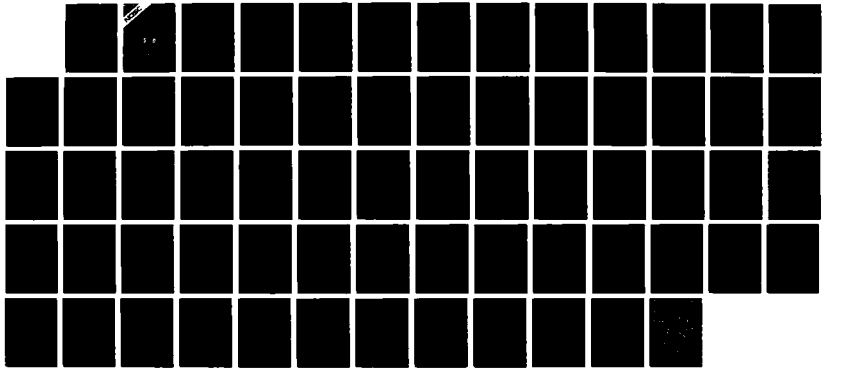

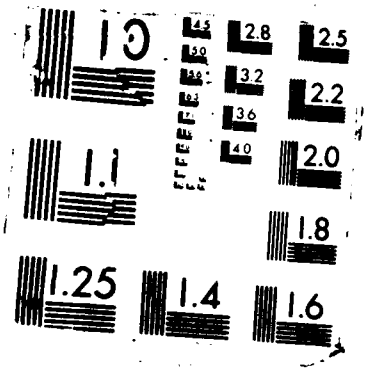
2.8
2.5
3.2
2.2
3.6
2.0
1.8
1.1
1.25
1.4
1.6

NAVAL OCEAN SYSTEMS CENTER San Diego, California 92152-5000

(12)

NOSC TD 1075

Technical Document 1075
April 1987

Evaluation of a Dual-Lidar Method for Measuring Aerosol Extinction

M. R. Paulson

NAVAL OCEAN SYSTEMS CENTER

San Diego, California 92152-5000

E. G. SCHWEIZER, CAPT, USN
Commander

R. M. HILLYER
Technical Director

ADMINISTRATIVE INFORMATION

The work described in this report was performed from October 1986 to March 1987 by the Modeling Branch, Code 544, of the Ocean and Atmospheric Sciences Division of the Naval Ocean Systems Center. This task was funded under the Office of Naval Technology, Office of the Chief of Naval Research, program element 62759N, project W59551.

Released by
J.A. Ferguson, Head
Modeling Branch

Under authority of
J.H. Richter, Head
Ocean and Atmospheric
Sciences Division

RT

UNCLASSIFIED
SECURITY CLASSIFICATION OF THIS PAGE

REPORT DOCUMENTATION PAGE

1a REPORT SECURITY CLASSIFICATION UNCLASSIFIED	1b RESTRICTIVE MARKINGS
2a SECURITY CLASSIFICATION AUTHORITY	3 DISTRIBUTION/AVAILABILITY OF REPORT Approved for public release; distribution is unlimited.
2b DECLASSIFICATION/DOWNGRADING SCHEDULE	
4 PERFORMING ORGANIZATION REPORT NUMBER(S) NOSC TD 1075	5 MONITORING ORGANIZATION REPORT NUMBER(S)
6a NAME OF PERFORMING ORGANIZATION Naval Ocean Systems Center 6b OFFICE SYMBOL (if applicable) Code 544	7a NAME OF MONITORING ORGANIZATION
6c ADDRESS (City, State and ZIP Code) San Diego, CA 92152-5000	7b ADDRESS (City, State and ZIP Code)
8a NAME OF FUNDING/SPONSORING ORGANIZATION Office of Naval Technology Office of Chief of Naval Research 8b OFFICE SYMBOL (if applicable) ONT	9 PROCUREMENT INSTRUMENT IDENTIFICATION NUMBER
8c ADDRESS (City, State and ZIP Code) Arlington, VA 22217	10 SOURCE OF FUNDING NUMBERS PROGRAM ELEMENT NO: 62759N PROJECT NO: W59551 TASK NO: 540-CDB6 AGENCY ACCESSION NO: DN488 760

11 TITLE (include Security Classification)
Evaluation of a Dual-Lidar Method for Measuring Aerosol Extinction

12 PERSONAL AUTHOR(S)
M.R. Paulson

13a TYPE OF REPORT	13b TIME COVERED	14 DATE OF REPORT (Year, Month, Day)	15 PAGE COUNT
Final	FROM Oct 1986 TO Mar 1987	April 1987	66

16 SUPPLEMENTARY NOTATION

17 COSATI CODES			18 SUBJECT TERMS (Continue on reverse if necessary and identify by block number)
FIELD	GROUP	SUB-GROUP	Two-lidar method; Visiocellometer lidars; S(R) curves; Extinction coefficient profiles; Backscatter coefficient

19 ABSTRACT (Continue on reverse if necessary and identify by block number)

This report describes a method for determining aerosol distributions in the atmosphere using a technique that obtains extinction coefficient profiles and integrated extinction between two points. To implement this scheme, two lidars are set up at opposite ends of a propagation path and pointed toward each other. Since two equations are available to solve for the two unknowns, no assumptions are required concerning aerosol distributions.

20 DISTRIBUTION/AVAILABILITY OF ABSTRACT	21 ABSTRACT SECURITY CLASSIFICATION
☐ UNCLASSIFIED/UNLIMITED ☒ SAME AS RPT ☐ DTIC USERS	UNCLASSIFIED
22a NAME OF RESPONSIBLE INDIVIDUAL M.R. Paulson	22b TELEPHONE (include Area Code) (619) 225-2976 22c OFFICE SYMBOL Code 544

DD FORM 1473, 84 JAN

83 APR EDITION MAY BE USED UNTIL EXHAUSTED
ALL OTHER EDITIONS ARE OBSOLETE

UNCLASSIFIED
SECURITY CLASSIFICATION OF THIS PAGE

DD FORM 1473, 84 JAN

CONTENTS

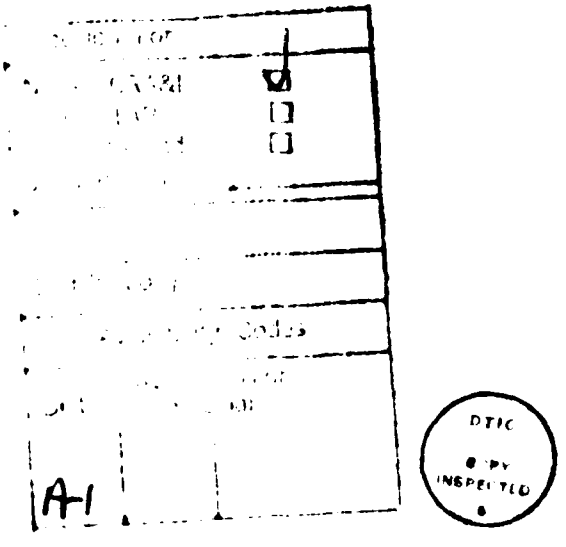

ILLUSTRATIONS

Figure

TABLES

Table

1.0 INTRODUCTION

This document describes a technique for obtaining atmospheric extinction coefficient profiles by using two lidars. With a single lidar, some assumptions must be made about the atmospheric conditions, since there is only one equation, but two unknowns. One assumption sometimes made is that the aerosol distributions in the atmosphere are horizontally homogeneous. More frequently assumed is that the atmospheric backscatter-to-extinction ratio is a constant. Even if this were true, this ratio would still have to be determined.

With the two-lidar technique, no assumptions are necessary, since there are now two equations and two unknowns. An additional advantage of the technique is that the lidar constant resulting from geometric characteristics of the optics and the laser pulse energy need not be known. However, the lidar receiver gains must still be accurately calibrated.

A block diagram of a two-lidar system is shown in figure 1-1. The two lidars are separated and pointed along nearly the same path, but in opposite directions. The second lidar site has a sensor that detects when the first lidar is fired. This outputs a signal through a delay circuit, which then triggers, or fires, the second lidar. Alternatively, with appropriate time delay, a trigger signal could be sent via landline, to the second lidar. The output of each lidar could be recorded at each site, along with an accurate time reference; or the outputs from the two lidars could be recorded on a common recording device, along with a time reference.

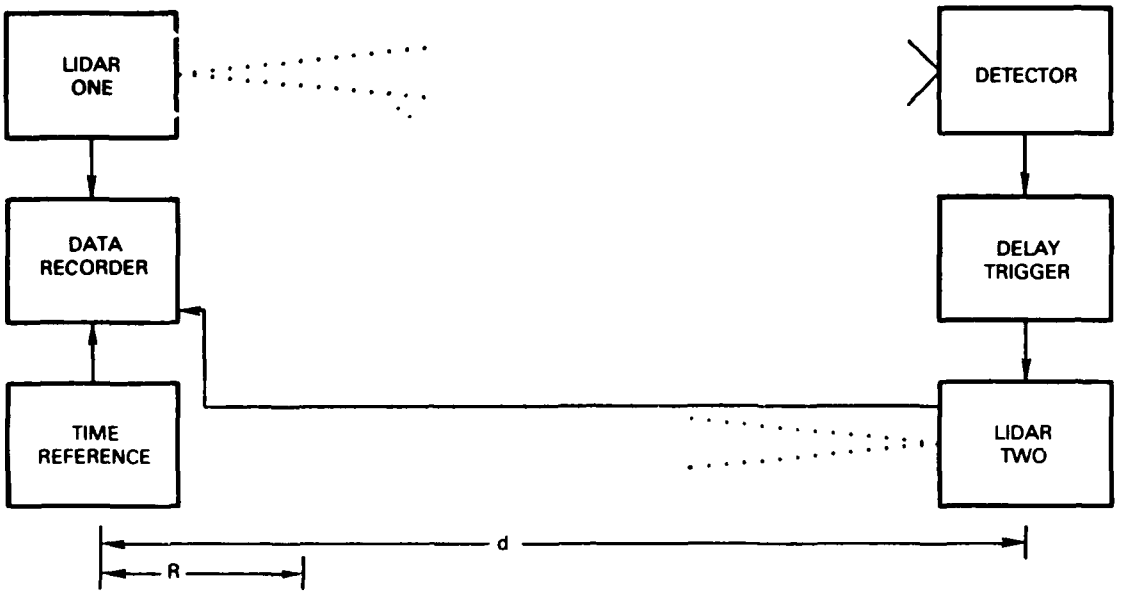

Figure 1-1. Block diagram of a possible two-lidar system.

2.0 MATHEMATICAL DERIVATIONS

2.1 EXTINCTION COEFFICIENT PROFILES

The quantity S(R) is the natural logarithm of the backscattered power received from range R multiplied by R^2. If the two lidars are separated a distance d, as shown in figure 1-1, and the origin is at lidar 1, the equation for S(R) for the first lidar is

$$S_1(R) = \mathrm{Ln}(C_{11}) + \mathrm{Ln}[\beta(R)] - 2\int_0^R \sigma(r)\,dr, \tag{1}$$

and that for the second lidar is

$$S_2(R) = \mathrm{Ln}(C_{12}) + \mathrm{Ln}[\beta(R)] - 2\int_R^d \sigma(r)\,dr, \tag{2}$$

where C_{11} and C_{12} are the instrumentation constants for each of the lidars. The $\sigma(r)$ is the extinction coefficient at range r, and $\beta(R)$ is the backscatter coefficient at range R.

If equation 2 is subtracted from equation 1, we get

$$S_1(R) - S_2(R) = \mathrm{Ln}(C_{11}) - \mathrm{Ln}(C_{12}) - 2\int_0^R \sigma(r)\,dr + 2\int_R^d \sigma(r)\,dr. \tag{3}$$

Since

$$\int_R^d \sigma(r)\,dr = \int_0^d \sigma(r)\,dr - \int_0^R \sigma(r)\,dr, \tag{4}$$

equation 3 becomes

$$S_1(R) - S_2(R) = \mathrm{Ln}(C_{11}) - \mathrm{Ln}(C_{12}) - 4\int_0^R \sigma(r)\,dr + 2\int_0^d \sigma(r)\,dr. \tag{5}$$

Taking the difference between equations 1 and 2 eliminates the backscatter coefficient. Then, taking the derivative of equation 5 eliminates the requirement that instrumentation constants C_{11} and C_{12} be known, and we get

$$dS_1(R) - dS_2(R) = -4\ \sigma(R)\,dR \tag{6}$$

or

$$\sigma(R) = \frac{\dfrac{dS_2(R)}{dR} - \dfrac{dS_1(R)}{dR}}{4}. \tag{7}$$

The calibration curves for each of the lidar receivers are still needed, however, and must be accurately known, since they affect the slope characteristics of the S(R) curves.

Because the propagation for the two lidars is in opposite directions with respect to the origin, the slopes of $S_1(R)$ and $S_2(R)$ should have opposite signs under homogeneous atmospheric conditions.

2.2 INTEGRATED EXTINCTION AND VISIBILITY

While integrated extinction can be obtained by integrating the extinction coefficient profile, it can be obtained more directly. If equation 3 is written for two different distances, R_1 and R_2, we get

$$S_1(R_1) - S_2(R_1) = \mathrm{Ln}(C_{11}) - \mathrm{Ln}(C_{12}) - 4\int_0^{R_1} \sigma(r)dr + 2\int_0^{d} \sigma(r)dr \quad (8)$$

and

$$S_1(R_2) - S_2(R_2) = \mathrm{Ln}(C_{11}) - \mathrm{Ln}(C_{12}) - 4\int_0^{R_2} \sigma(r)dr + 2\int_0^{d} \sigma(r)dr. \quad (9)$$

Subtracting equation 9 from equation 8 gives

$$[S_1(R_1) - S_2(R_1)] - [S_1(R_2) - S_2(R_2)] = -4\int_0^{R_1} \sigma(r)dr + 4\int_0^{R_2} \sigma(r)dr. \quad (10)$$

Using the following equation

$$\int_{R_1}^{R_2} \sigma(r)dr = \int_0^{R_2} \sigma(r)dr - \int_0^{R_1} \sigma(r)dr, \quad (11)$$

we get

$$\int_{R_1}^{R_2} \sigma(r)dr = \frac{[S_1(R) - S_2(R_1)] - [S_1(R_2) - S_2(R_2)]}{4}. \quad (12)$$

Again, the instrumentation constants drop out.

If atmospheric conditions were homogeneous, this could be used to calculate visibility by using the equation

$$\mathrm{Vis} = \frac{3.912(R_2 - R_1)}{\int_{R_1}^{R_2} \sigma(r)dr}, \quad (13)$$

which is the Koschmieder relationship with the extinction coefficient replaced by an average extinction coefficient over the interval R_1 to R_2.

3.0 EXPERIMENTAL MEASUREMENTS

3.1 EQUIPMENT SETUP

The lidars used for these measurements were visioceilometer lidars (Lentz, 1982) operating at a 1.06-μm wavelength with a nominal pulse energy of about 10 mJ and a pulse width of 6 nsec. The two lidars were set up at opposite ends of a 1-km path and pointed towards each other. Lidar #025090 (#0) was located at building 323, about 30 to 35 meters above the ocean surface. Lidar #025091 (#1) was at building 593 at about 130 to 135 meters above the ocean and southeast of building 323. Lidar #0 was pointed about 3 or 4 meters above lidar #1, and lidar #1 was pointed about 3 or 4 meters west of lidar #0.

A test sequence usually consisted of 25 shots at approximately 45-second to 1-minute intervals. This was controlled by how fast the data for each shot could be recorded. Timing of the lidar shots was coordinated over a radio link to ensure that the two lidars were fired within about 1 second of each other. The data were recorded at each site on Memodyne cassette recorders for subsequent processing.

3.2 LIDAR CALIBRATION

Lidar #1 was calibrated in March 1986 (Ferguson & Paulson, 1986), and the calibration was found to agree closely with the calibration curve provided by the manufacturer. While lidar #0 was not calibrated at that time, the two lidars were later fired together along a common path. The receiver gain constants of lidar #0 were then adjusted so that a least-squares fit to a straight line of the S(R) returns agreed, on average, for the two lidars, for about 25 lidar shots. An example of this is shown in figure 3-1.

While the gain constant for lidar #0 appeared to be steady, the DC-offset value varied considerably.

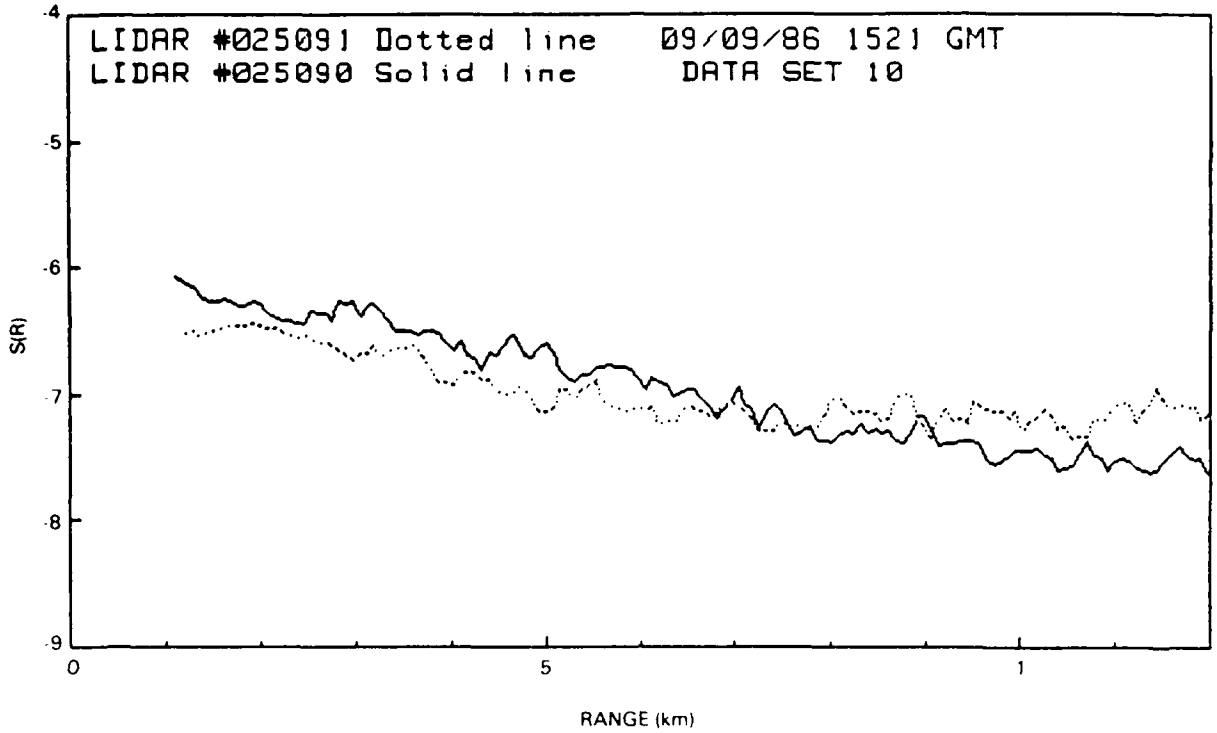

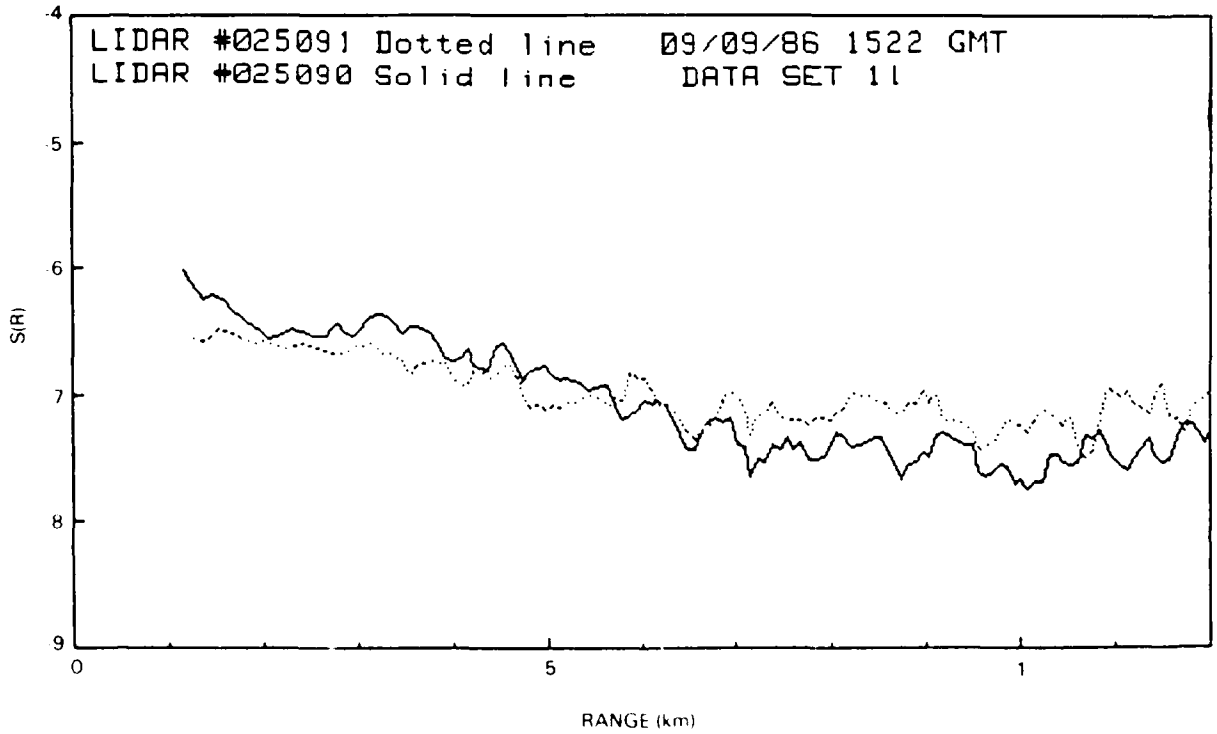

Figure 3-1 Comparison of S(R) curves for the two lidars over a common path.

4.0 DATA ANALYSIS

Data were taken on 27, 28, and 30 October 1986 during conditions of reduced visibility. (See figures 4-1 and 4-2.) Data were also taken on 4 November 1986, when visibility was quite good. The raw data were adjusted for receiver calibration and were range-compensated to produce S(R) curves for each of the examples. Additional examples are found in Appendix A. Evidently, many of the atmospheric irregularities one lidar sees are also seen by the other. If the two lidars had been aligned exactly on the same path, this agreement would probably have been even better. However, they probably should not be pointed directly at each other. Even if the pulse from one lidar did not damage the detector of the other, it would probably saturate the detector to the point where it would not record the return from its own pulse.

Additional improvement might have been obtained if the time delay between the two lidar shots had been reduced to a small fraction of a second. The lidar separation of 0.9825 km is accurate to within one 7.5-meter range cell.

To try a slightly shorter path, on 28 October lidar #0 was relocated south of building 323, near a radar site. In this case, the lidar separation was 0.6375 km.

4.1 EXTINCTION COEFFICIENT PROFILES

In applying equations 6 and 7, the differences between $S_1(R)$ and $S_2(R)$ were calculated first, then the derivative as a function of range was taken to obtain extinction coefficient profiles. Some data smoothing was necessary, however, before taking the derivative. Usually 11-point running averages were used to accomplish this. This is equal to an 82.5-meter running average.

Theoretically, the slope of the S(R) difference curves should never go positive, and the extinction coefficient should never be less than zero. However, minor differences in what each lidar sees may cause the extinction coefficient profile to sometimes dip slightly below the zero line. Better signal-to-noise ratios for the two lidars might reduce this effect.

A range increment of 15 points was used in calculating the derivatives of the S(R) difference curves. This corresponds to a running range interval of 112.5 meters. Figures 4-3 and 4-4 show examples of S(R) difference curves for 27 and 30 October, respectively, along with the corresponding extinction coefficient profiles. These correspond to the S(R) curves for data set 2 in figure 4-1 and for data set 3 in figure 4-2. Other examples are included in Appendix B.

4.2 INTEGRATED EXTINCTION AND VISIBILITY

Equation 12 was used to get the integrated extinction between 0.12 and 0.81 km for each lidar shot on 27 and 30 October, and 4 November. On 28 October, these distances were 0.12 and 0.51 km. Additionally, equation 13 was used to show what the visibility would have been if the atmospheric conditions had been homogenous. The results are shown in tables 4-1 and 4-2.

The results show improving atmospheric conditions on 28 and 30 October over those on 27 October and very good visibility conditions on 4 November. This agrees with what was observed visually.

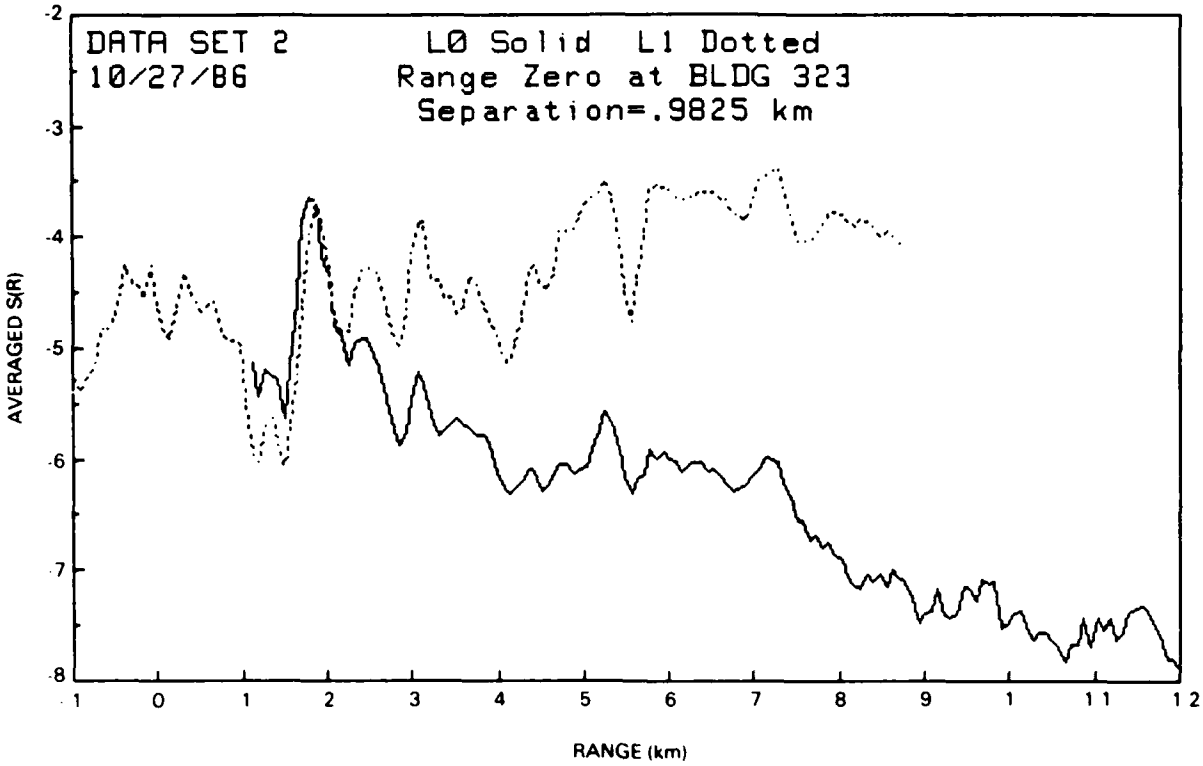

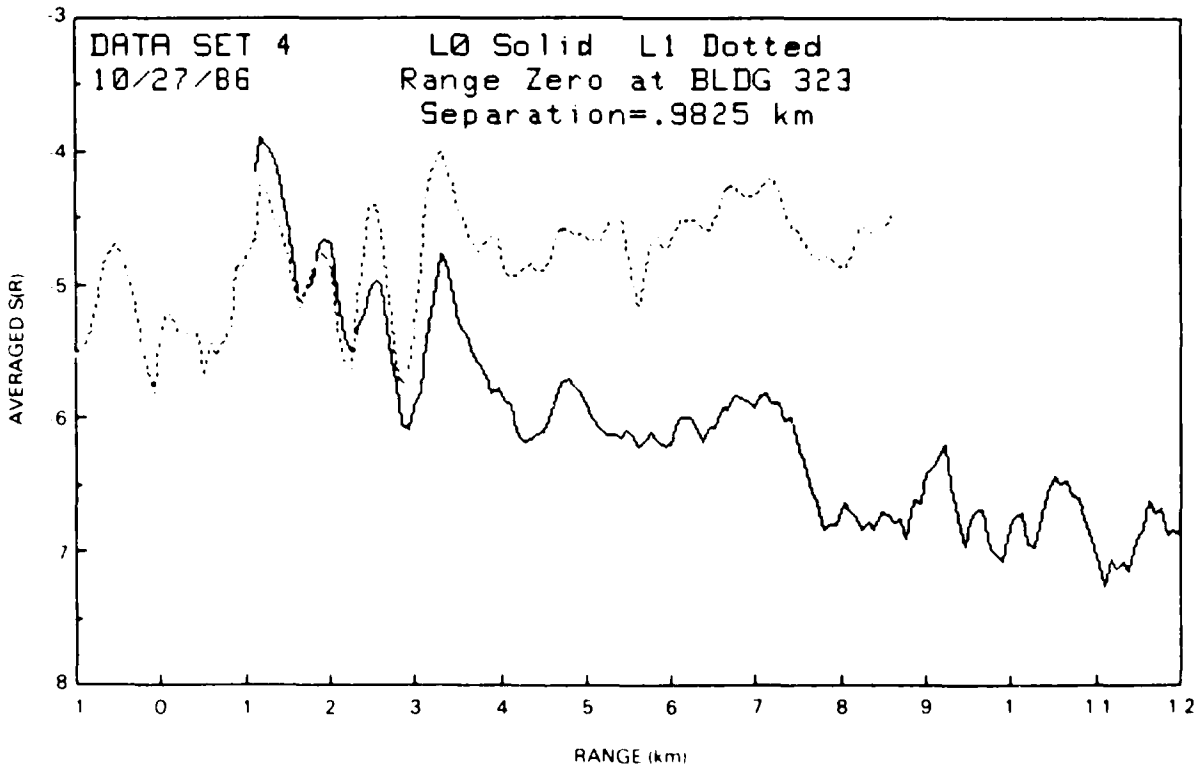

Figure 4-1 Examples of S(R) data for the two-lidar method. Solid line is for lidar #0, and dotted line is for lidar #1. Curves are 3-point running averages.

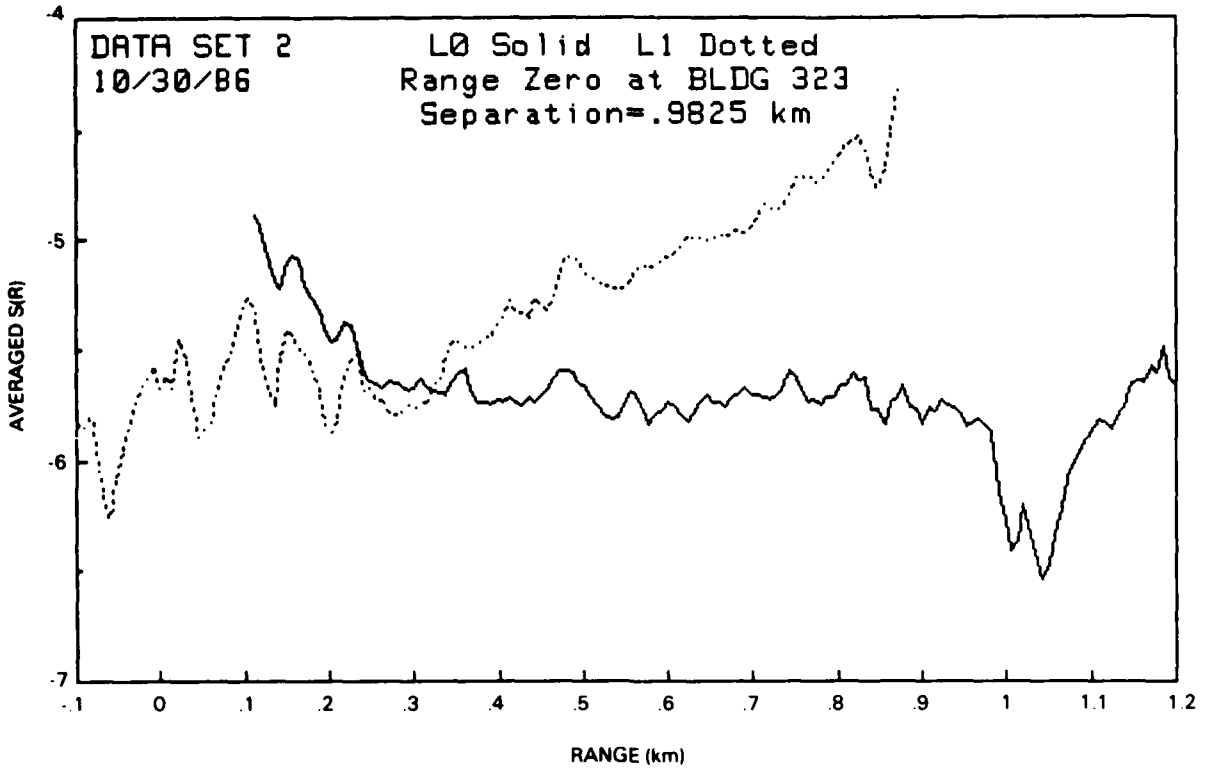

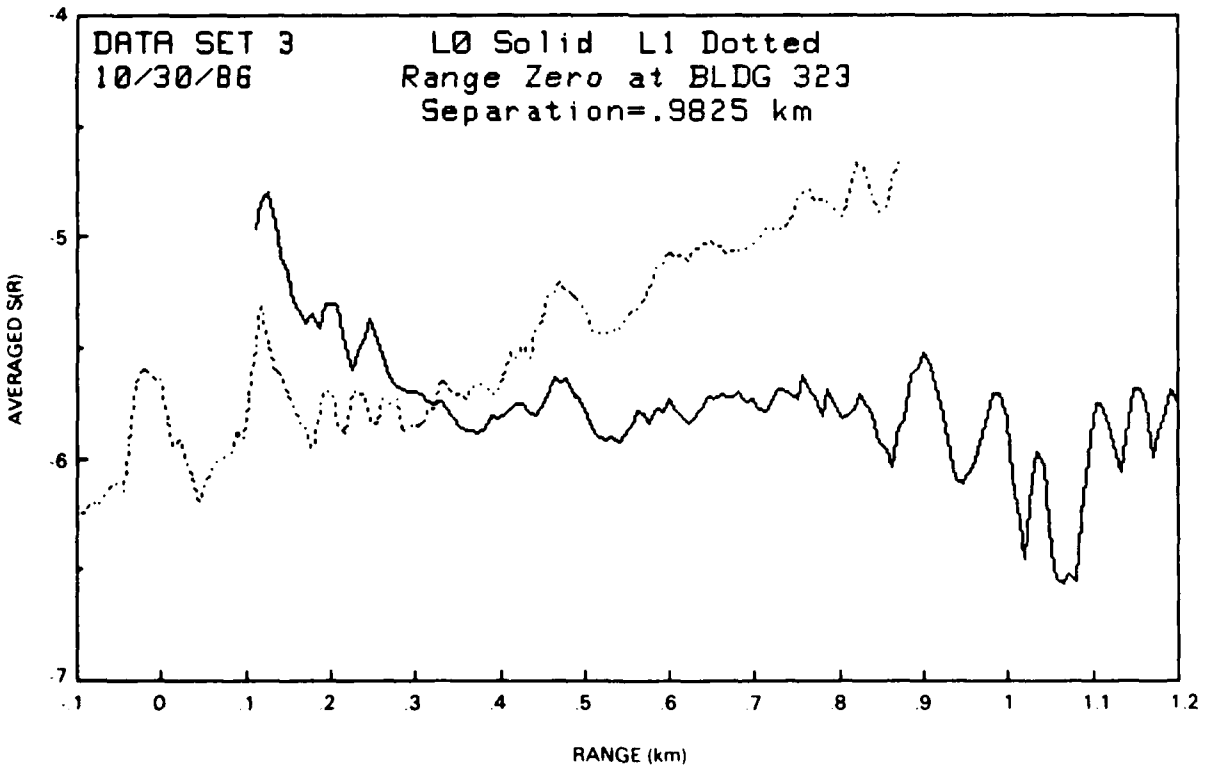

Figure 4-2. The same as figure 4-1, but for 30 October 1986. The vertical scale is expanded compared to figure 4-1.

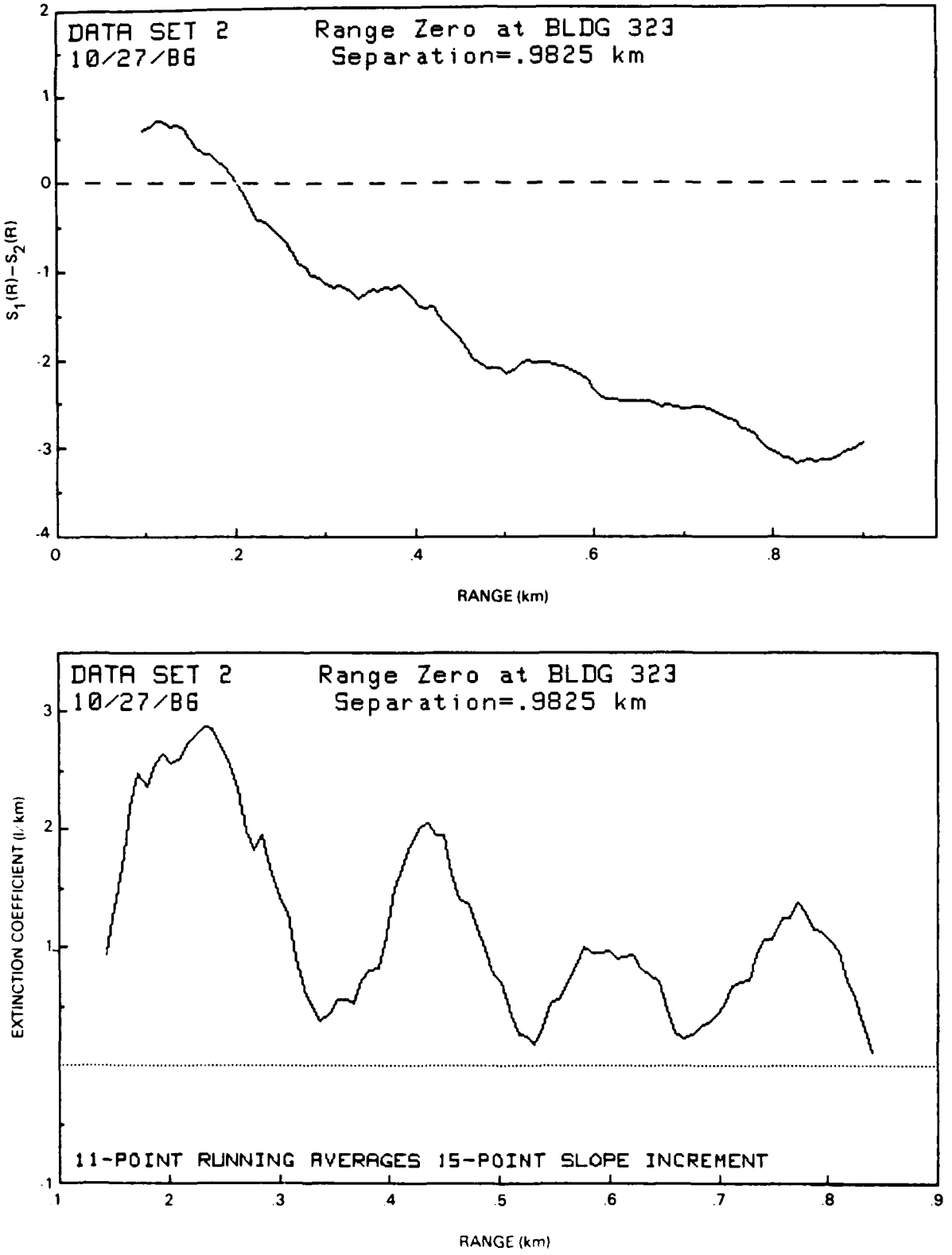

Figure 4-3. $S_1(R) - S_2(R)$ curve and extinction coefficient profile for 27 October 1986 for data set 2.

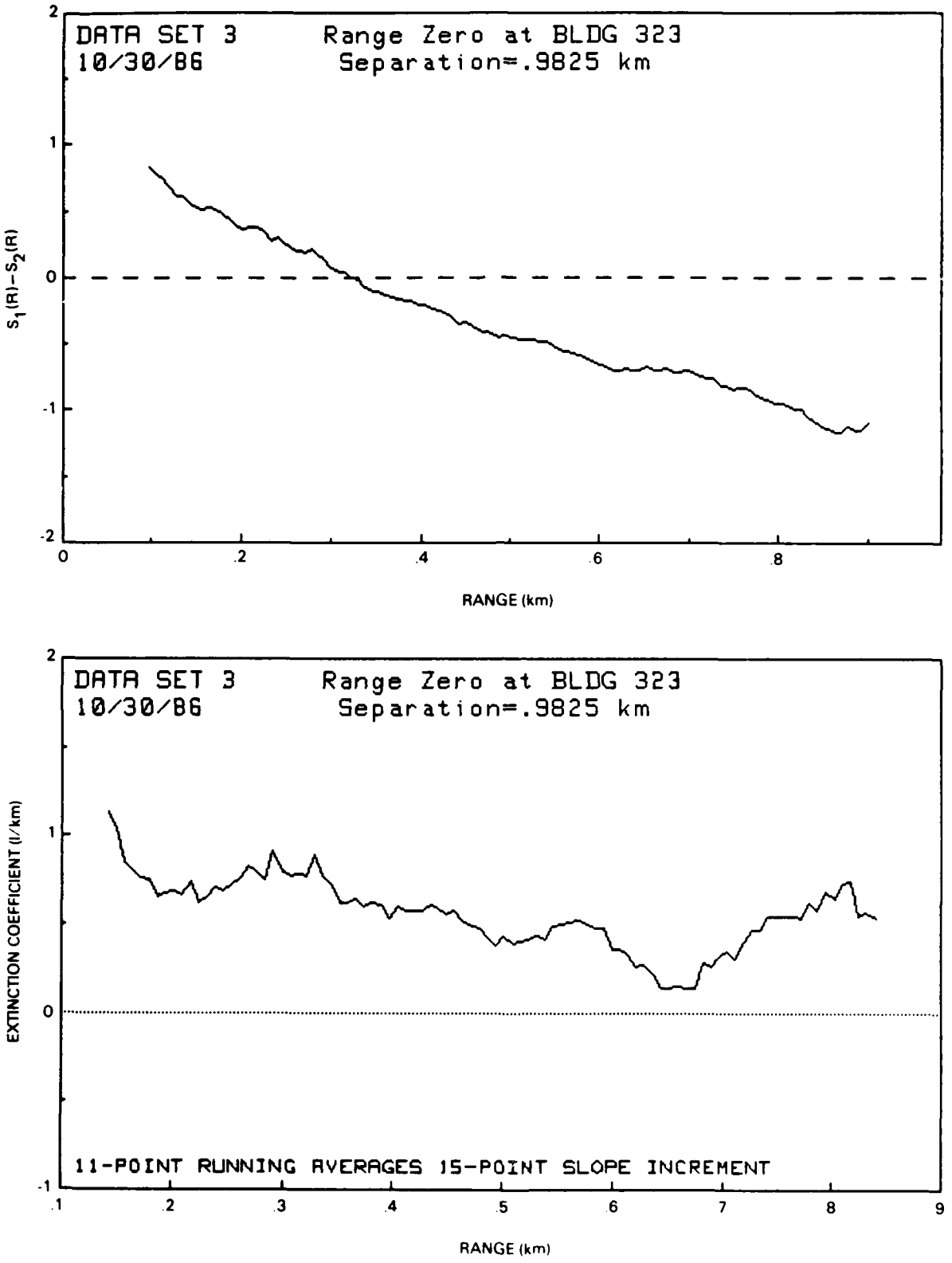

Figure 4-4. The same as figure 4-3, but for 30 October 1986.

Table 4-1. Values of integrated extinction from 0.12 to 0.81 km for 27 October 1986 and from 0.12 to 0.51 km for 28 October 1986. The visibilities are an indication of what the visibility would have been if atmospheric conditions had been homogenous.

Date	Data Set	Integrated Extinction	Visibility (km)
10/27/86	2	0.953	2.83
	3	0.737	3.66
	4	0.635	4.25
	5	0.715	3.78
	6	0.791	3.41
	7	0.653	4.14
	8	0.766	3.48
	9	0.920	2.93
	10	1.178	2.29
	11	1.058	2.55
	12	1.077	2.51
	13	0.831	3.25
	14	1.007	2.68
	15	0.953	2.83
	16	1.020	2.65
	17	0.949	2.84
	18	0.792	3.41
	19	1.132	2.38
	20	0.973	2.77
	21	0.851	3.17
	22	0.993	2.72
10/28/86	2	0.228	6.68
	3	0.326	4.68
	4	0.234	6.52
	5	0.279	5.47
	6	0.254	6.02
	7	0.259	5.90
	8	0.204	7.48
	9	0.285	5.36
	10	0.254	6.00
	12	0.154	9.91
	13	0.211	7.22
	14	0.256	5.96
	15	0.233	6.56
	16	0.222	6.88
	17	0.176	8.65
	18	0.193	7.89
	19	0.268	5.69
	20	0.250	6.10
	21	0.251	6.07
	22	0.227	6.73
	23	0.297	5.14
	24	0.310	4.93

Table 4-2. Integrated extinction from 0.12 to 0.81 km for 30 October 1986 and 4 November 1986. The visibilities indicated show what the visibility would have been if atmospheric conditions had been homogeneous.

Date	Data Set	Integrated Extinction	Visibility (km)
10/30/86	2	0.402	6.71
	3	0.413	6.54
	4	0.400	6.75
	5	0.478	5.64
	6	0.409	6.60
	7	0.407	6.64
	8	0.433	6.24
	9	0.425	6.36
	10	0.469	5.76
	11	0.457	5.91
	12	0.422	6.40
	13	0.458	5.90
	14	0.381	7.08
	15	0.357	7.57
	16	0.353	7.64
	17	0.412	6.55
	18	0.429	6.29
	19	0.428	6.31
	20	0.458	5.89
	21	0.447	6.04
	22	0.430	6.28
	23	0.399	6.76
	24	0.376	7.18
11/04/86	2	0.180	14.96
	3	0.415	6.50
	4	0.184	14.65
	5	0.079	34.11
	6	0.191	14.10
	7	0.111	24.24
	8	0.154	17.52
	9	0.240	11.24
	10	0.212	12.74
	11	0.156	17.30

5.0 TEST OF A LIDAR INVERSION ALGORITHM

The results from the two-lidar approach can be used to evaluate lidar inversion algorithms. One of these algorithms requires that a value of extinction coefficient be known, or estimated, for a point at maximum range (Klett, 1981). The equation is

$$\sigma(r) = \frac{\text{EXP}\,[(S - S_m)/k]}{\frac{1}{\sigma_m} + \frac{2}{k}\int_r^{r_m} \text{EXP}[(S - S_m)/k]\,dr'} \,. \qquad (14)$$

where $\sigma(m)$ is the extinction at maximum range, and k is taken as 1. This equation must assume that the backscatter-to-extinction ratio remains constant as well as that $\sigma(m)$ be known. Although there have been attempts to improve on this technique (Klett, 1985), the method used in equation 14 will be studied here.

Since the two-lidar method provides an extinction coefficient profile between the two lidars, a value of extinction coefficient can be chosen from opposite ends of the profile. The value is used as the far-point extinction coefficient, $\sigma(m)$, for each of the lidars. This has been done for several lidar shots and for equation 14, used with the corresponding separate S(R) profiles. The lower graph in figure 5-1 shows some results for data set 4 on 30 October 1986. The two lidars agree quite well, but the curves do not closely follow that of the two-lidar method shown in the upper graph. Another example for data set 2 on 27 October 1986 is shown in the lower graph of figure 5-2. Here there are some differences between the two extinction profiles, although they tend to agree in general. They do not follow the two-lidar extinction coefficient profile very well, though. Figure 5-3 for the following data set shows major differences between the extinction coefficient profiles for the two lidars, while figure 5-4 again shows some agreement.

In most cases, the extinction coefficient profiles from the stable inversion method do not agree well with the extinction coefficient profile produced by the two-lidar method. It also appears that the extinction coefficient profiles calculated separately with the two lidars disagree widely from one data sample to the next. This occurs even though the calculations of the coefficient profiles use the same S(R) data that were used in the two-lidar method to obtain the far-point extinction coefficients used in equation 14. One possible explanation is that the backscatter coefficient may be varying along the propagation path. Some computer-generated S(R) curves were used to test this.

Figure 5-5 shows a known extinction coefficient profile in the upper graph and a known backscatter coefficient profile in the lower graph. For each of the two lidars, these profiles were used to generate S(R) curves with a separation equal to that used in the experiments. These two S(R) curves were used in the dual-lidar method to obtain the extinction coefficient profile shown in figure 5-6. Note that it agrees well with the profile used to generate the data.

The two S(R) curves were then used with the far-point, or stable, inversion method to obtain extinction coefficient profiles for each of the lidars. The results are shown in figure 5-7. While the two curves have the same general shape, one is much larger than the true extinction coefficient profile, and the other is much lower.

Variation in the dc offset for lidar #0 might shift its extinction coefficient profile slightly up or down, with respect to that of lidar #1, but this should not affect its shape. The dc shift should have no effect, however, in the case of the two lidar method.

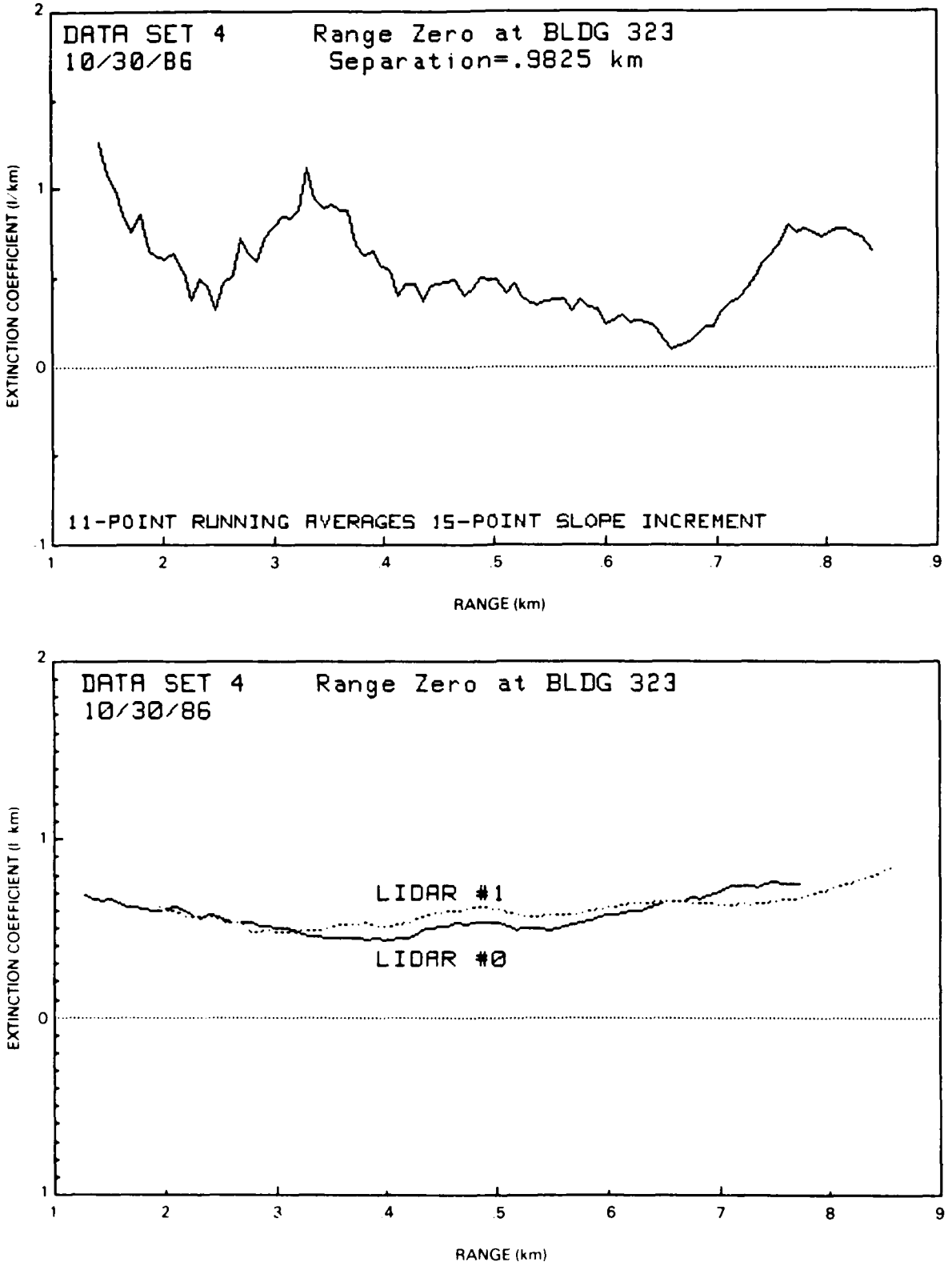

Figure 5-1 Comparison of extinction coefficient profiles using the "stable inversion technique" with the results from the two-lidar method.

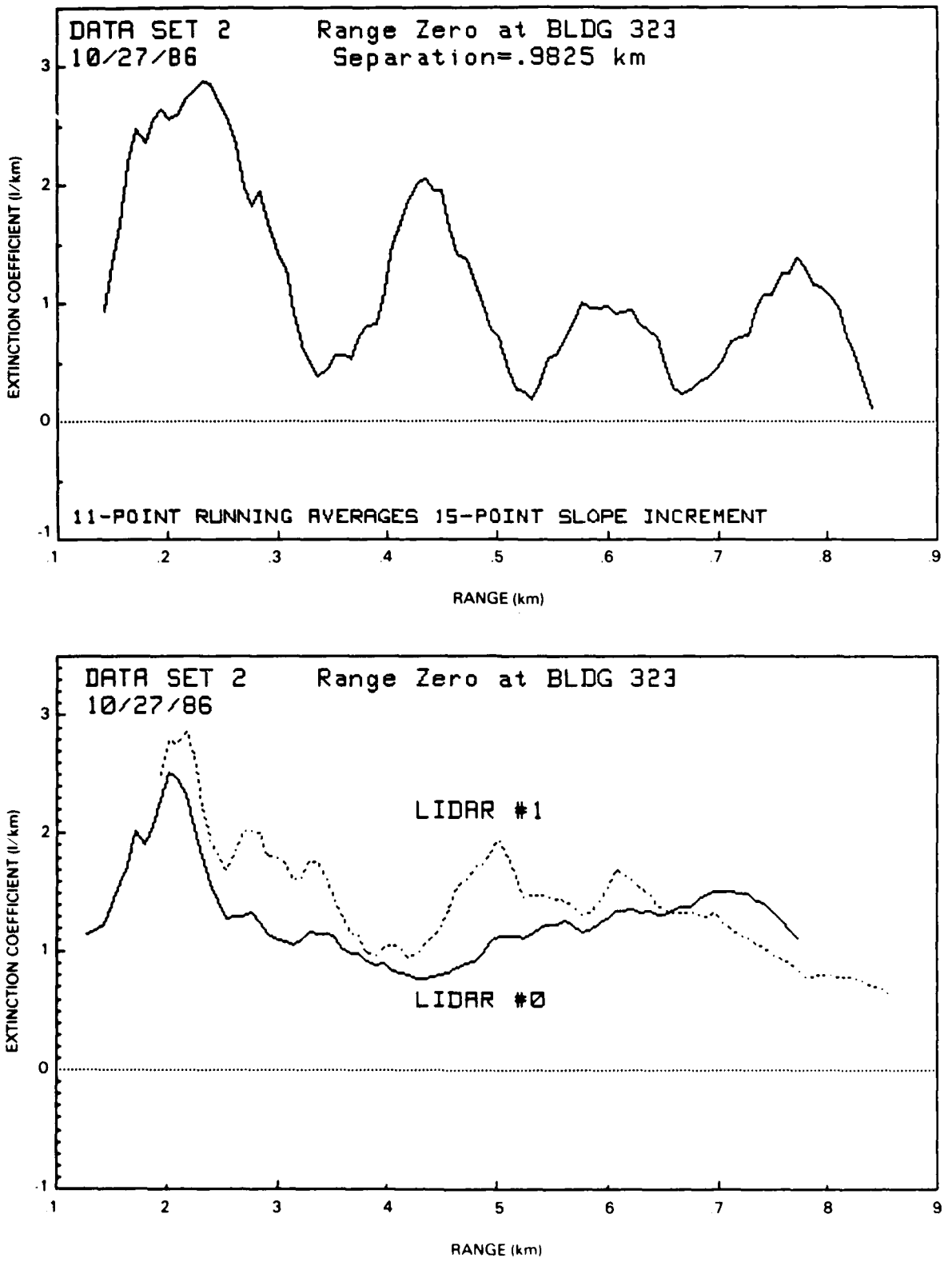

Figure 5-2. The same as figure 5-1, but for data set 2 on 27 October 1986.

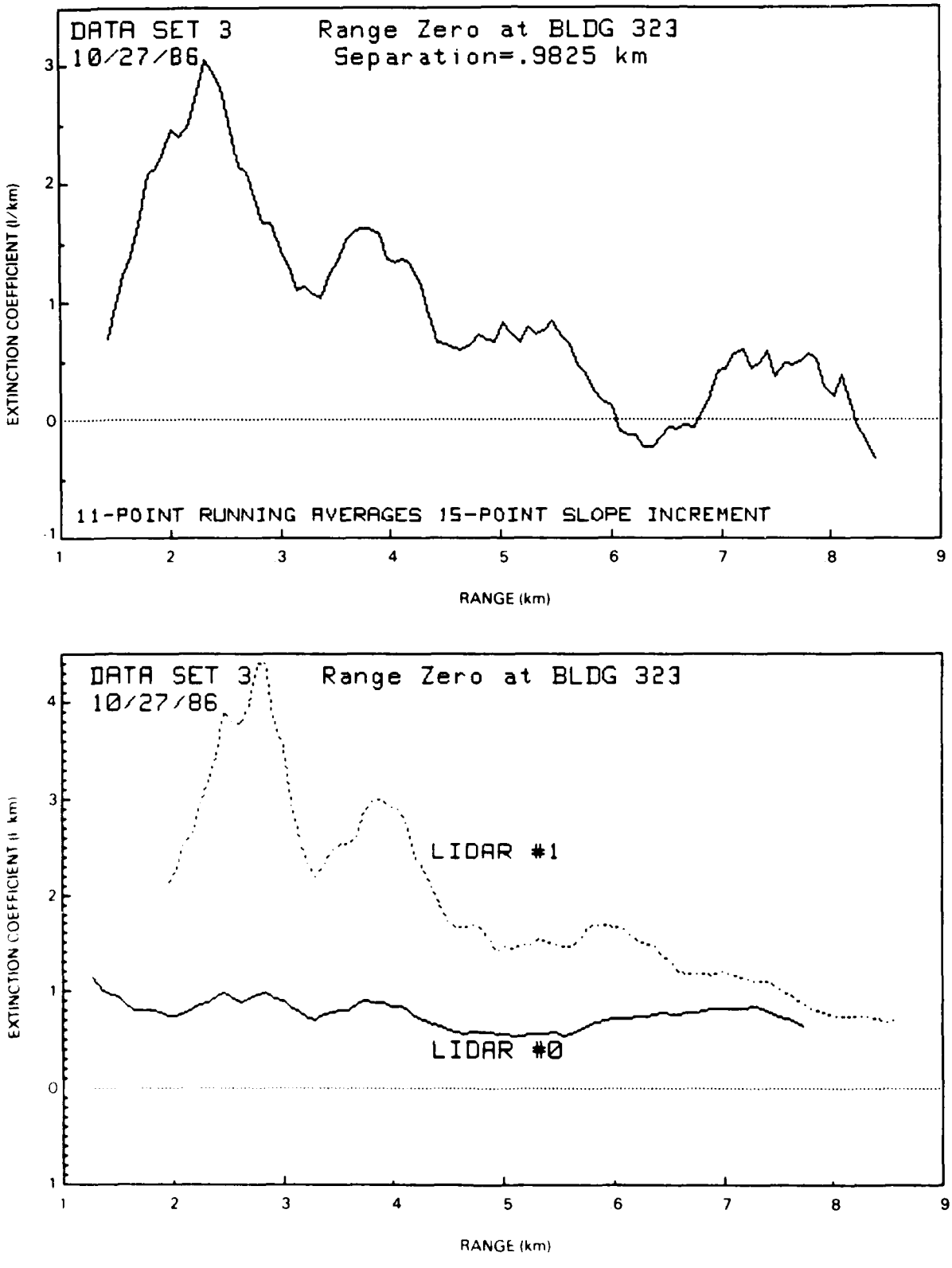

Figure 5-3 The same as figure 5-1, but for data set 3 on 27 October 1986.

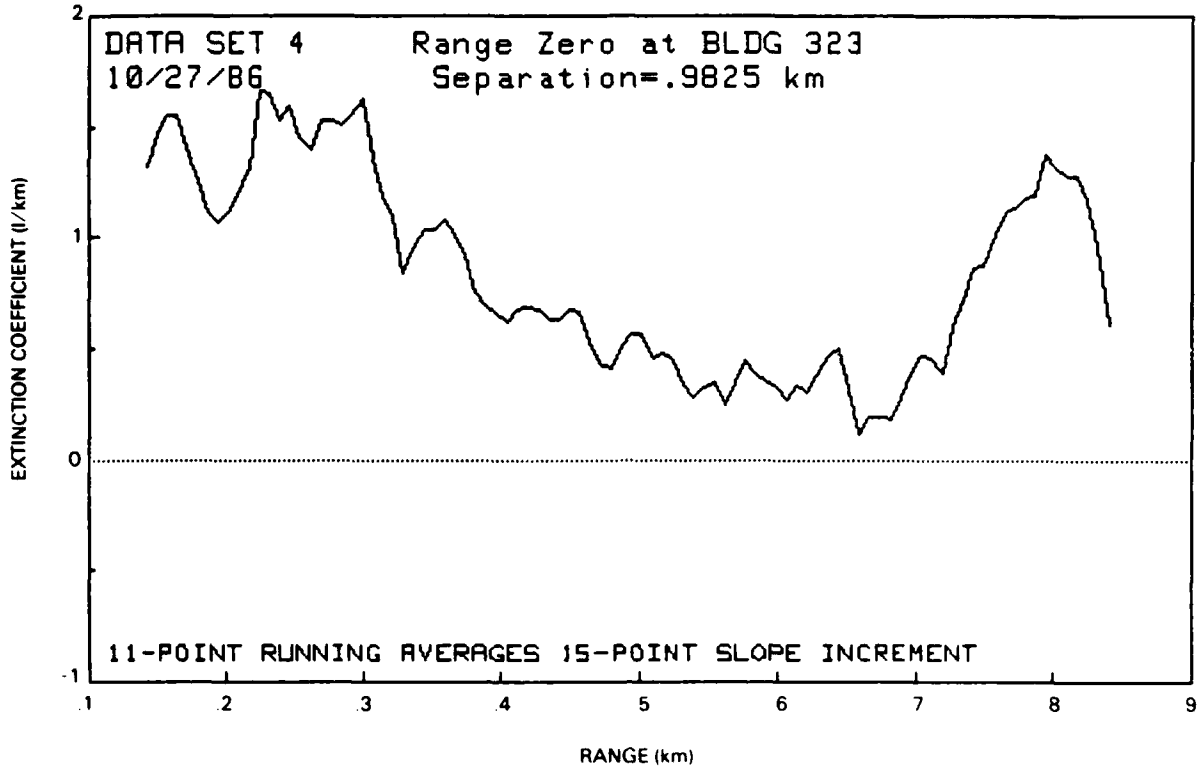

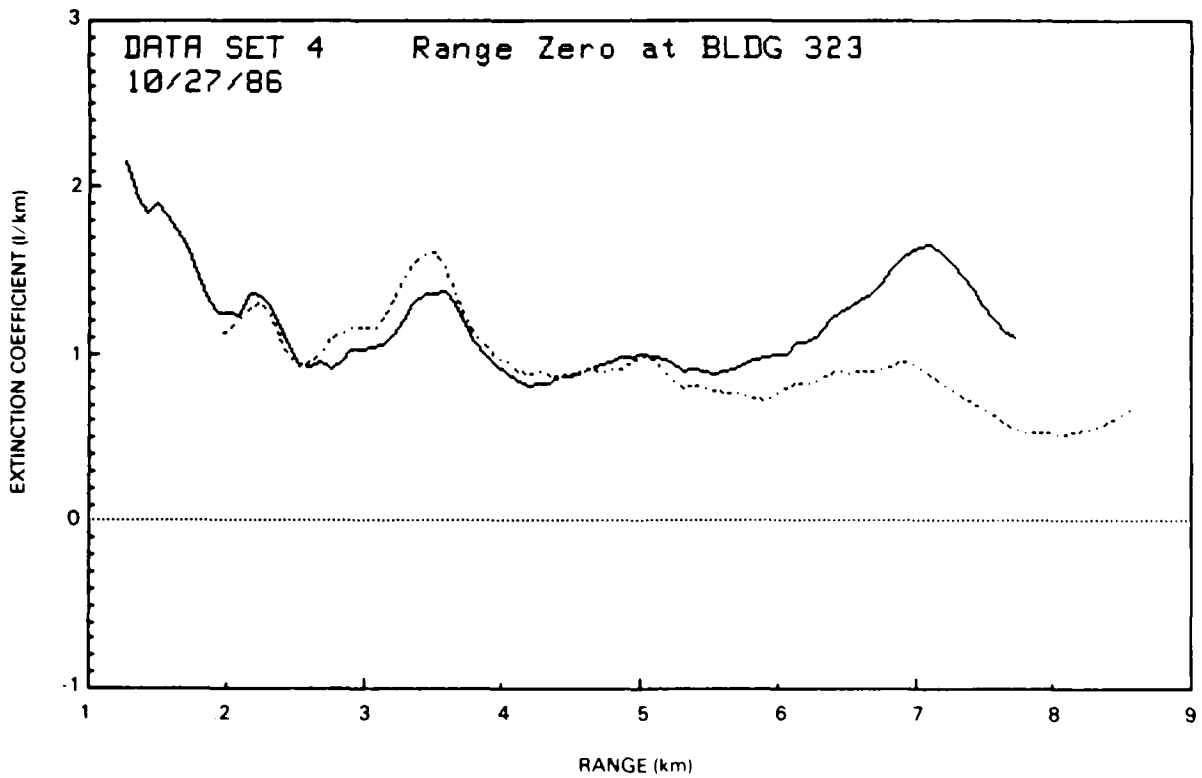

Figure 5-4. The same as figure 5-1, but for data set 4 on 27 October 1986.

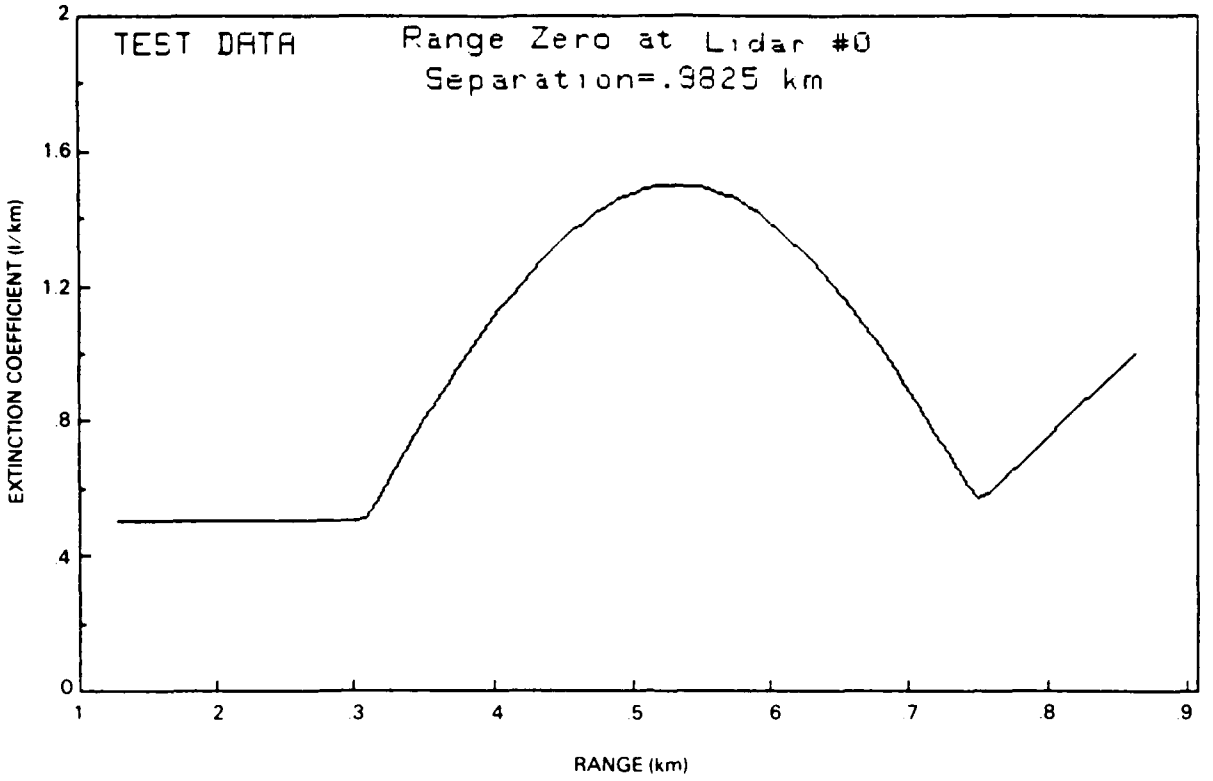

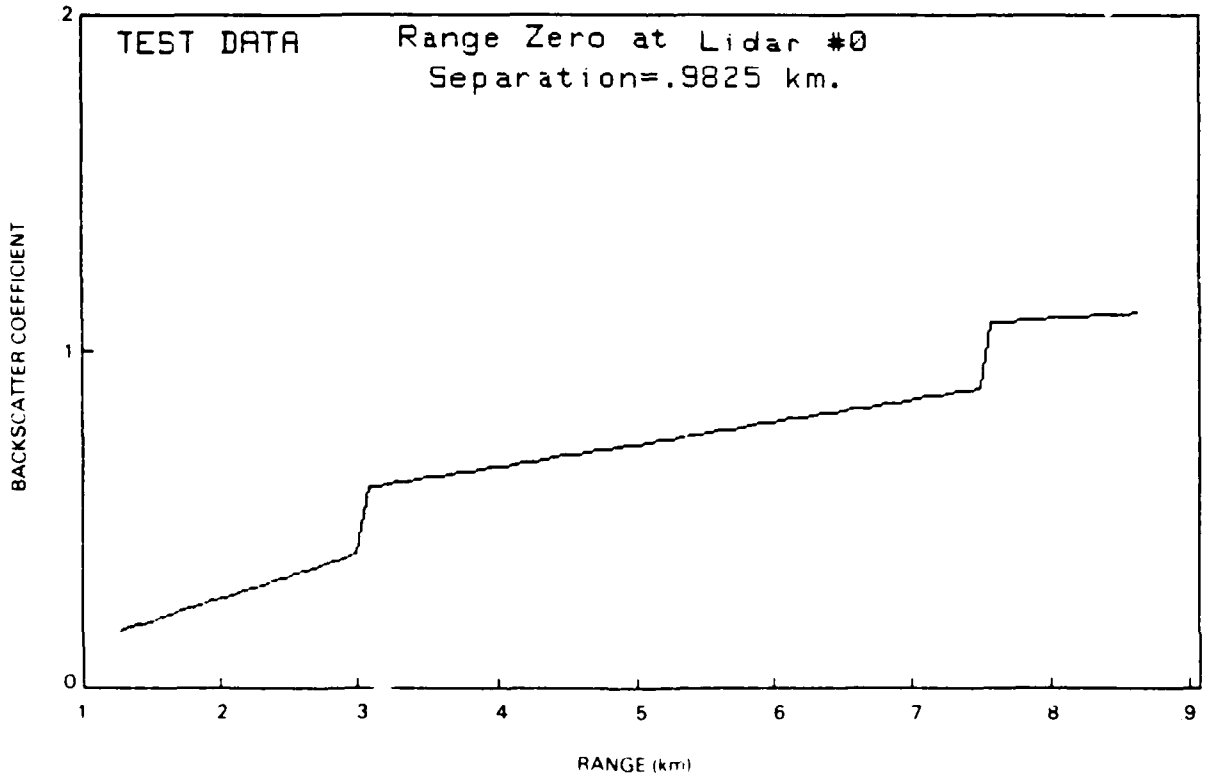

Figure 5 5 Upper graph is the extinction coefficient profile and lower graph is the backscatter coefficient profile used to generate S(R) data for the two lidars

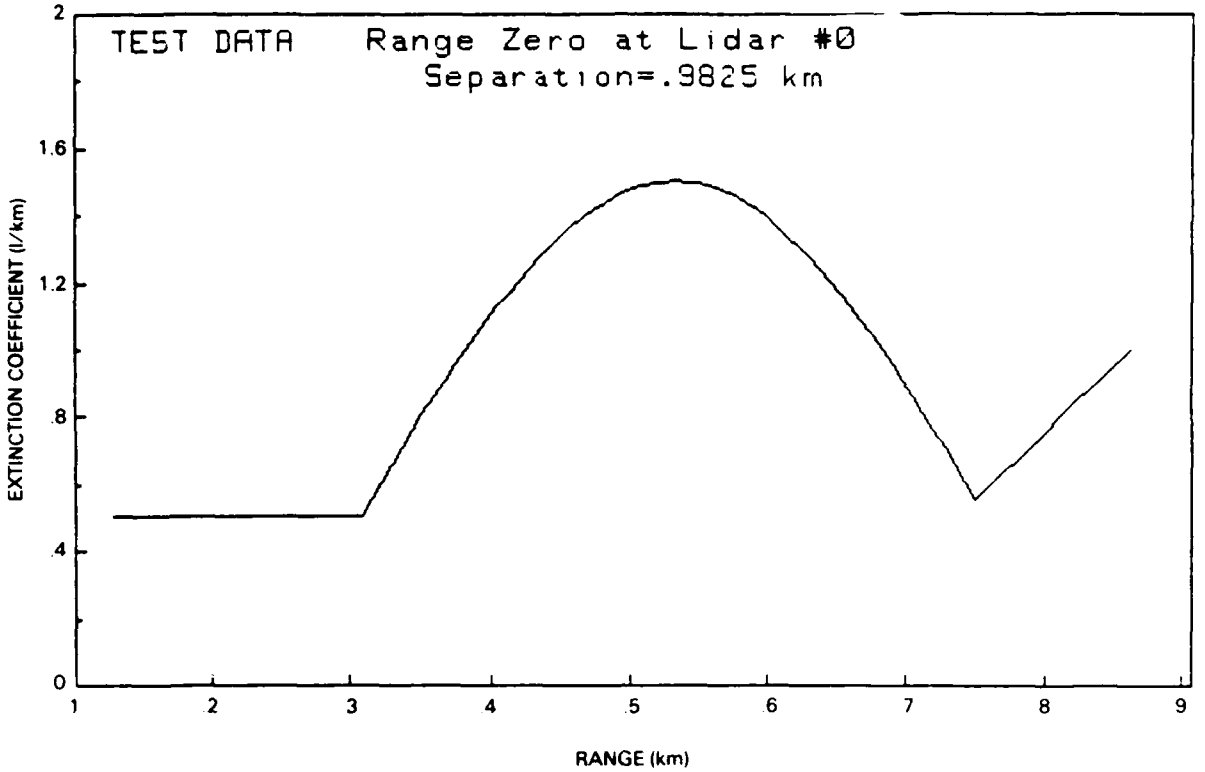

Figure 5-6. Extinction coefficient profile calculated with the dual lidar method. Compare this to the upper graph in figure 5-5.

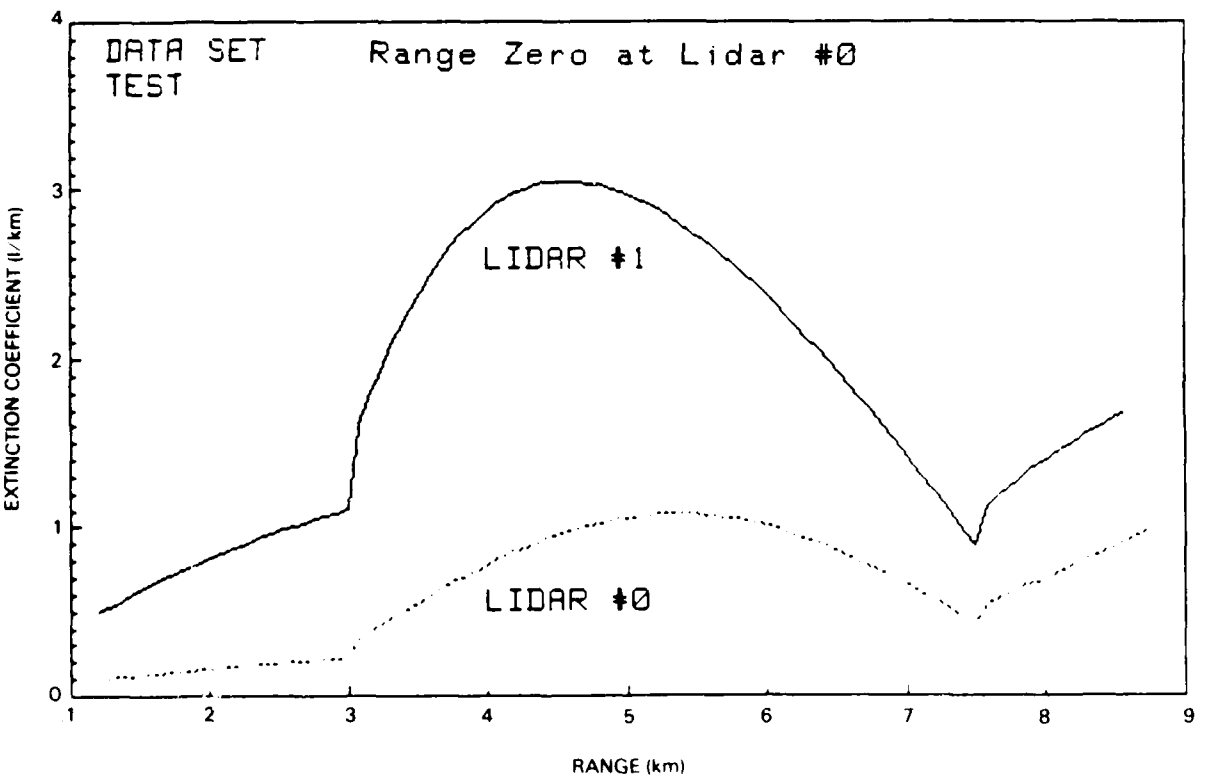

Figure 5-7. Extinction coefficient profiles calculated with the use of the stable inversion method and the computer-generated S(R) data. The results differ greatly for the two lidars.

6.0 SUMMARY

A method has been described here for obtaining extinction coefficient profiles and integrated extinction between two points. This method uses two lidars set up at opposite ends of a propagation path and pointed toward each other. No assumptions need be made about the aerosol distributions, since two equations are available to solve for the two unknowns. With accurately calibrated lidars, once the extinction coefficient profile is determined, the results can be used to separately calculate backscatter coefficient profiles for each of the lidars. These can then be compared.

Limited tests of the far-point inversion algorithm method of obtaining extinction coefficient profiles show large differences from that obtained by the two-lidar method, as well as large differences between the two lidars. A test of the two methods with known computer-generated S(R) data suggests that this is caused by the backscatter coefficient varying along the propagation path. The study merits further investigation.

While the visioceilometers used here were useful for demonstrating the two-lidar technique, a better system is needed. In particular, higher-energy output is needed to provide better signal-to-noise ratios and to allow a greater range separation. Second, a more automated method of firing the lidars and recording the data is also needed. Accurate system calibration is required, too. In addition, the visioceilometers have many unnecessary circuits that introduce needless delays in the system and noise into the output.

The two-lidar technique will not provide slant-path visibilities on a routine basis. However, when properly implemented, it may be a useful research tool for studying atmospheric aerosol characteristics when used with other atmospheric-measurement techniques.

7.0 REFERENCES

Ferguson, J. A. and M. R. Paulson. 1986."Calibration of the Hand Held Lidars Used by the Naval Ocean Systems Center," NOSC TD 996.

Klett, J. D. 1981. "Stable Analytical Inversion Solution for Processing Lidar Returns," *Applied Optics*, Vol. 20, No. 2, pp 211-220.

Klett, J. D. 1985. "Lidar Inversion with Variable Backscatter/Extinction Ratios," *Applied Optics*, Vol. 24, No. 11, pp 1638-1643.

Lentz, W. J. 1982. "The visioceilometer: A Portable Visibility and Cloud Ceiling Height Lidar," Atmospheric Sciences Laboratory TR 0105.

APPENDIX A
EXAMPLES OF S(R) CURVES FOR THE TWO LIDARS

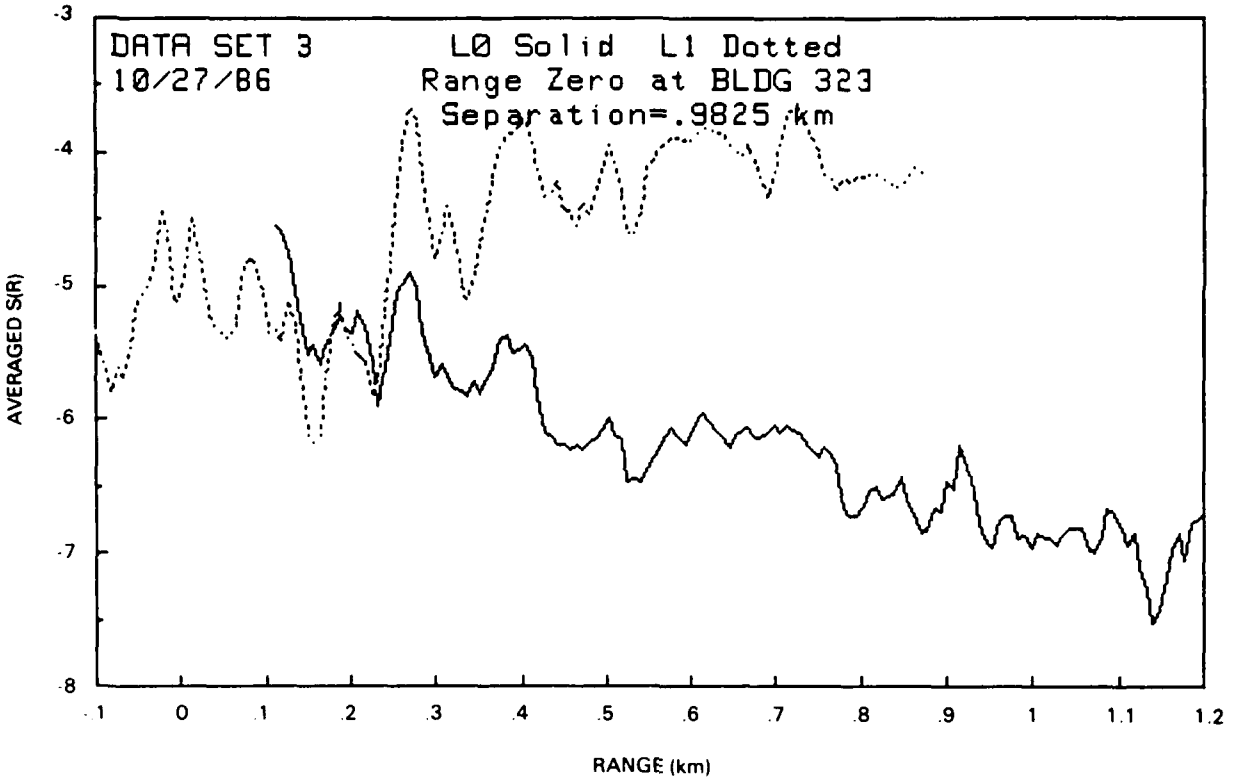
DATA SET 3
10/27/86
L0 Solid L1 Dotted
Range Zero at BLDG 323
Separation=.9825 km
AVERAGED S(R)
-3
-4
-5
-6
-7
-8
-.1
0
.1
.2
.3
.4
.5
.6
.7
.8
.9
1
1.1
1.2
RANGE (km)

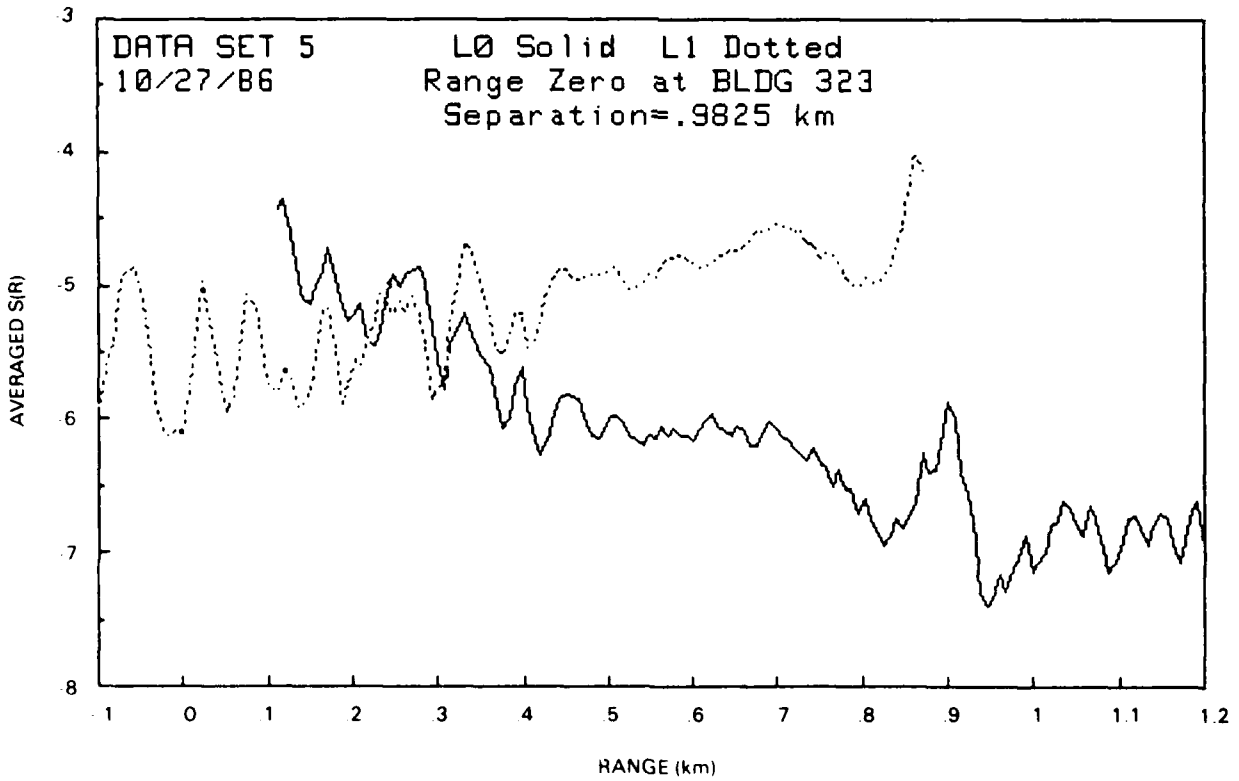
DATA SET 5
10/27/86
L0 Solid L1 Dotted
Range Zero at BLDG 323
Separation=.9825 km
AVERAGED S(R)
-3
-4
-5
-6
-7
-8
-.1
0
.1
.2
.3
.4
.5
.6
.7
.8
.9
1
1.1
1.2
RANGE (km)

Figure A-1.

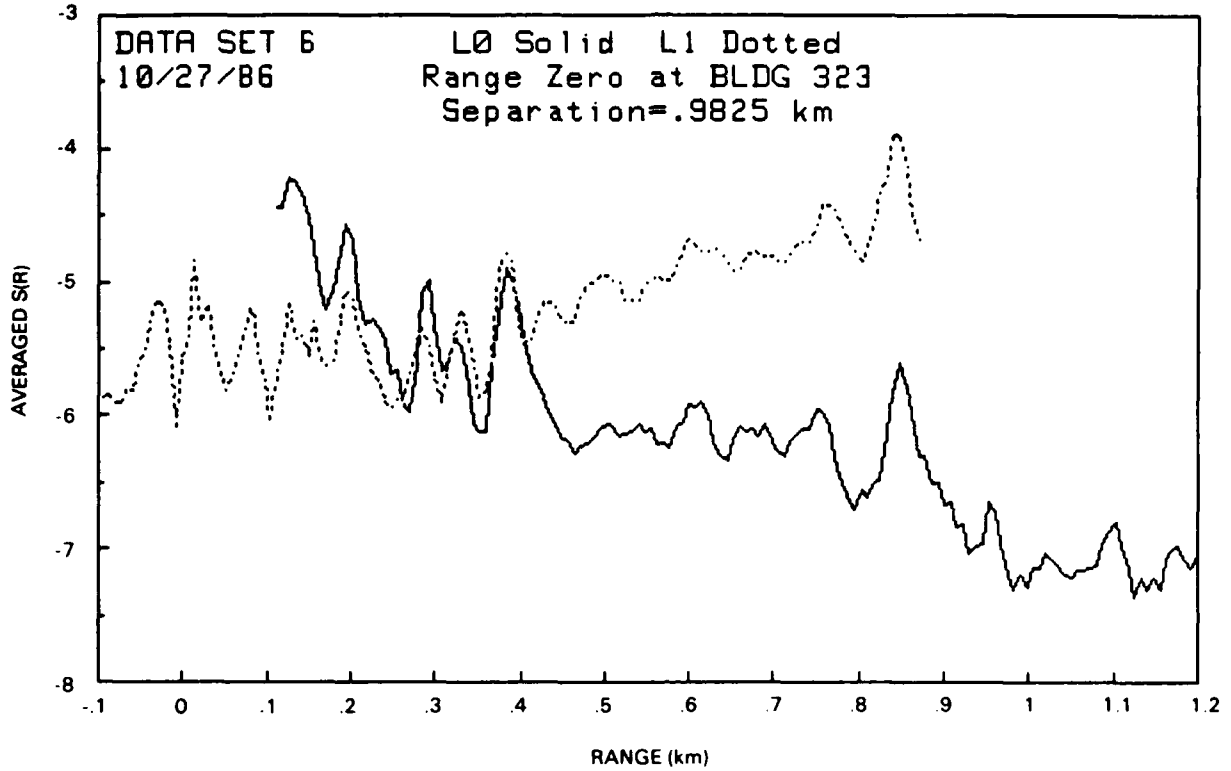
DATA SET 6
10/27/86
L0 Solid L1 Dotted
Range Zero at BLDG 323
Separation=.9825 km
AVERAGED S(R)
-3
-4
-5
-6
-7
-8
-.1
0
.1
.2
.3
.4
.5
.6
.7
.8
.9
1
1.1
1.2
RANGE (km)

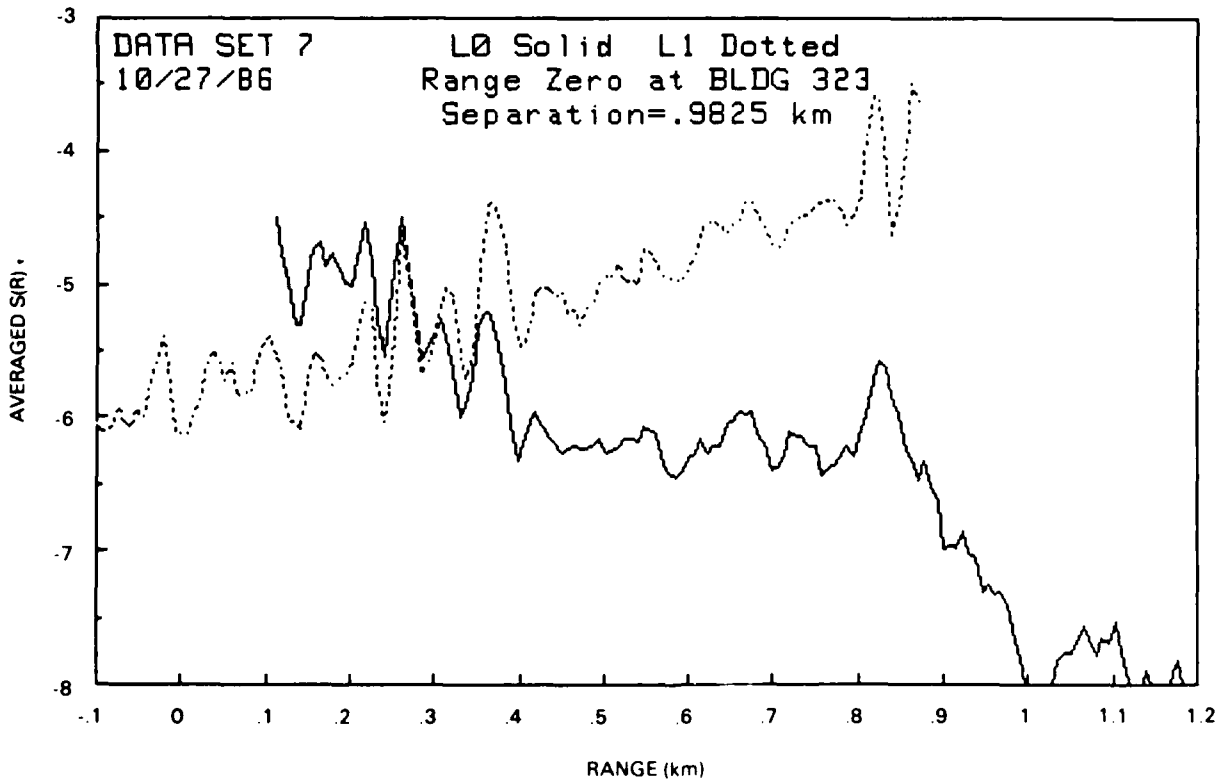
DATA SET 7
10/27/86
L0 Solid L1 Dotted
Range Zero at BLDG 323
Separation=.9825 km
AVERAGED S(R)
-3
-4
-5
-6
-7
-8
-.1
0
.1
.2
.3
.4
.5
.6
.7
.8
.9
1
1.1
1.2
RANGE (km)

Figure A-2.

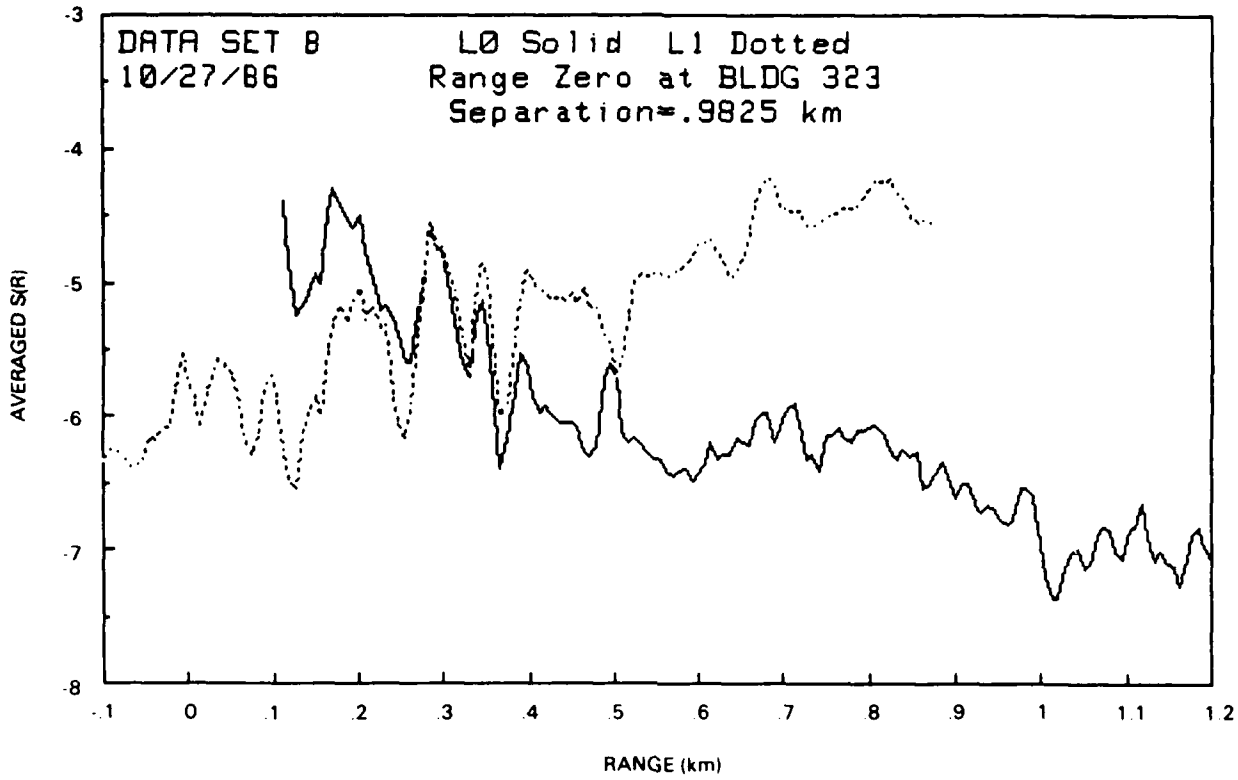
DATA SET 8
10/27/86
L0 Solid L1 Dotted
Range Zero at BLDG 323
Separation=.9825 km
AVERAGED S(R)
-3
-4
-5
-6
-7
-8
.1
0
.1
.2
.3
.4
.5
.6
.7
.8
.9
1
1.1
1.2
RANGE (km)

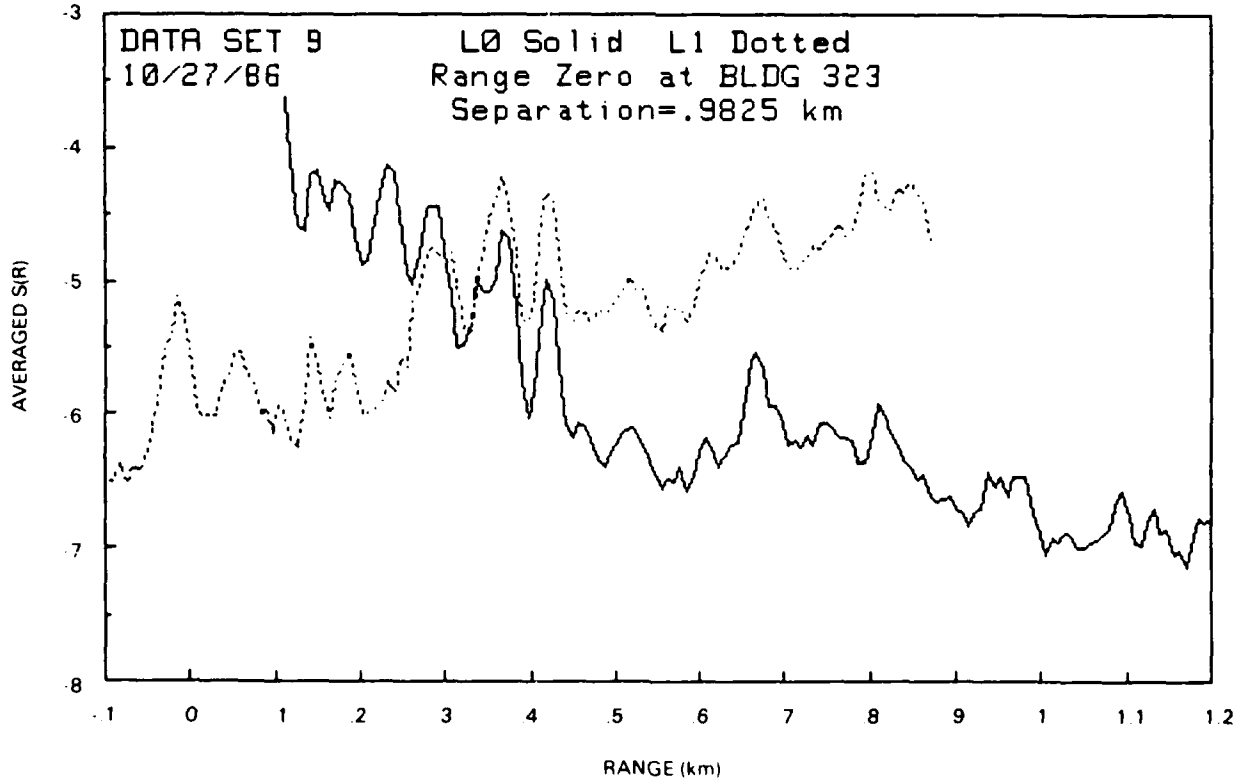
DATA SET 9
10/27/86
L0 Solid L1 Dotted
Range Zero at BLDG 323
Separation=.9825 km
AVERAGED S(R)
-3
-4
-5
-6
-7
-8
.1
0
1
.2
3
4
.5
6
7
8
9
1
1.1
1.2
RANGE (km)

Figure A-3.

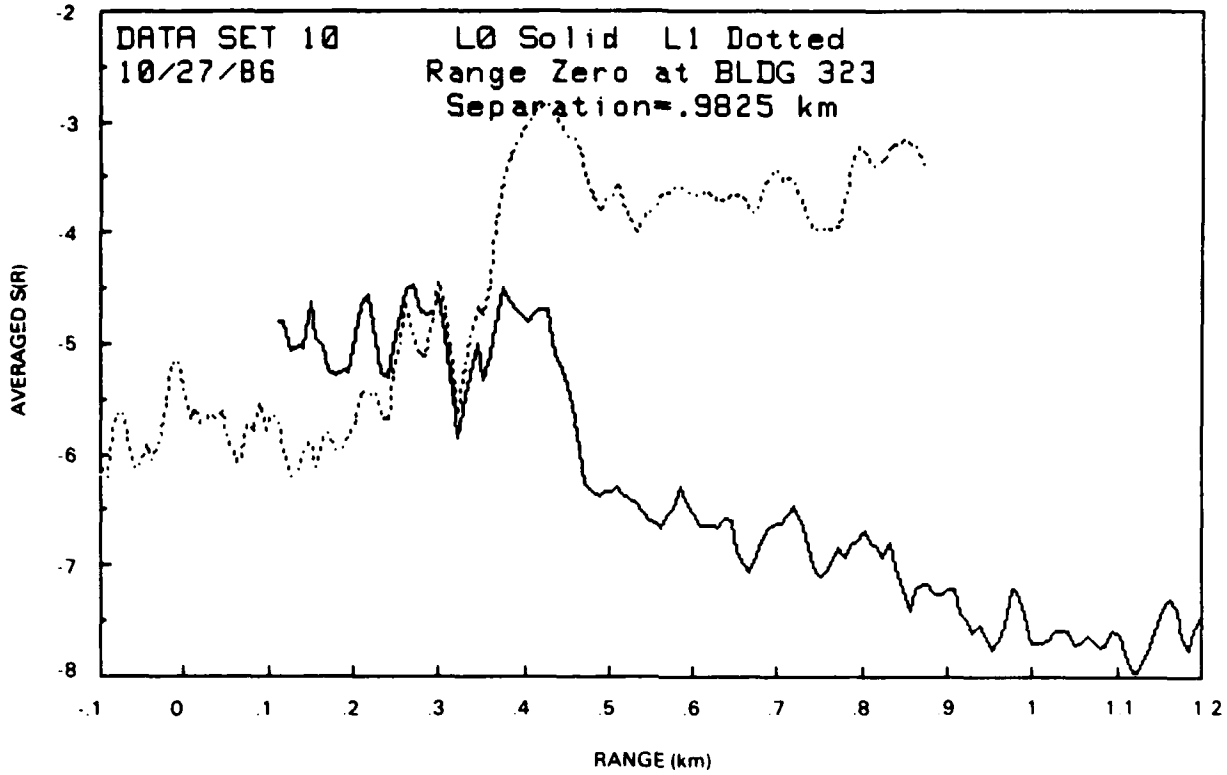
DATA SET 10
10/27/86
L0 Solid L1 Dotted
Range Zero at BLDG 323
Separation=.9825 km
AVERAGED S(R)
RANGE (km)

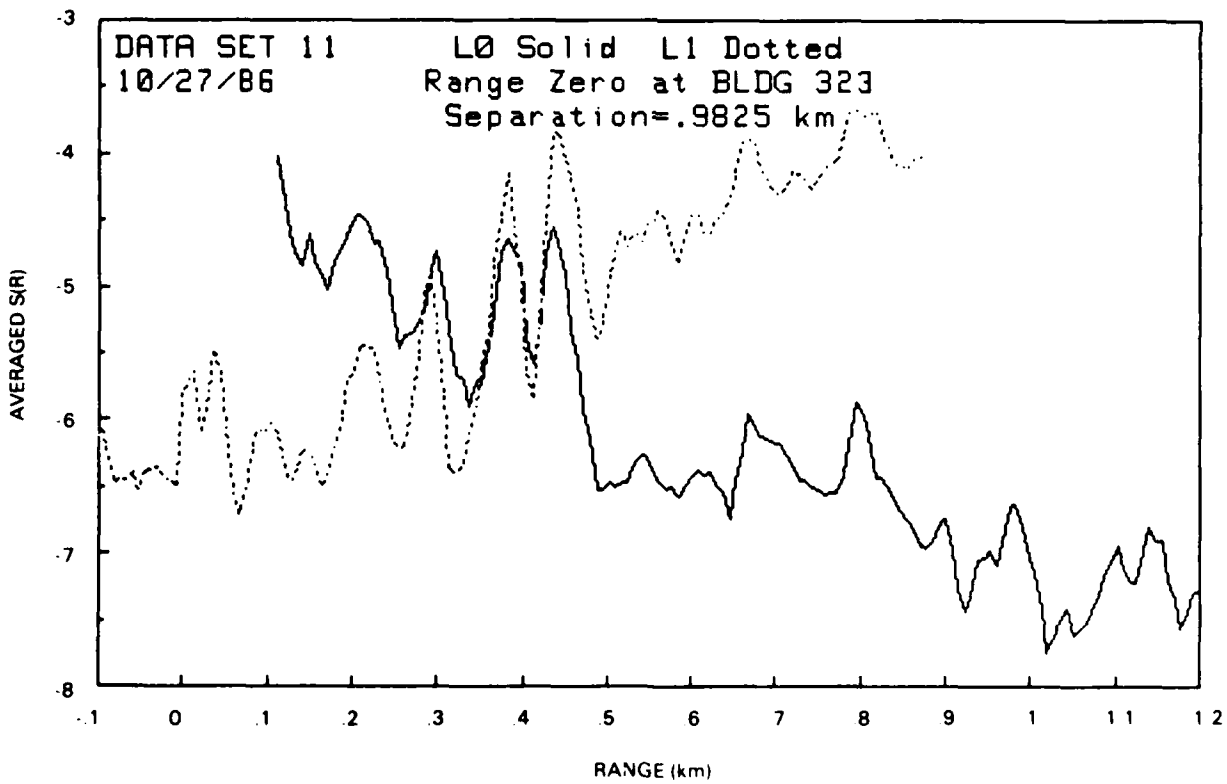
DATA SET 11
10/27/86
L0 Solid L1 Dotted
Range Zero at BLDG 323
Separation=.9825 km
AVERAGED S(R)
RANGE (km)

Figure A-4

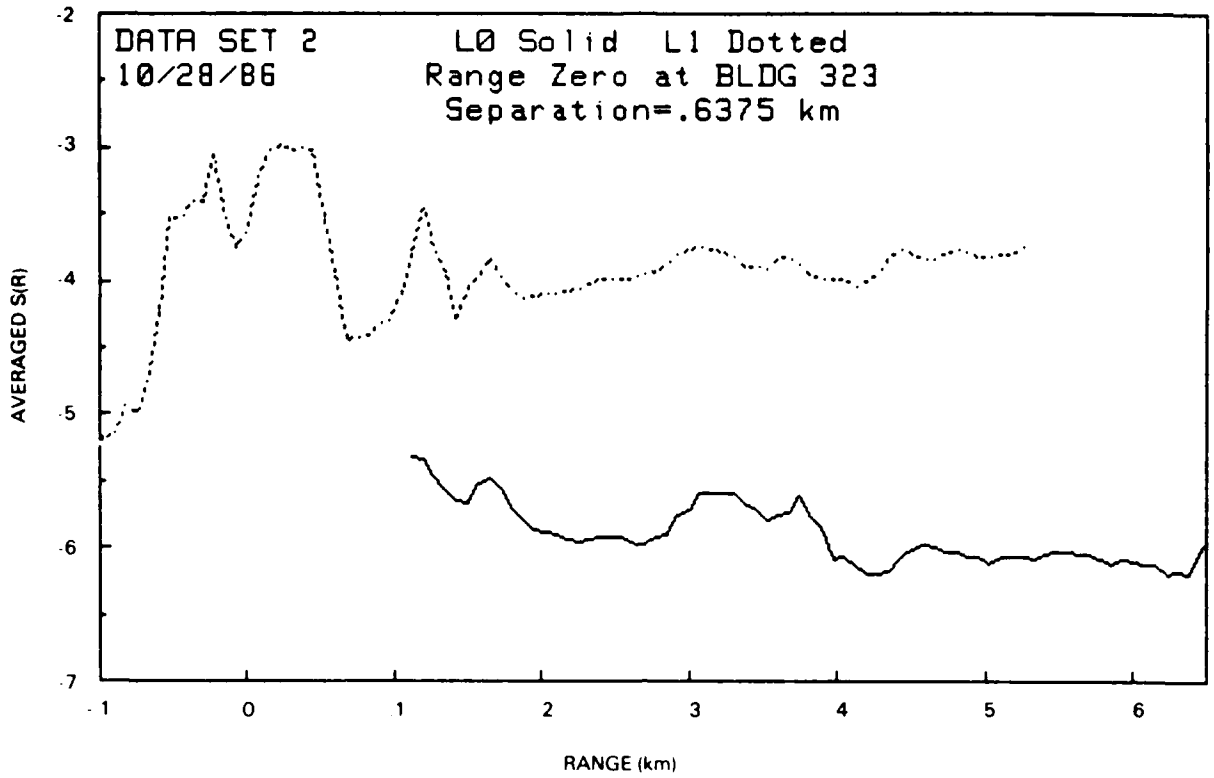
DATA SET 2
10/28/86
L0 Solid L1 Dotted
Range Zero at BLDG 323
Separation=.6375 km
AVERAGED S(R)
-2
-3
-4
-5
-6
-7
-1
0
1
2
3
4
5
6
RANGE (km)

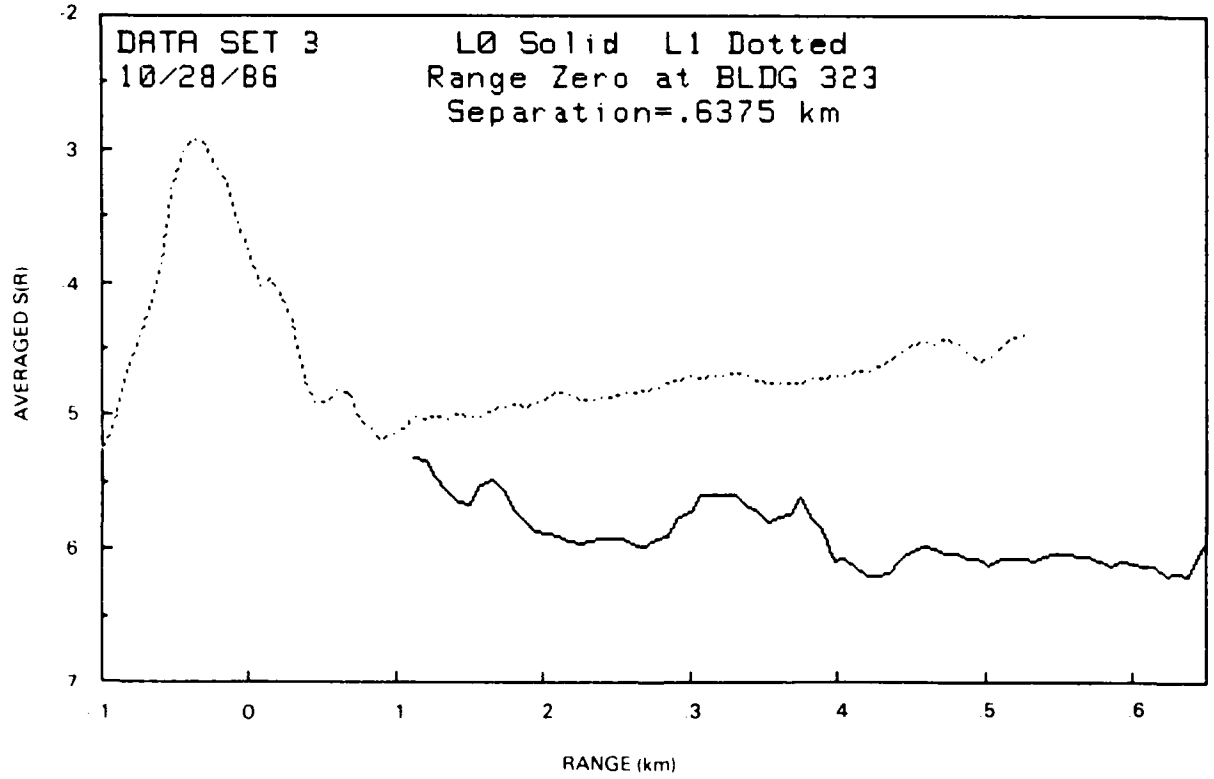
DATA SET 3
10/28/86
L0 Solid L1 Dotted
Range Zero at BLDG 323
Separation=.6375 km
AVERAGED S(R)
-2
3
4
5
6
7
-1
0
1
2
3
4
5
6
RANGE (km)

Figure A-5.

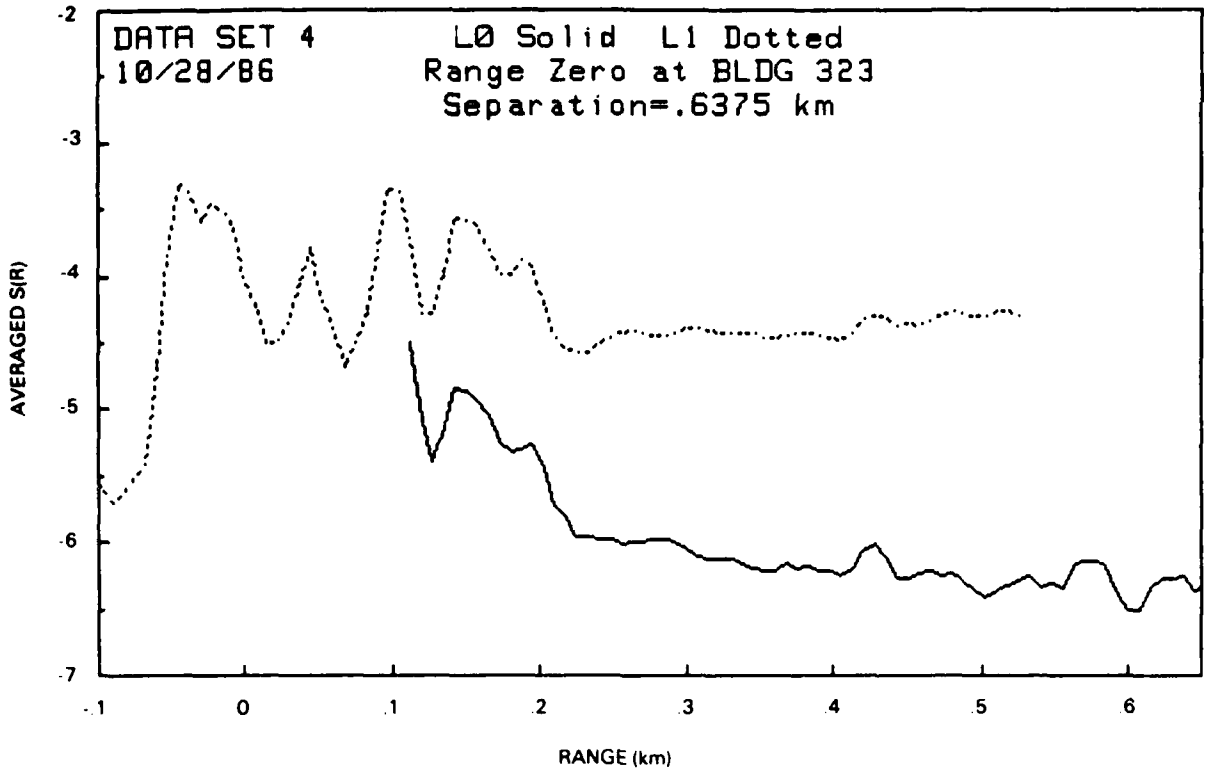
DATA SET 4
10/28/86
L0 Solid L1 Dotted
Range Zero at BLDG 323
Separation=.6375 km
AVERAGED S(R)
-2
-3
-4
-5
-6
-7
-.1
0
.1
.2
.3
.4
.5
.6
RANGE (km)

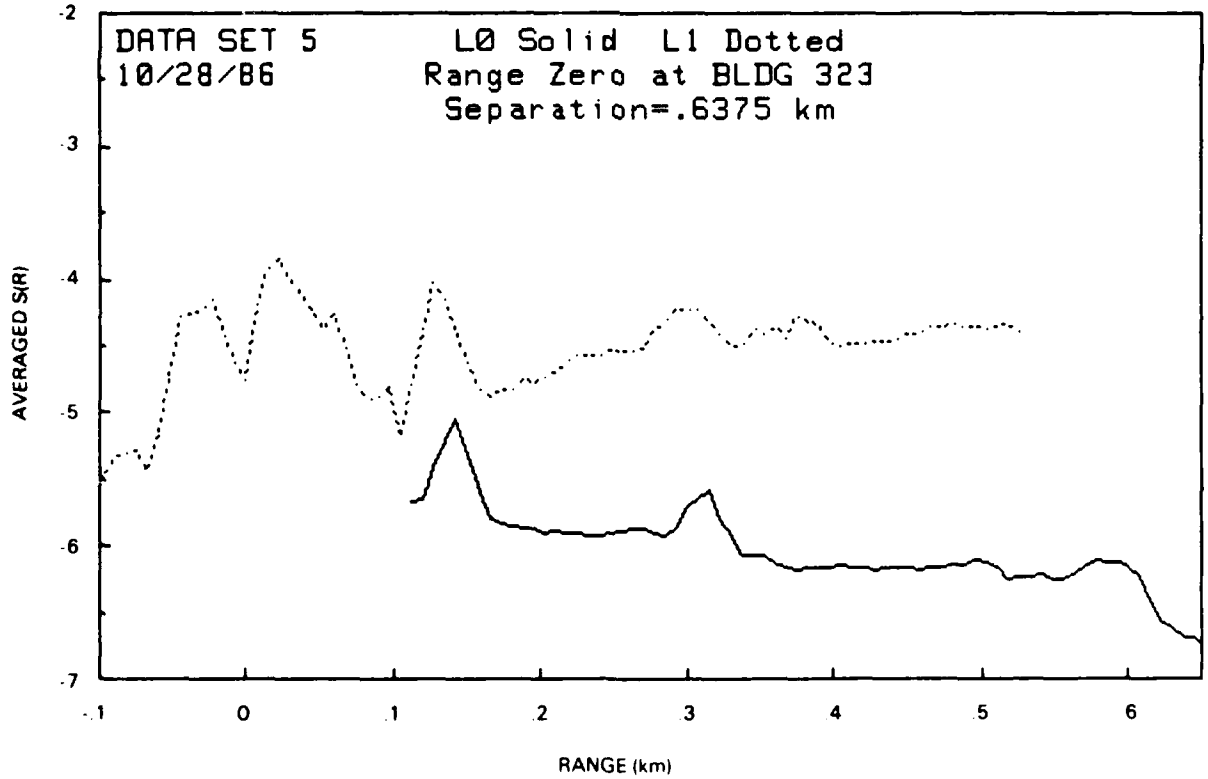
DATA SET 5
10/28/86
L0 Solid L1 Dotted
Range Zero at BLDG 323
Separation=.6375 km
AVERAGED S(R)
-2
-3
-4
-5
-6
-7
-.1
0
.1
.2
.3
.4
.5
.6
RANGE (km)

Figure A-6.

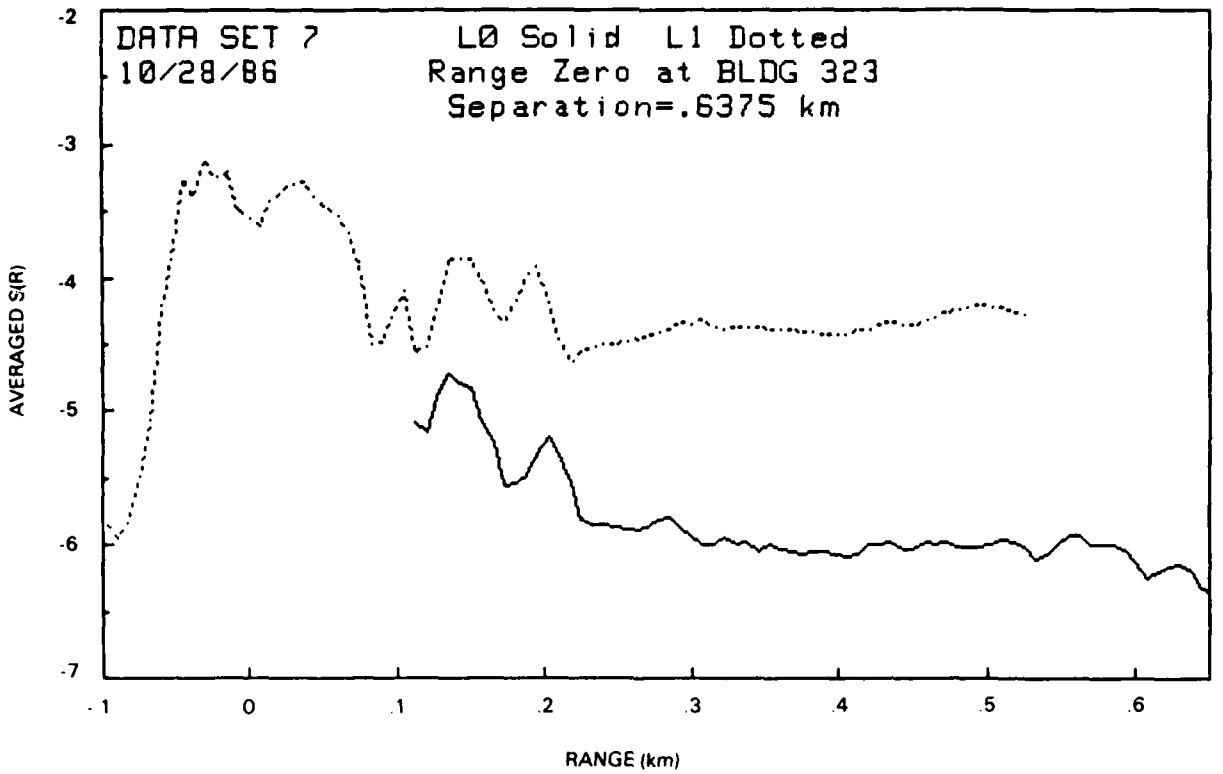
DATA SET 7
10/28/86
L0 Solid L1 Dotted
Range Zero at BLDG 323
Separation=.6375 km
AVERAGED S(R)
-2
-3
-4
-5
-6
-7
-.1
0
.1
.2
.3
.4
.5
.6
RANGE (km)

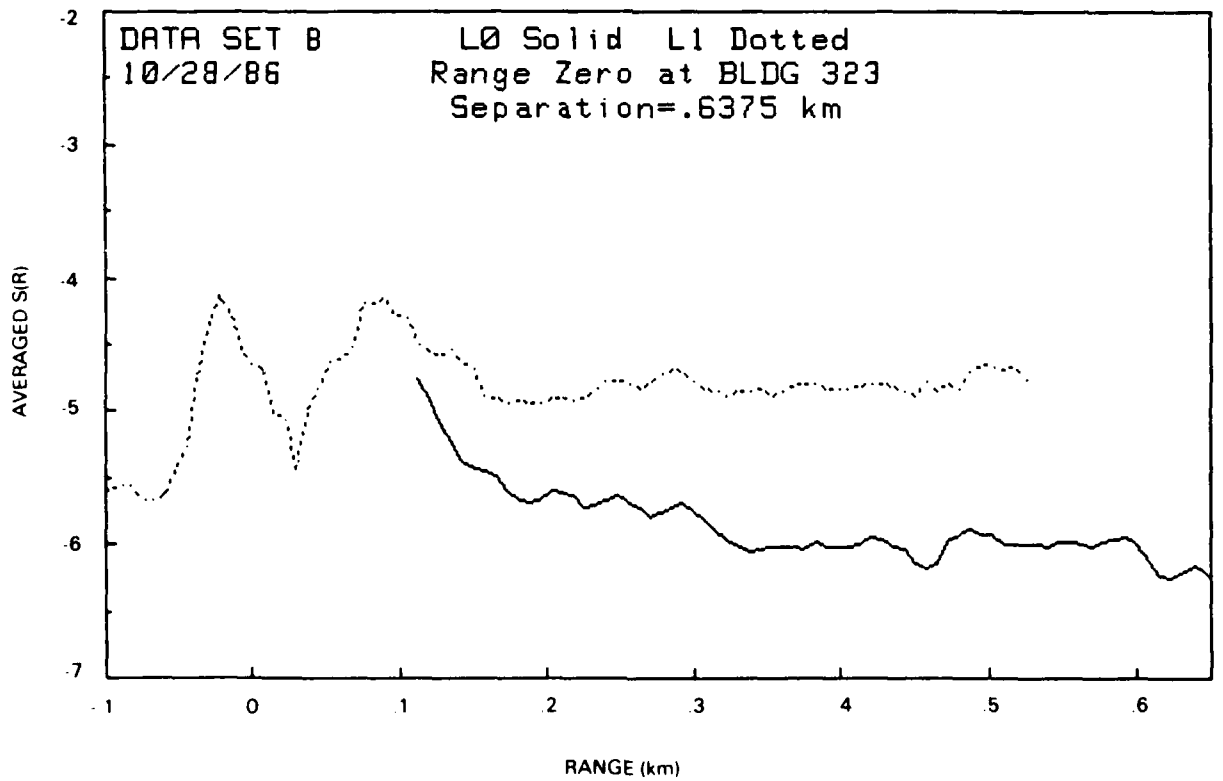
DATA SET 8
10/28/86
L0 Solid L1 Dotted
Range Zero at BLDG 323
Separation=.6375 km
AVERAGED S(R)
-2
-3
-4
-5
-6
-7
-.1
0
.1
.2
.3
.4
.5
.6
RANGE (km)

Figure A-7.

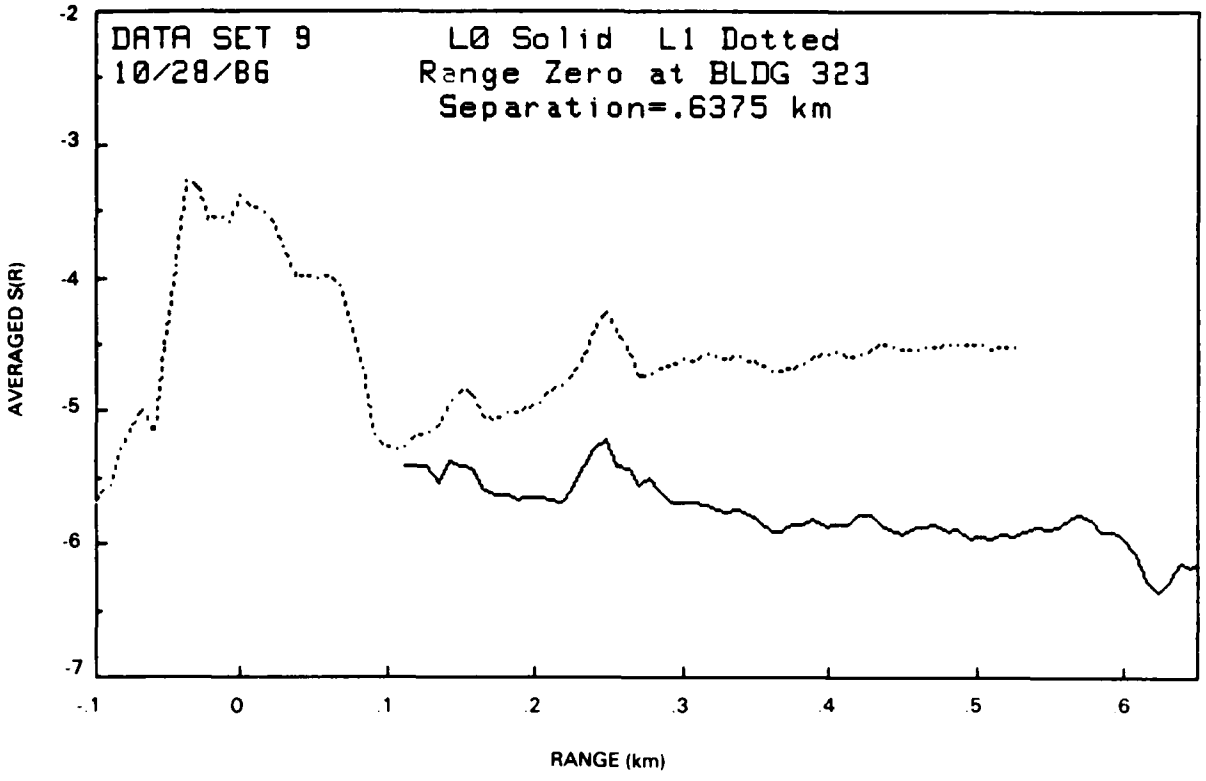
DATA SET 9
10/28/86
L0 Solid L1 Dotted
Range Zero at BLDG 323
Separation=.6375 km
AVERAGED S(R)
-2
-3
-4
-5
-6
-7
-.1
0
.1
.2
.3
.4
.5
6
RANGE (km)

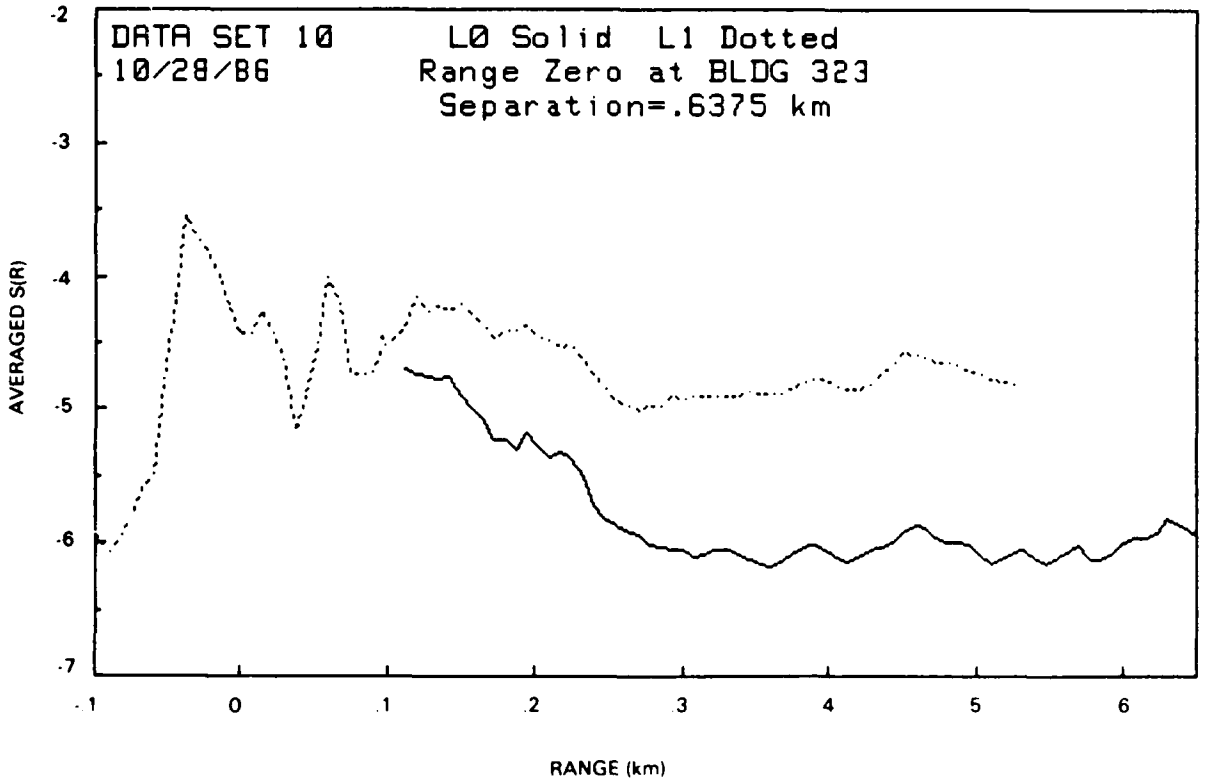
DATA SET 10
10/28/86
L0 Solid L1 Dotted
Range Zero at BLDG 323
Separation=.6375 km
AVERAGED S(R)
-2
-3
-4
-5
-6
-7
-.1
0
.1
.2
.3
4
5
6
RANGE (km)

Figure A-8.

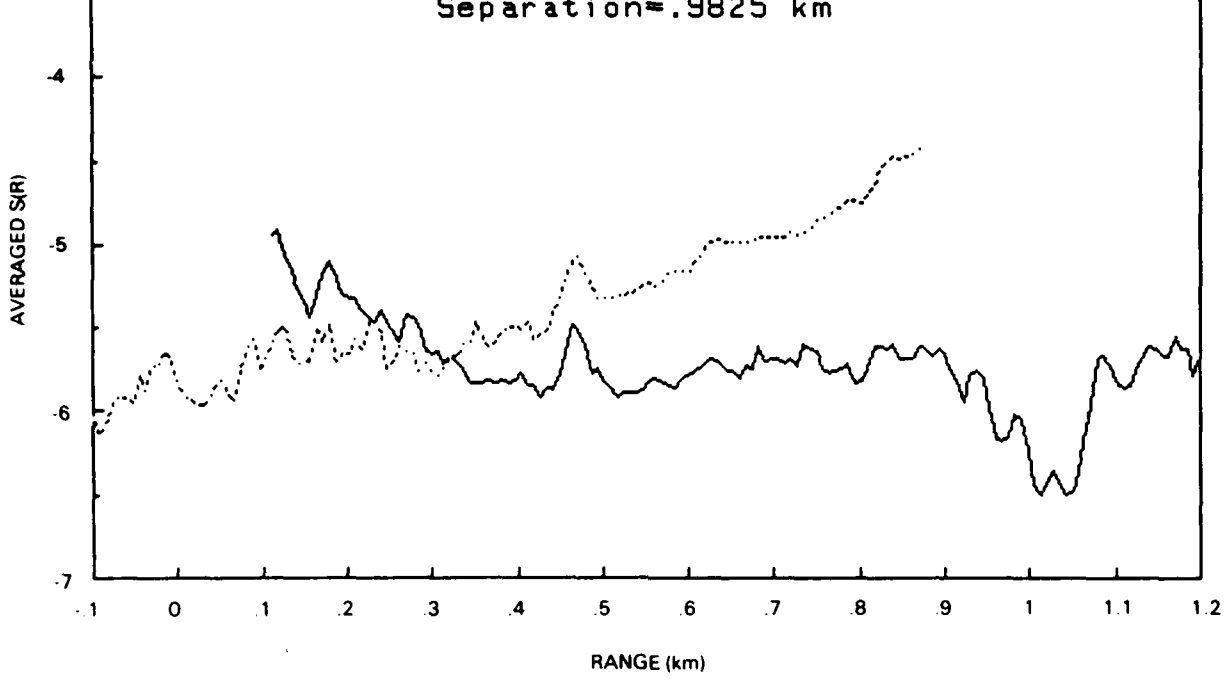
DATA SET 4
10/30/86
L0 Solid L1 Dotted
Range Zero at BLDG 323
Separation=.9825 km
AVERAGED S(R)
-3
-4
-5
-6
-7
-.1
0
.1
.2
.3
.4
.5
.6
.7
.8
.9
1
1.1
1.2
RANGE (km)

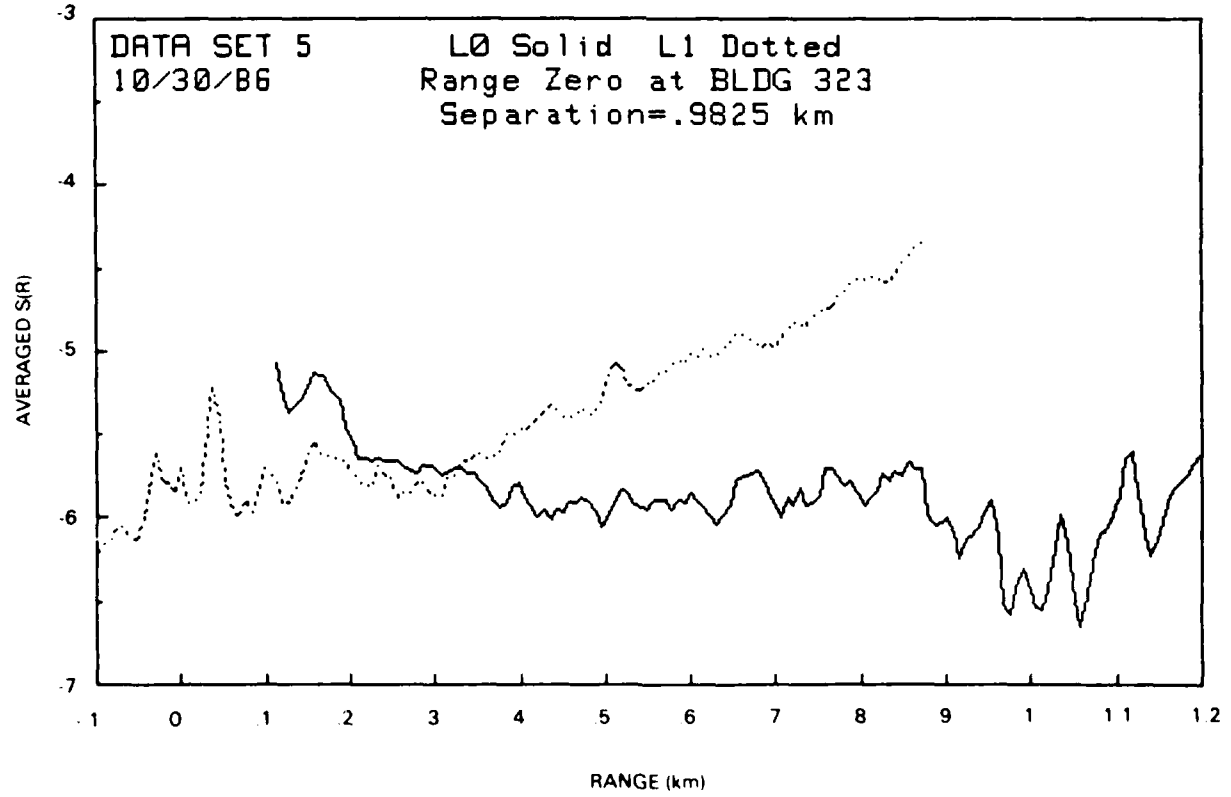
DATA SET 5
10/30/86
L0 Solid L1 Dotted
Range Zero at BLDG 323
Separation=.9825 km
AVERAGED S(R)
-3
-4
-5
-6
-7
-.1
0
.1
.2
3
4
.5
6
7
8
9
1
1.1
1.2
RANGE (km)

Figure A-9.

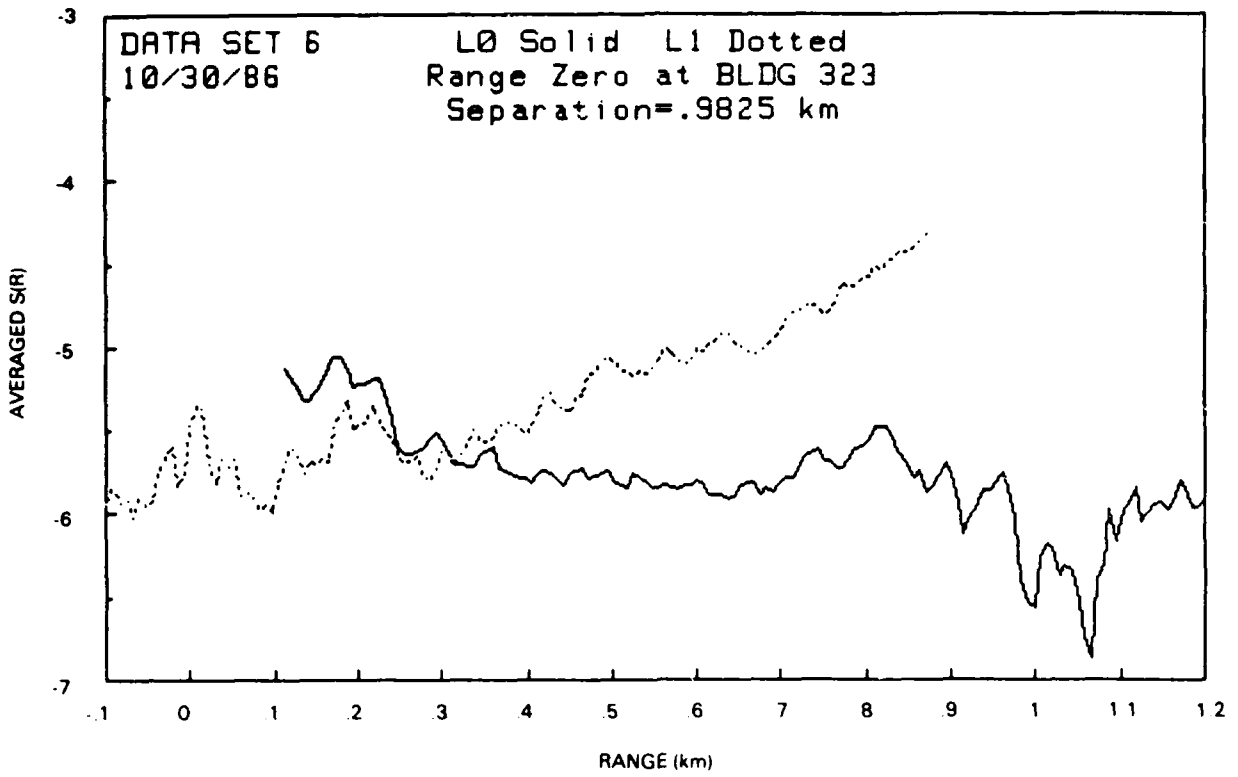
DATA SET 6
10/30/86
L0 Solid L1 Dotted
Range Zero at BLDG 323
Separation=.9825 km
AVERAGED S(R)
-3
-4
-5
-6
-7
-.1
0
1
.2
.3
.4
.5
.6
.7
.8
.9
1
1.1
1.2
RANGE (km)

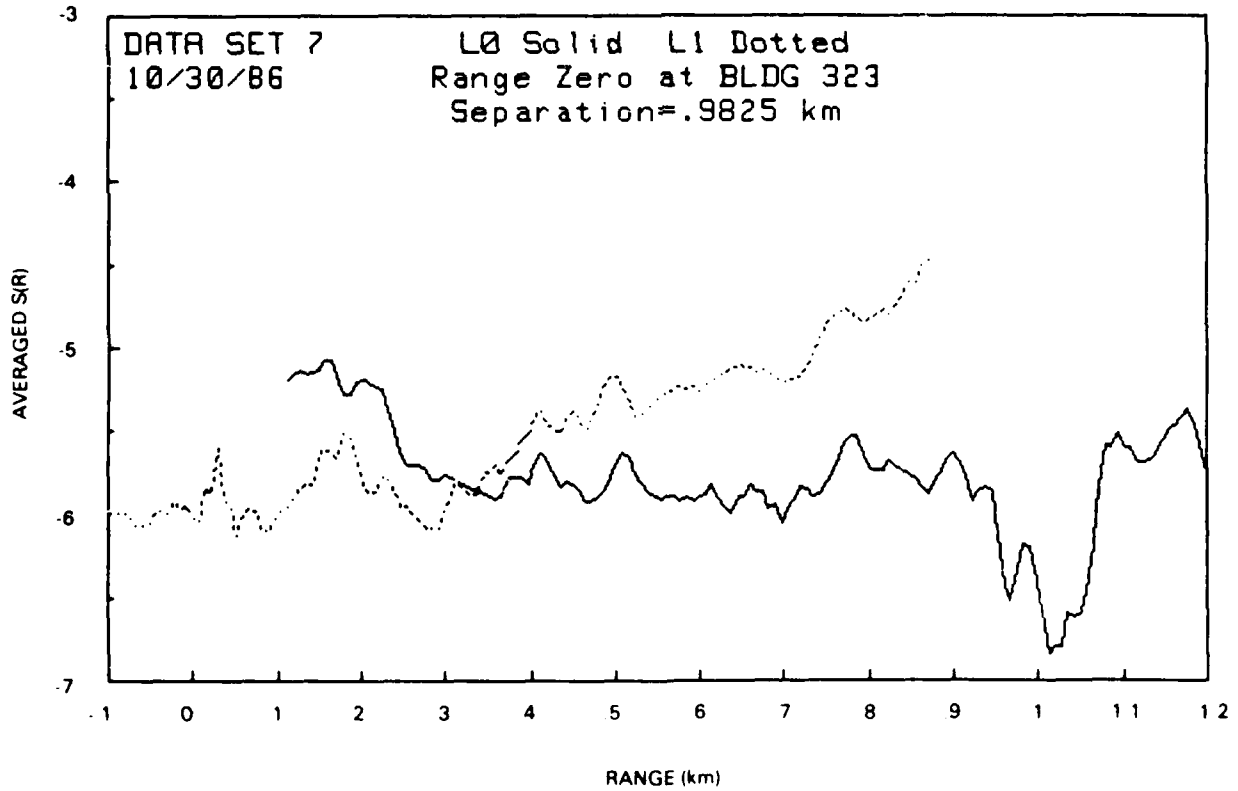
DATA SET 7
10/30/86
L0 Solid L1 Dotted
Range Zero at BLDG 323
Separation=.9825 km
AVERAGED S(R)
-3
-4
-5
-6
-7
-.1
0
1
2
3
4
5
6
7
8
9
1
1.1
1.2
RANGE (km)

Figure A-10.

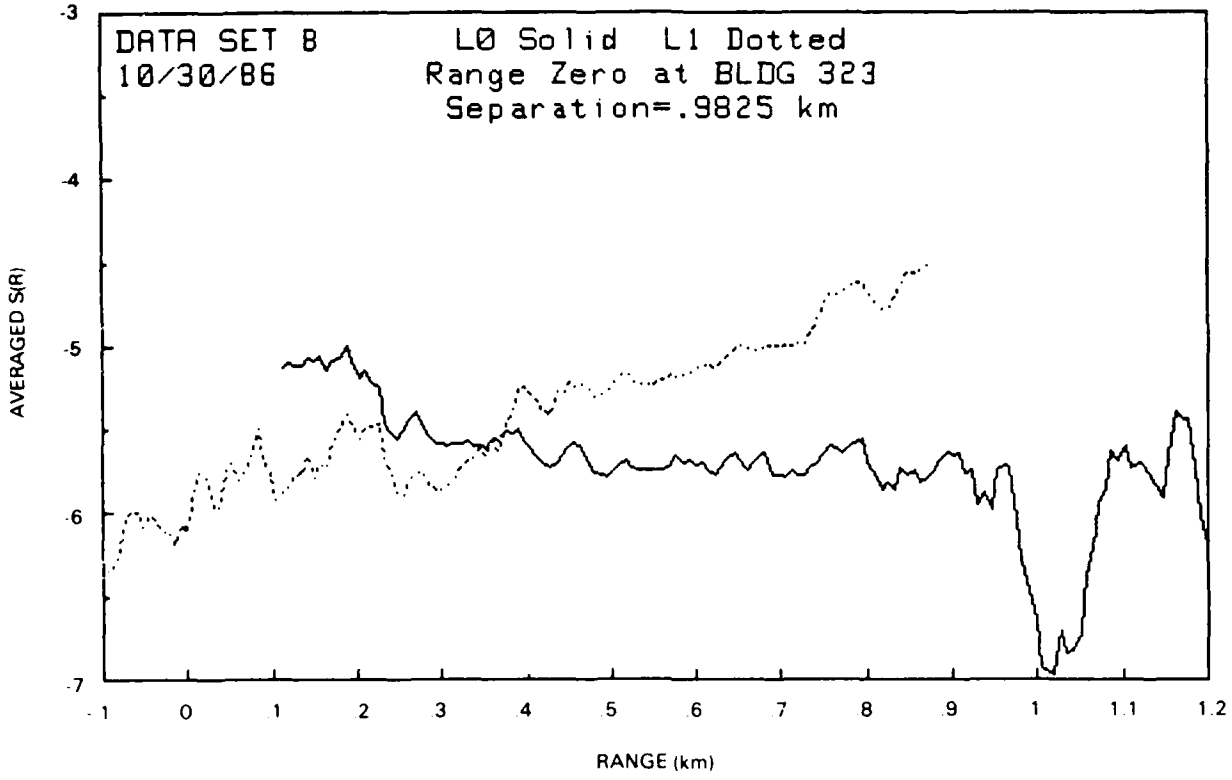
DATA SET 8
10/30/86
L0 Solid L1 Dotted
Range Zero at BLDG 323
Separation=.9825 km
AVERAGED S(R)
-3
-4
-5
-6
-7
-.1
0
.1
.2
.3
.4
.5
.6
.7
.8
.9
1
1.1
1.2
RANGE (km)

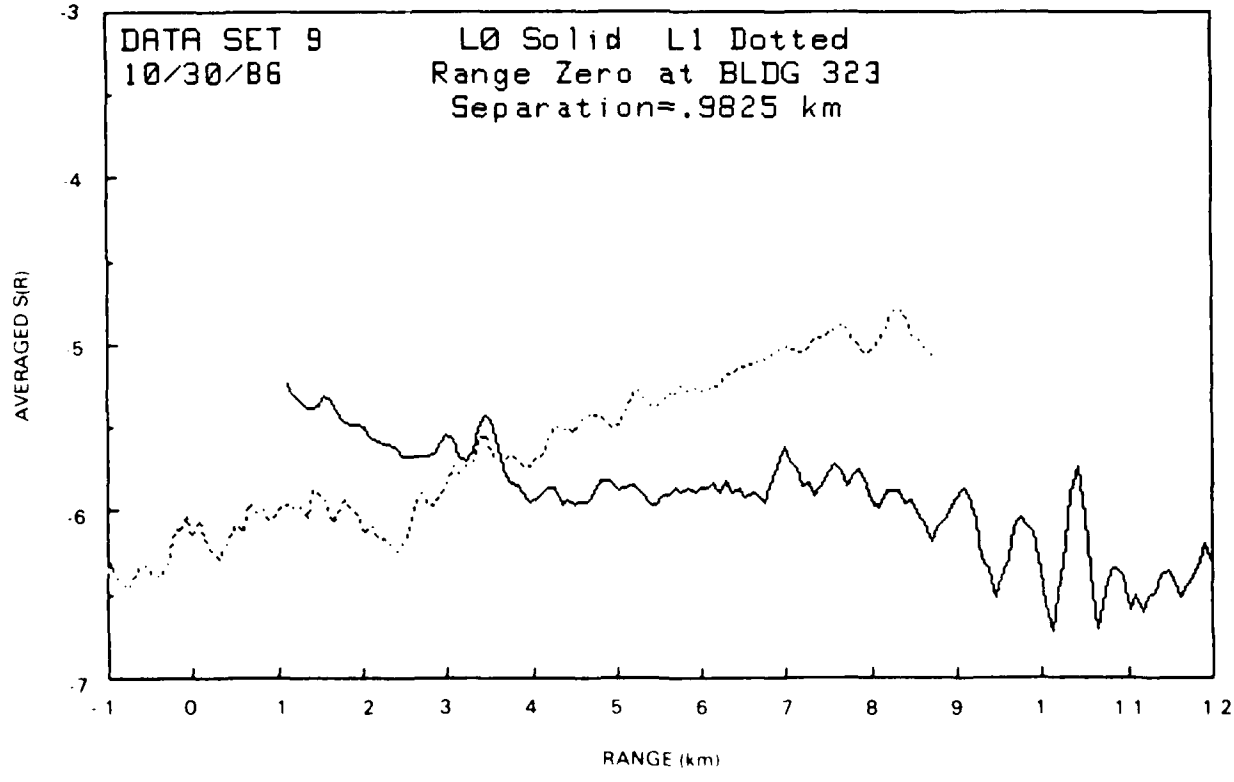
DATA SET 9
10/30/86
L0 Solid L1 Dotted
Range Zero at BLDG 323
Separation=.9825 km
AVERAGED S(R)
-3
-4
-5
-6
-7
-.1
0
1
2
3
4
5
6
7
8
9
1
1.1
1.2
RANGE (km)

Figure A-11

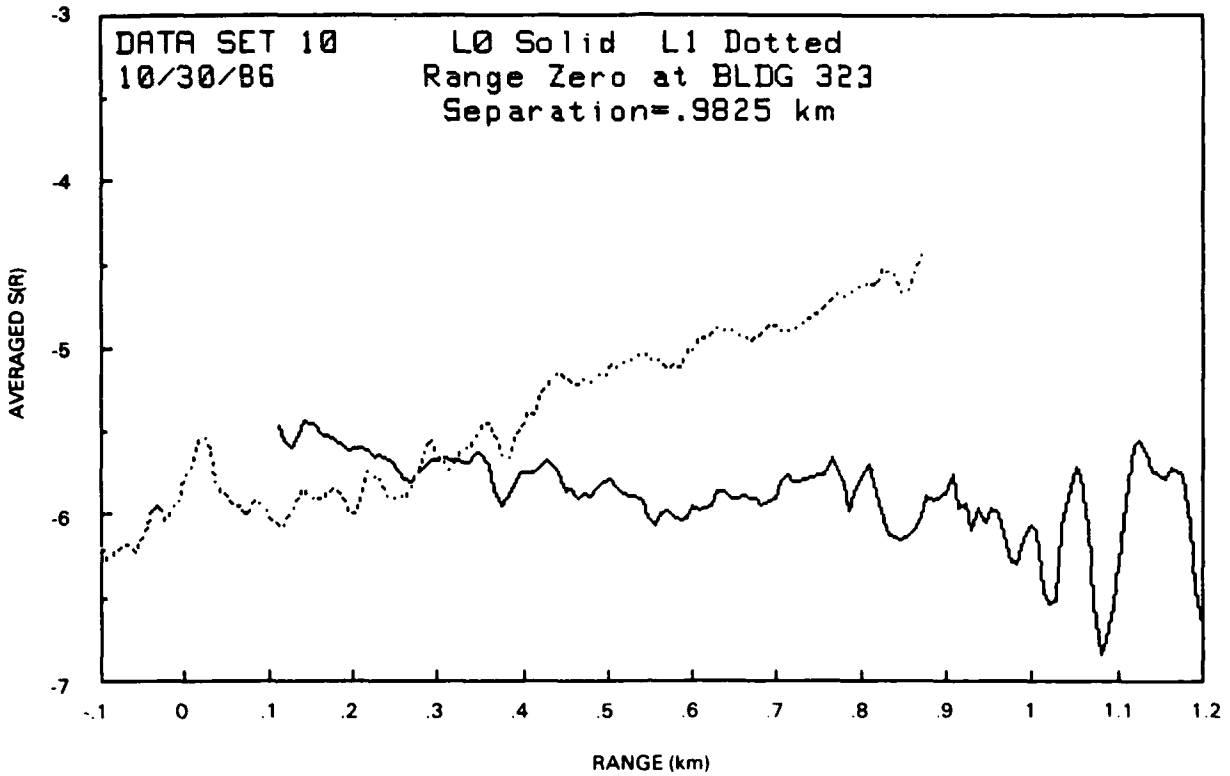
DATA SET 10
10/30/86
L0 Solid L1 Dotted
Range Zero at BLDG 323
Separation=.9825 km
AVERAGED S(R)
-3
-4
-5
-6
-7
-.1
0
.1
.2
.3
.4
.5
.6
.7
.8
.9
1
1.1
1.2
RANGE (km)

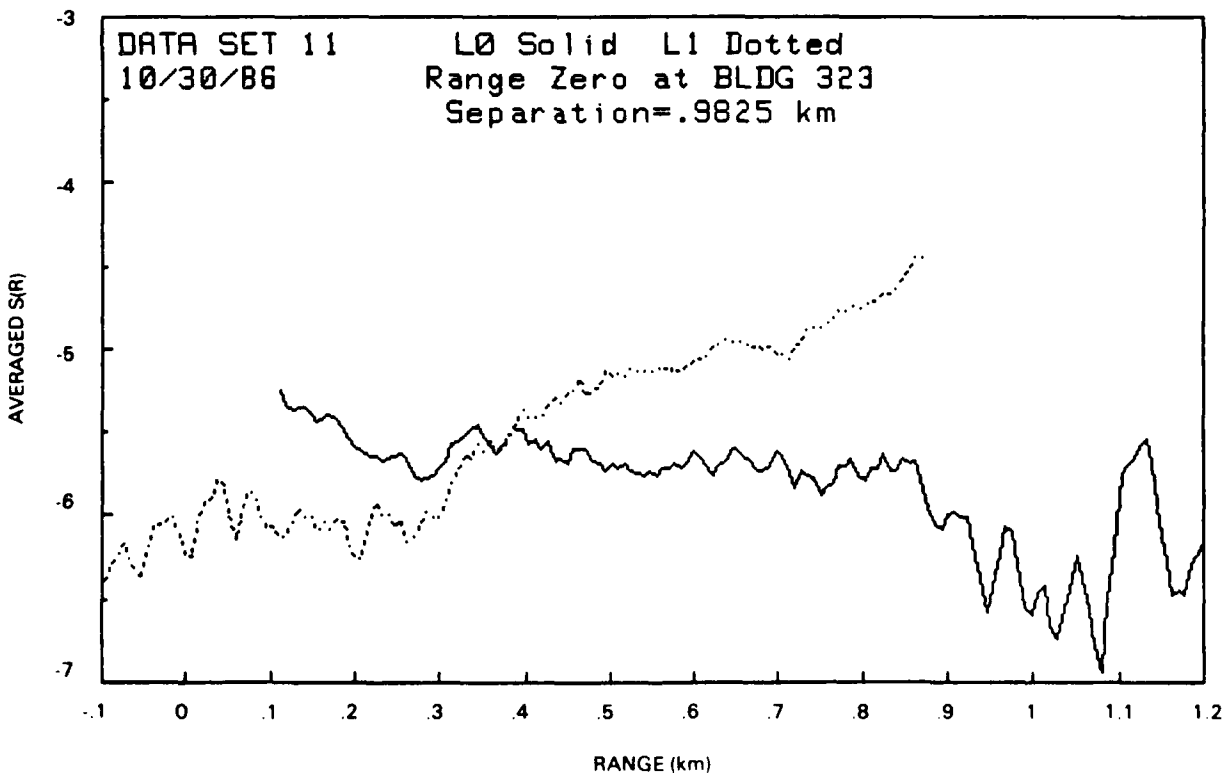
DATA SET 11
10/30/86
L0 Solid L1 Dotted
Range Zero at BLDG 323
Separation=.9825 km
AVERAGED S(R)
-3
-4
-5
-6
-7
-.1
0
.1
.2
.3
.4
.5
.6
.7
.8
.9
1
1.1
1.2
RANGE (km)

Figure A-12.

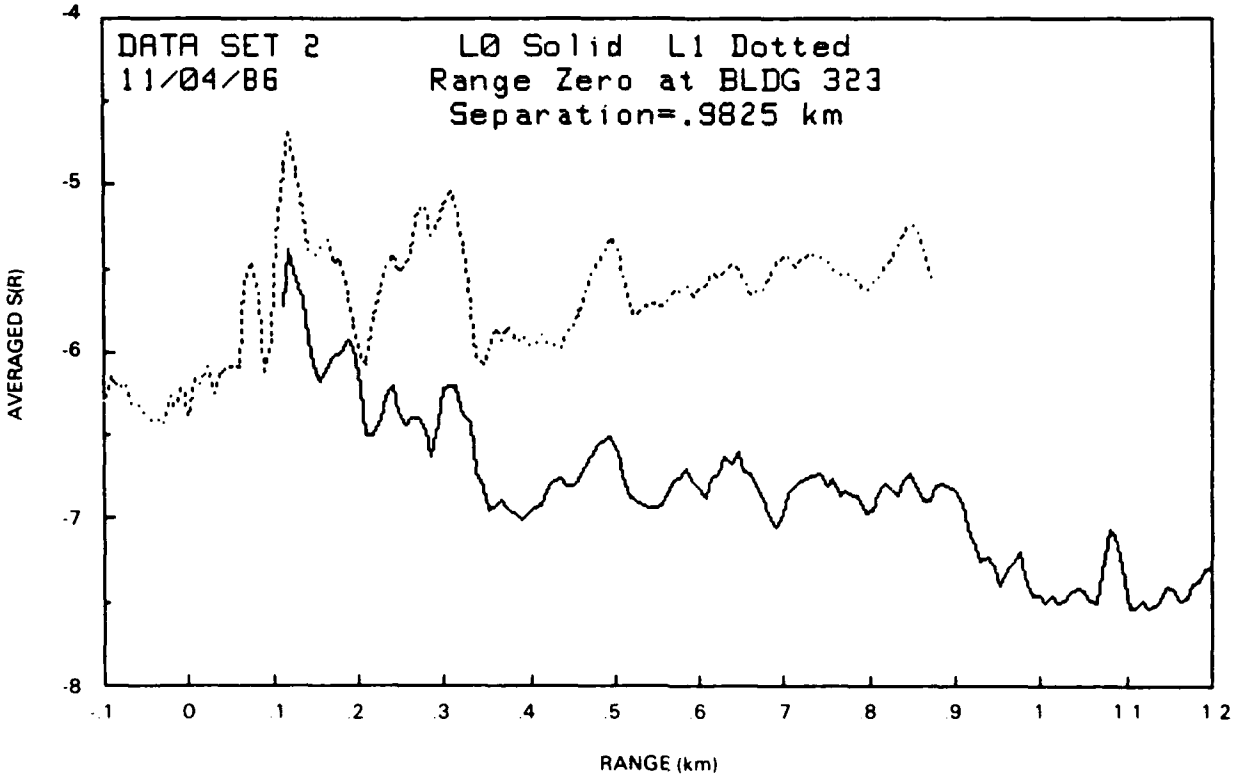
DATA SET 2
11/04/86
L0 Solid L1 Dotted
Range Zero at BLDG 323
Separation=.9825 km
AVERAGED S(R)
-4
-5
-6
-7
-8
.1
0
1
2
3
4
5
6
7
8
9
1
1 1
1 2
RANGE (km)

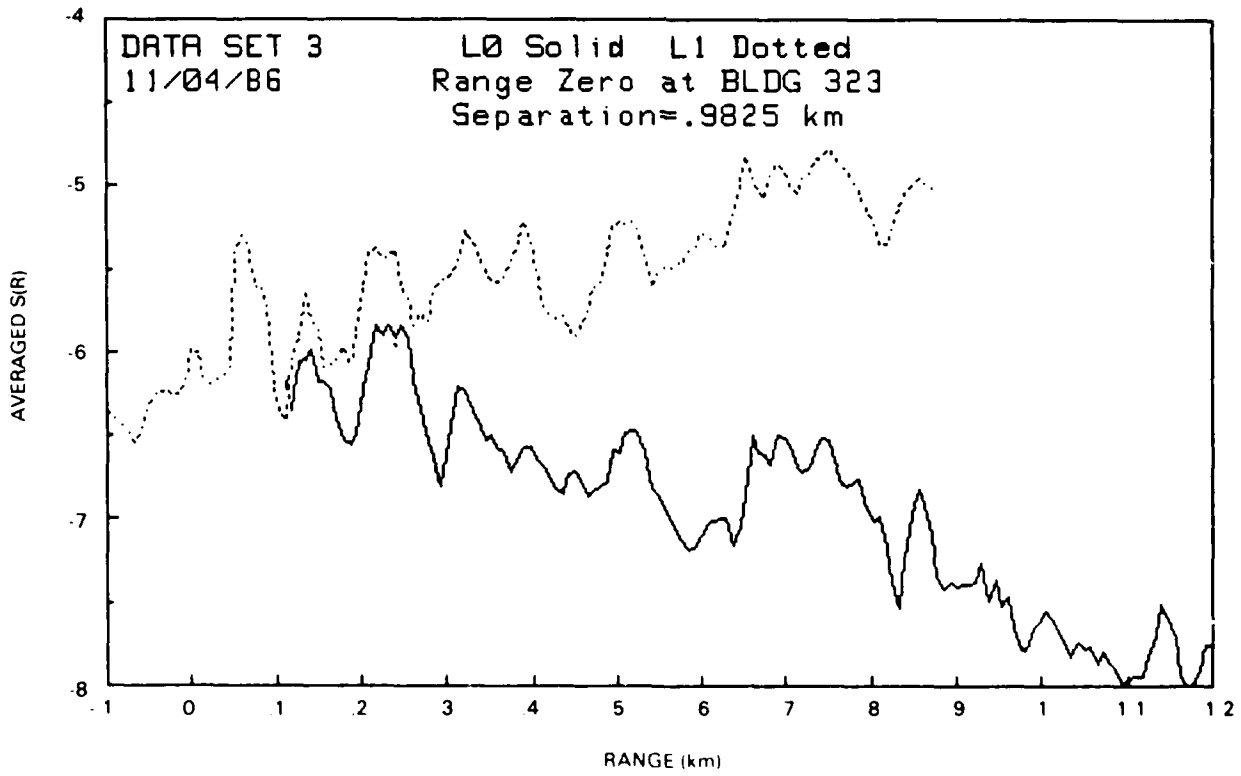
DATA SET 3
11/04/86
L0 Solid L1 Dotted
Range Zero at BLDG 323
Separation=.9825 km
AVERAGED S(R)
-4
-5
-6
-7
-8
.1
0
1
2
3
4
5
6
7
8
9
1
1 1
1 2
RANGE (km)

Figure A-13

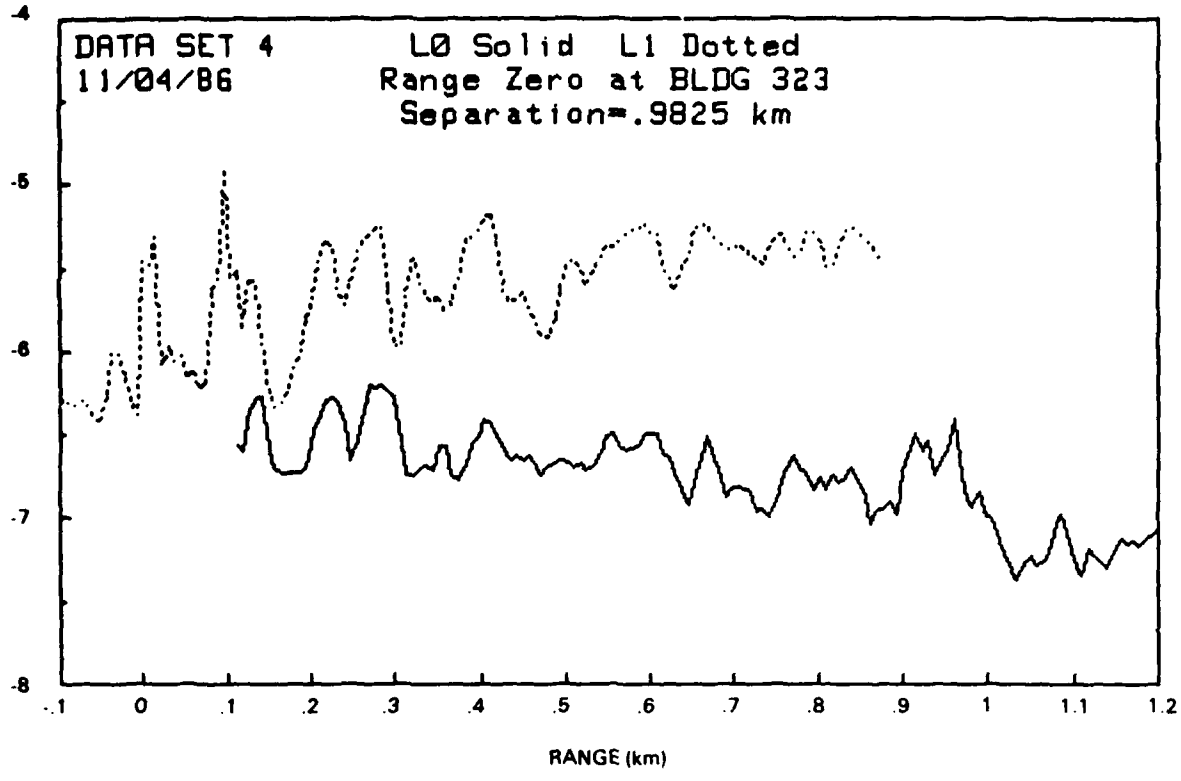
DATA SET 4
11/04/86
L0 Solid L1 Dotted
Range Zero at BLDG 323
Separation=.9825 km
-4
-5
-6
-7
-8
-.1
0
.1
.2
.3
.4
.5
.6
.7
.8
.9
1
1.1
1.2
RANGE (km)

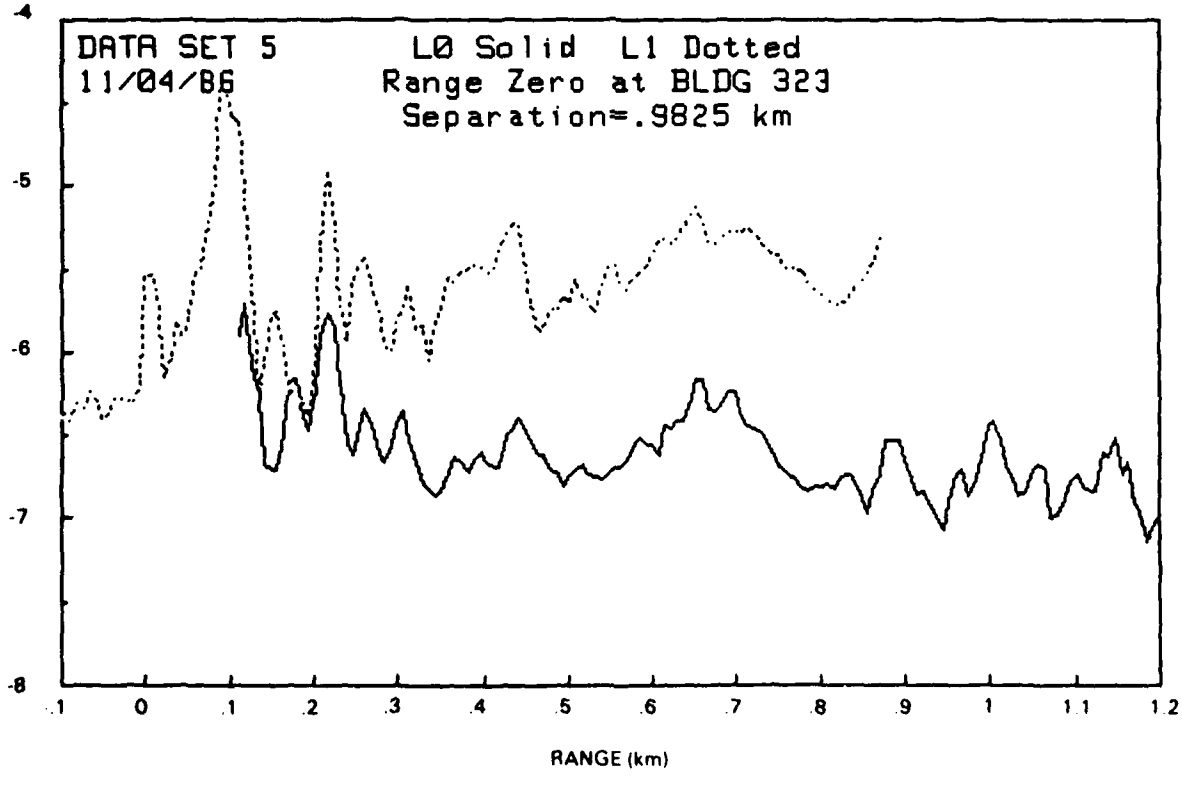
DATA SET 5
11/04/86
L0 Solid L1 Dotted
Range Zero at BLDG 323
Separation=.9825 km
-4
-5
-6
-7
-8
-.1
0
.1
.2
.3
.4
.5
.6
.7
.8
.9
1
1.1
1.2
RANGE (km)

Figure A-14.

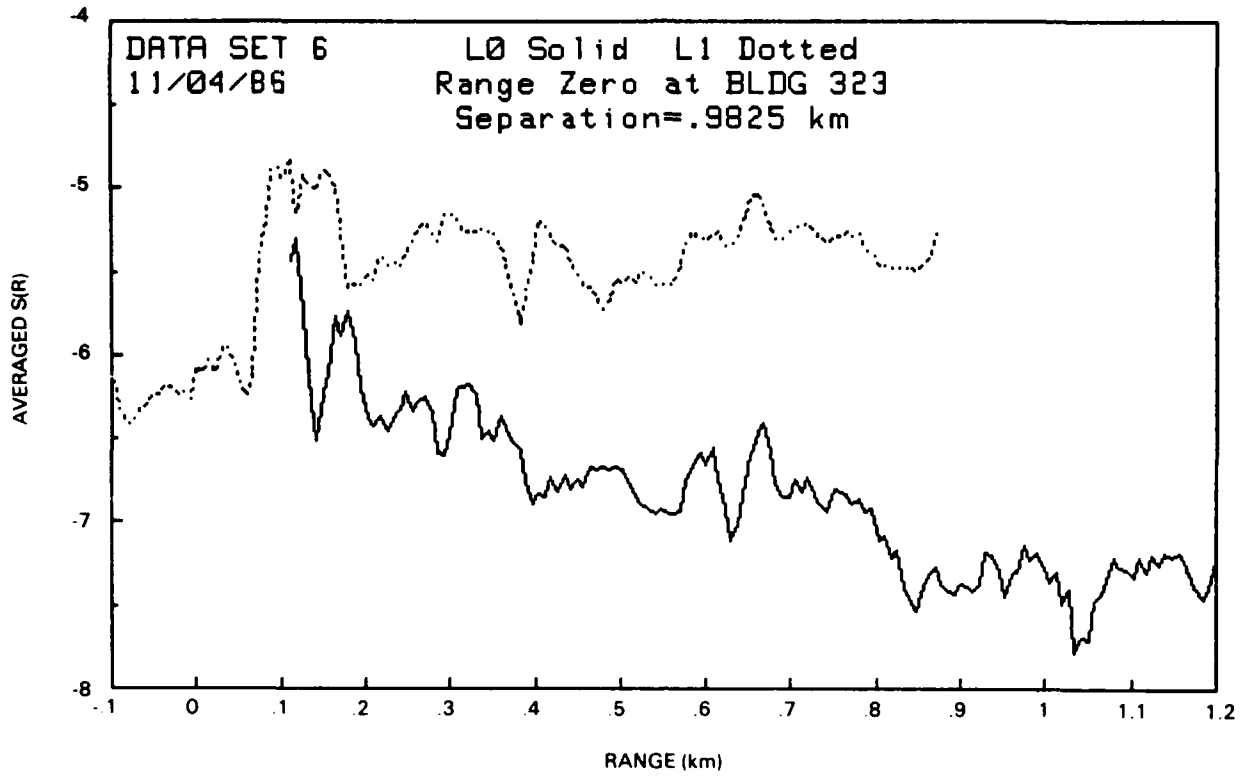
DATA SET 6
11/04/86
L0 Solid L1 Dotted
Range Zero at BLDG 323
Separation=.9825 km
AVERAGED S(R)
-4
-5
-6
-7
-8
.1
0
.1
.2
.3
.4
.5
.6
.7
.8
.9
1
1.1
1.2
RANGE (km)

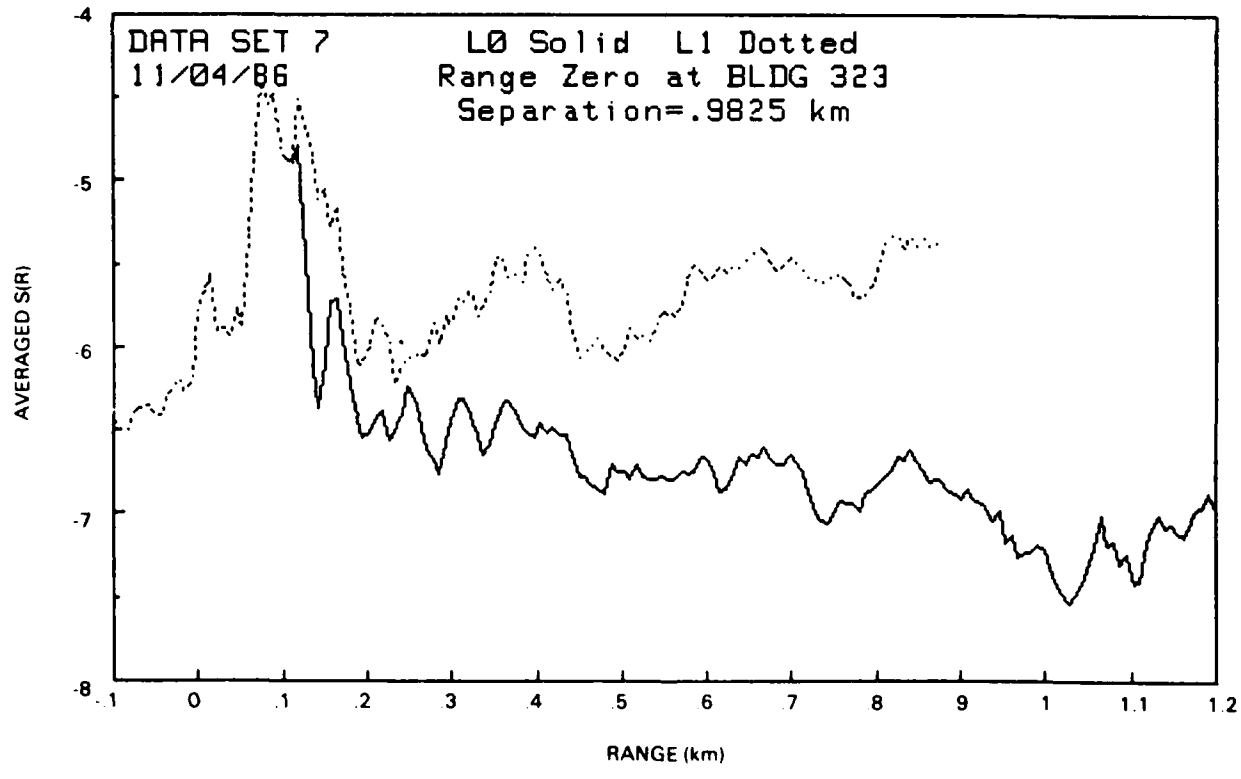
DATA SET 7
11/04/86
L0 Solid L1 Dotted
Range Zero at BLDG 323
Separation=.9825 km
AVERAGED S(R)
-4
-5
-6
-7
-8
.1
0
.1
.2
.3
.4
.5
6
7
8
9
1
1.1
1.2
RANGE (km)

Figure A-15.

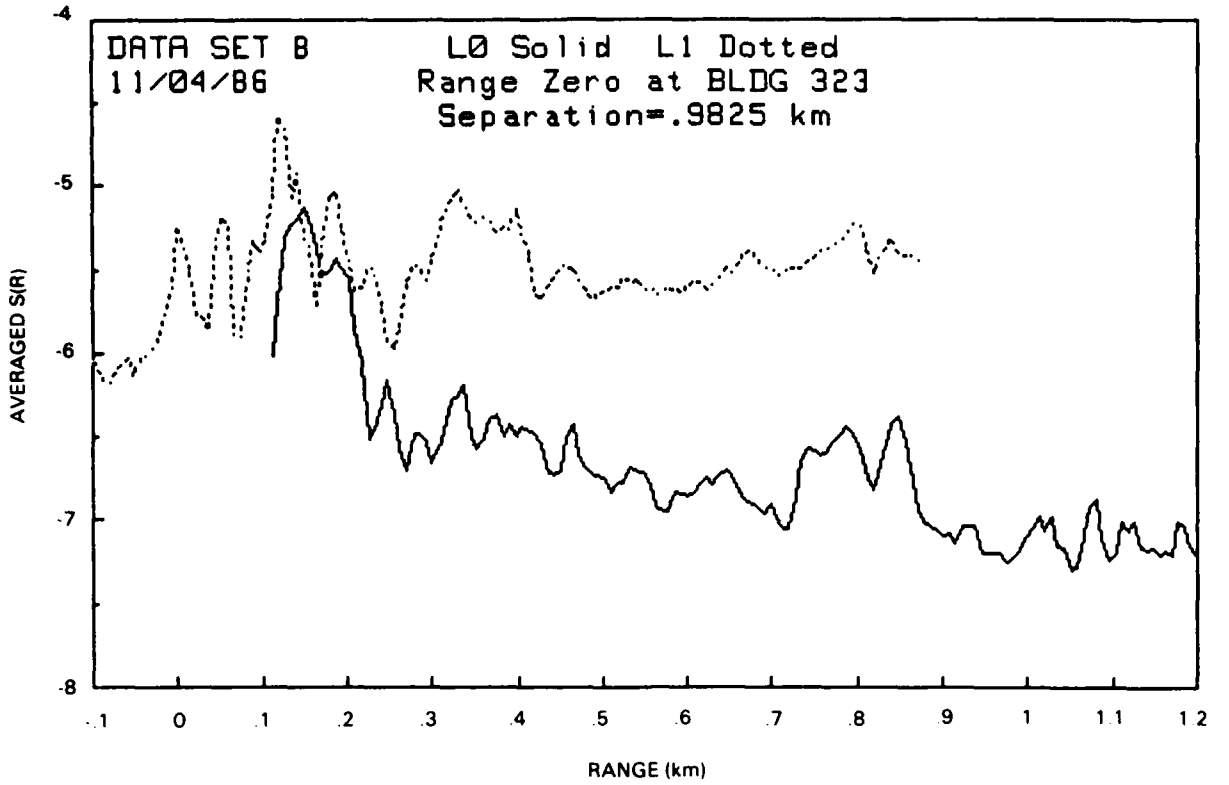
DATA SET 8
11/04/86
L0 Solid L1 Dotted
Range Zero at BLDG 323
Separation=.9825 km
AVERAGED S(R)
-4
-5
-6
-7
-8
.1
0
.1
.2
.3
.4
.5
.6
.7
.8
.9
1
1.1
1.2
RANGE (km)

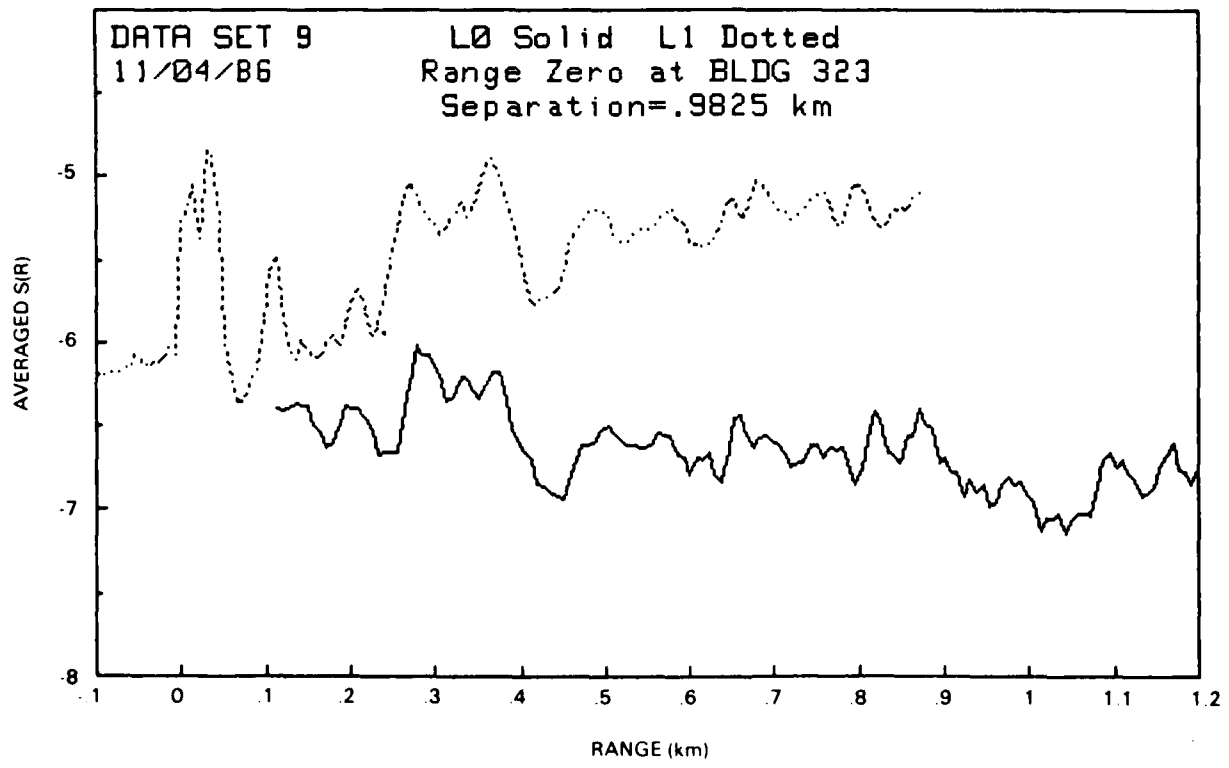
DATA SET 9
11/04/86
L0 Solid L1 Dotted
Range Zero at BLDG 323
Separation=.9825 km
AVERAGED S(R)
-5
-6
-7
-8
.1
0
.1
.2
.3
.4
.5
.6
.7
.8
.9
1
1.1
1.2
RANGE (km)

Figure A-16.

APPENDIX B

EXAMPLES OF S(R) DIFFERENCE CURVES AND EXTINCTION PROFILES

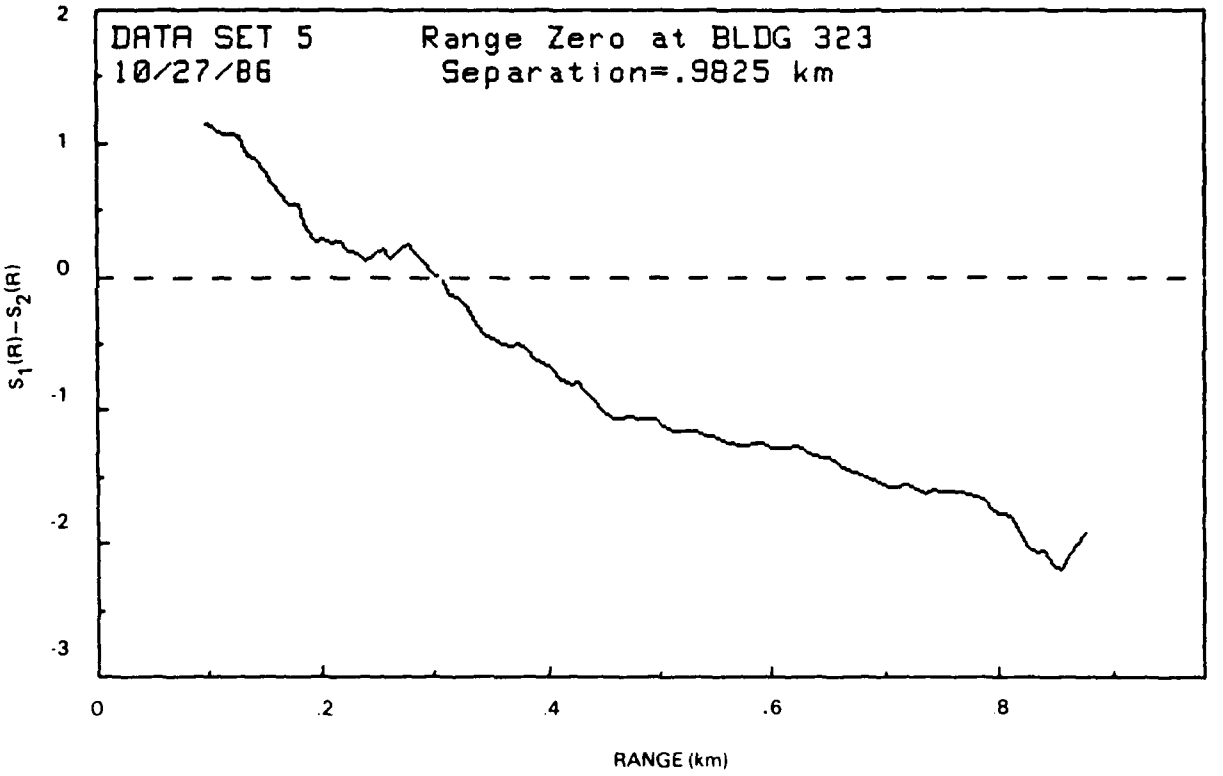
DATA SET 5
10/27/86
Range Zero at BLDG 323
Separation=.9825 km
$S_1(R)-S_2(R)$
2
1
0
-1
-2
-3
0
.2
.4
.6
.8
RANGE (km)

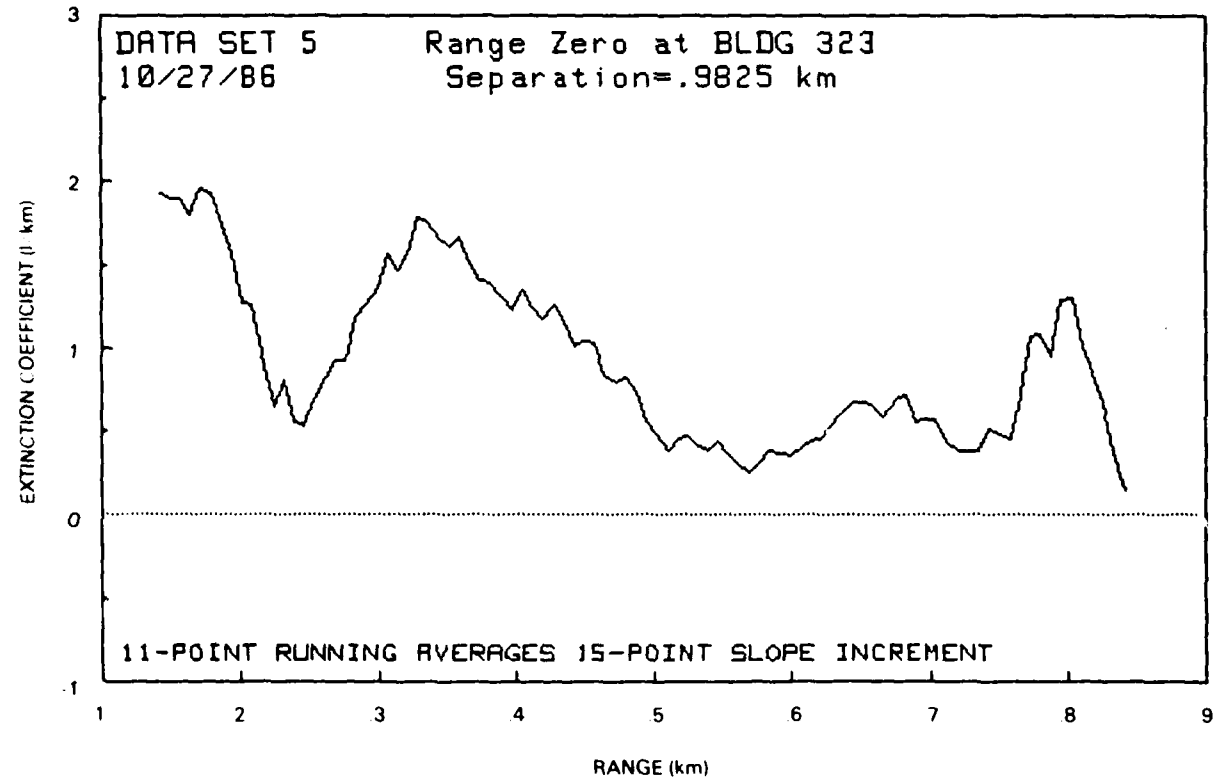
DATA SET 5
10/27/86
Range Zero at BLDG 323
Separation=.9825 km
EXTINCTION COEFFICIENT (1 km)
3
2
1
0
-1
11-POINT RUNNING AVERAGES 15-POINT SLOPE INCREMENT
1
2
3
4
5
6
7
8
9
RANGE (km)

Figure B-1.

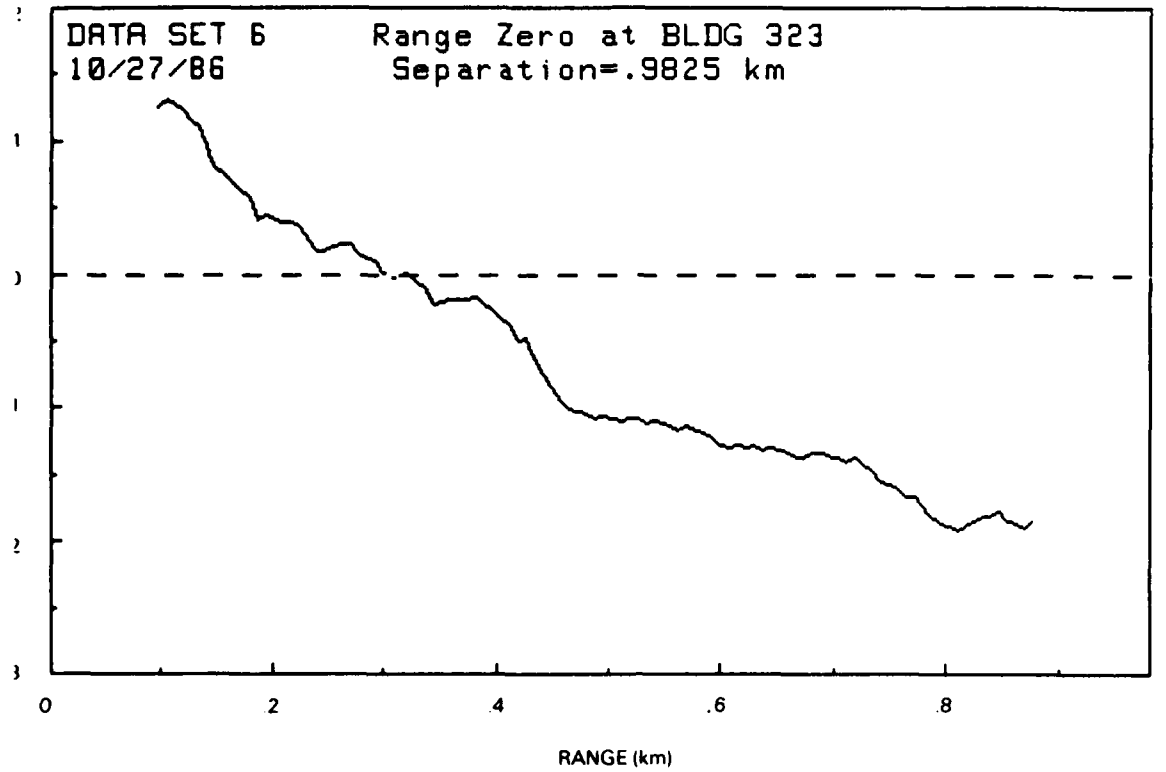
DATA SET 6
10/27/86
Range Zero at BLDG 323
Separation=.9825 km
0
2
.4
.6
.8
RANGE (km)

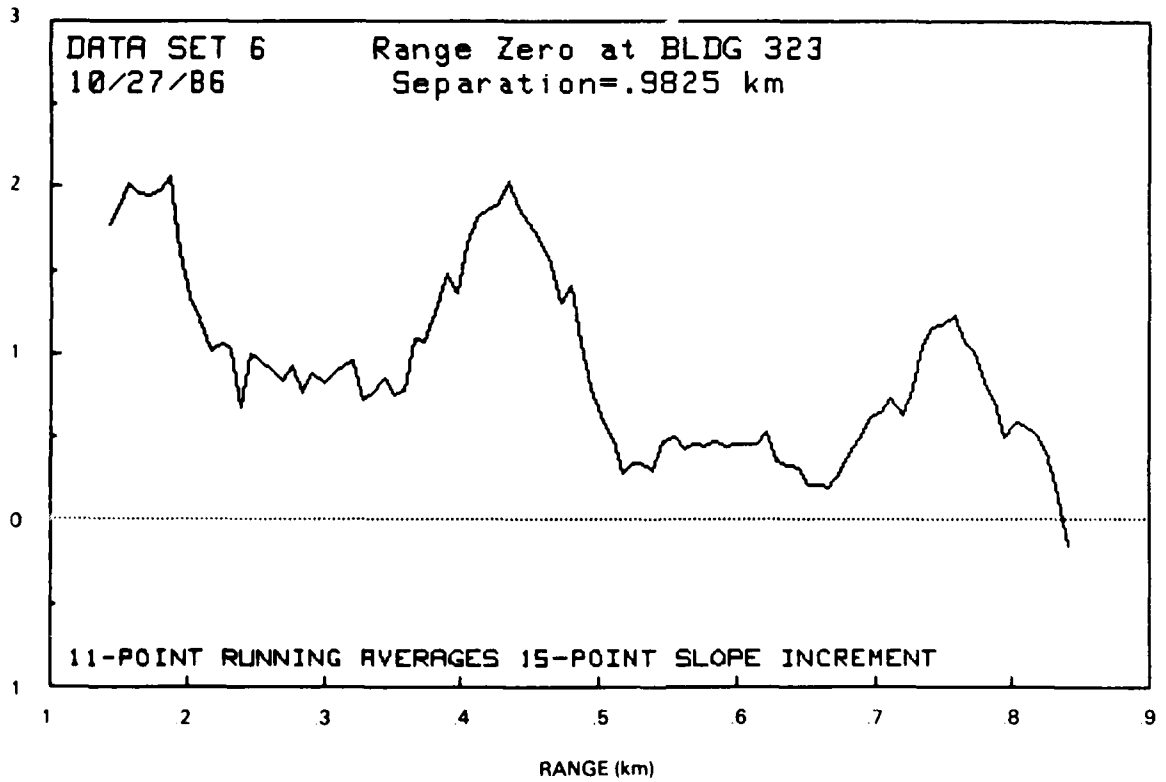
DATA SET 6
10/27/86
Range Zero at BLDG 323
Separation=.9825 km
11-POINT RUNNING AVERAGES 15-POINT SLOPE INCREMENT
1
2
3
4
5
6
7
8
9
RANGE (km)

Figure B-2.

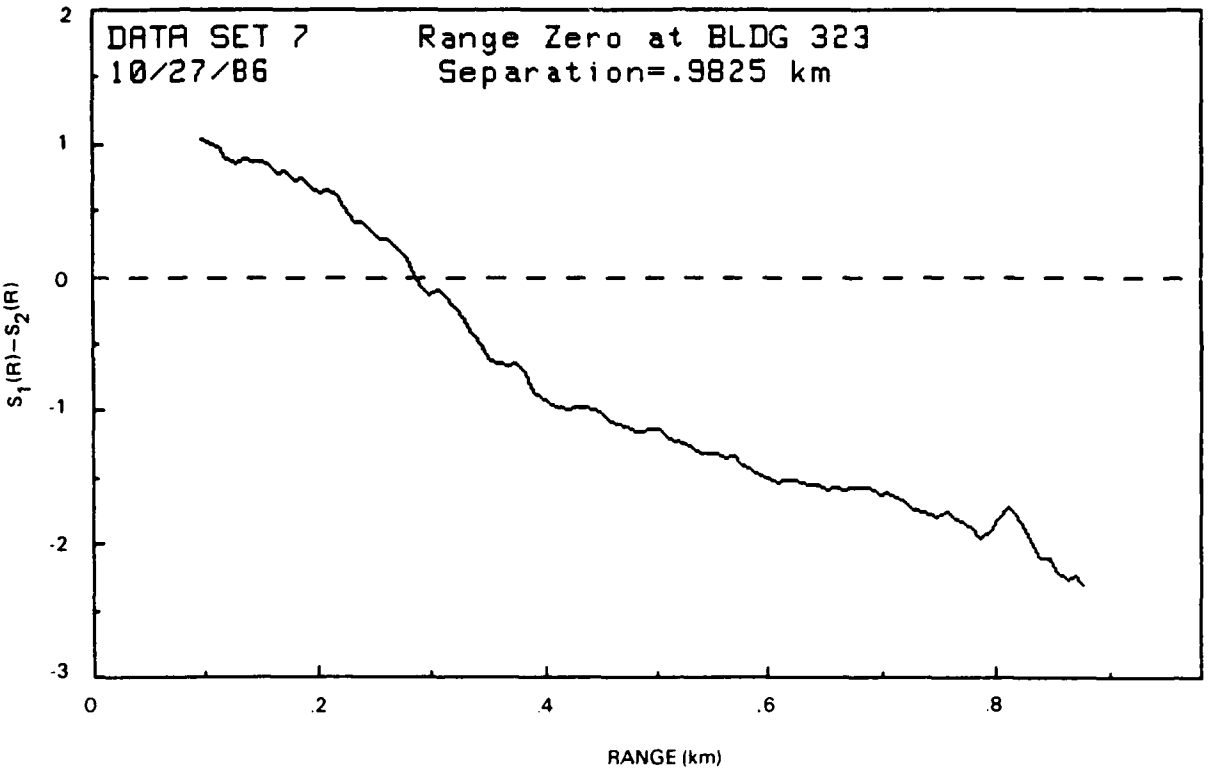
DATA SET 7
10/27/86
Range Zero at BLDG 323
Separation=.9825 km
$S_1(R)-S_2(R)$
RANGE (km)

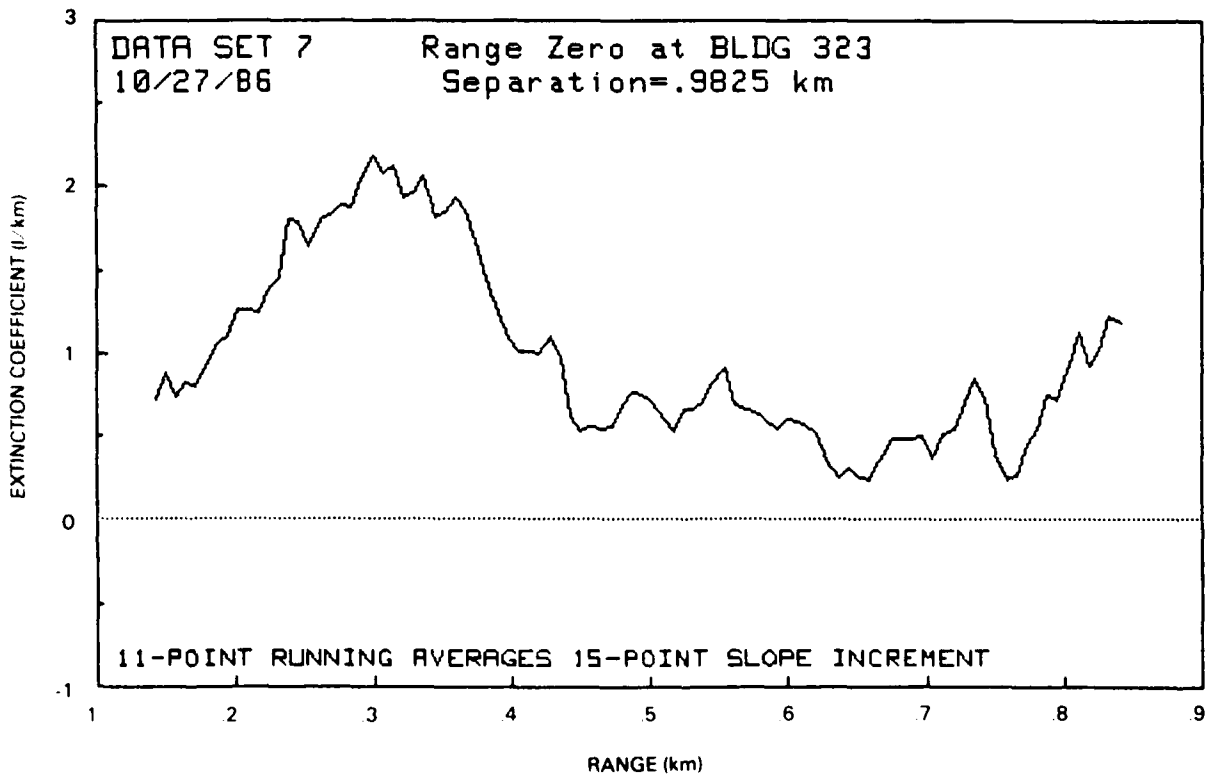
DATA SET 7
10/27/86
Range Zero at BLDG 323
Separation=.9825 km
EXTINCTION COEFFICIENT (1/km)
11-POINT RUNNING AVERAGES 15-POINT SLOPE INCREMENT
RANGE (km)

Figure B-3.

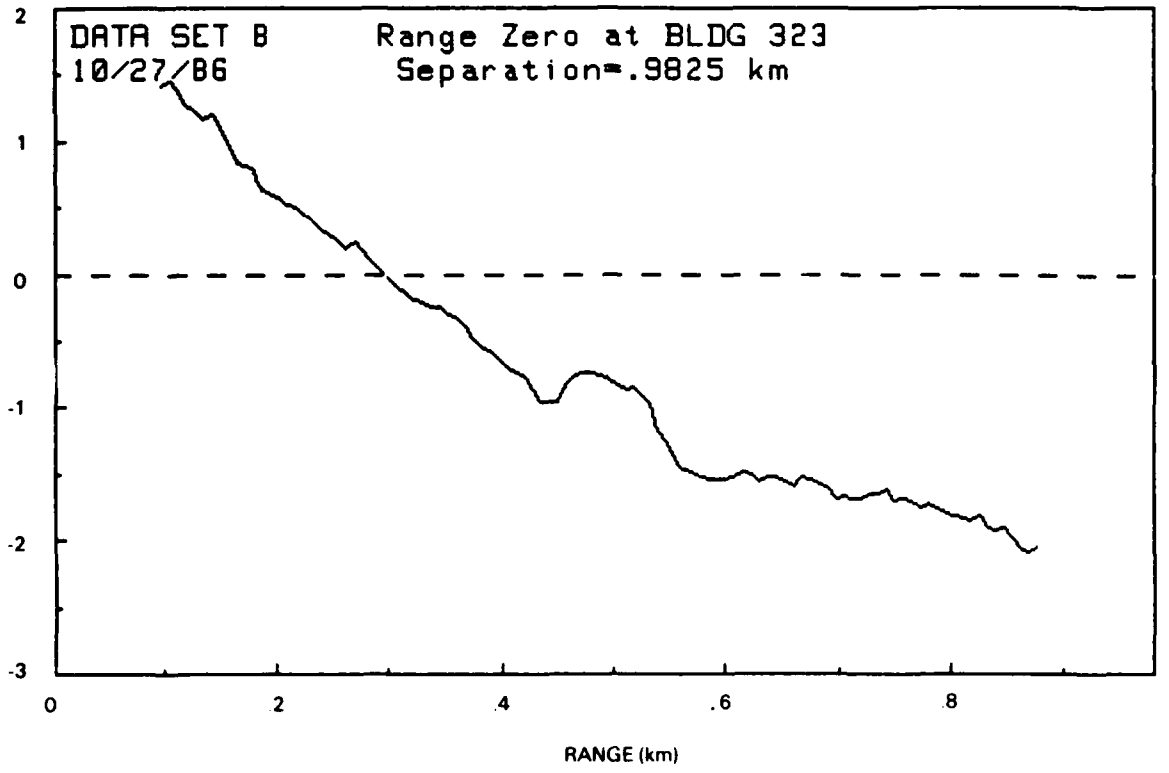
DATA SET B
10/27/86
Range Zero at BLDG 323
Separation=.9825 km
2
1
0
-1
-2
-3
0
.2
.4
.6
.8
RANGE (km)

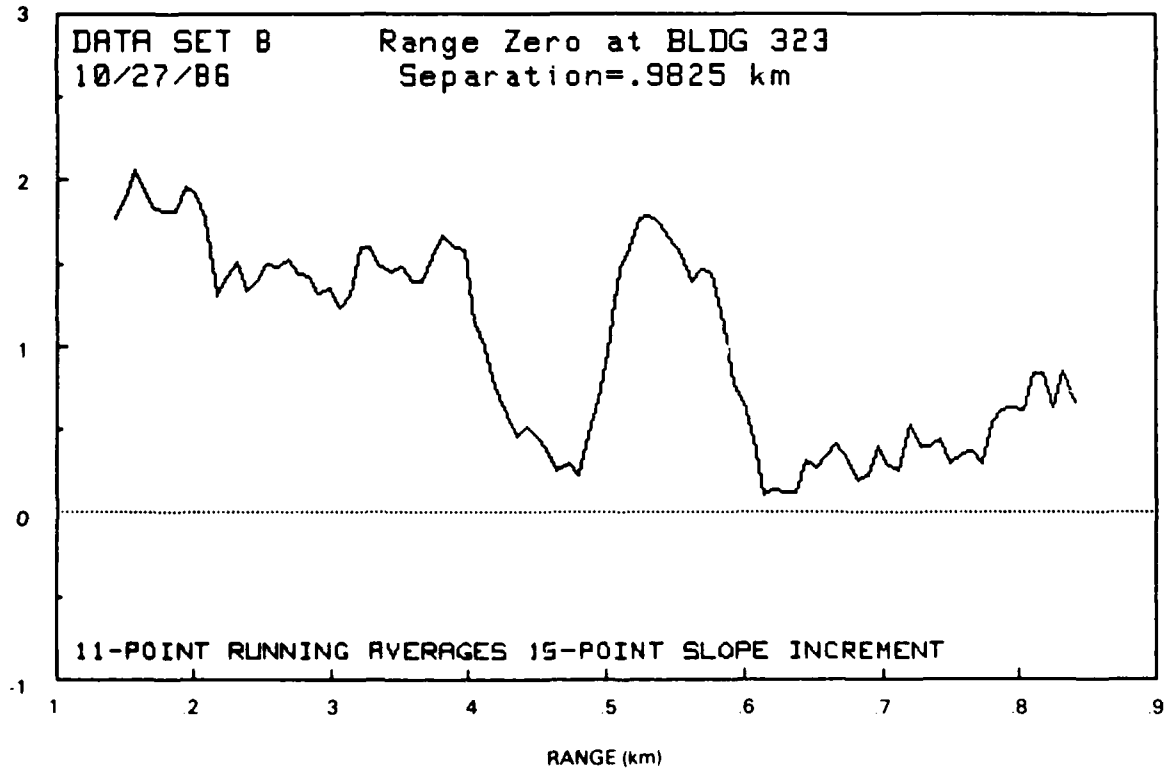
DATA SET B
10/27/86
Range Zero at BLDG 323
Separation=.9825 km
3
2
1
0
-1
11-POINT RUNNING AVERAGES 15-POINT SLOPE INCREMENT
1
.2
3
4
.5
.6
.7
.8
.9
RANGE (km)

Figure B-4.

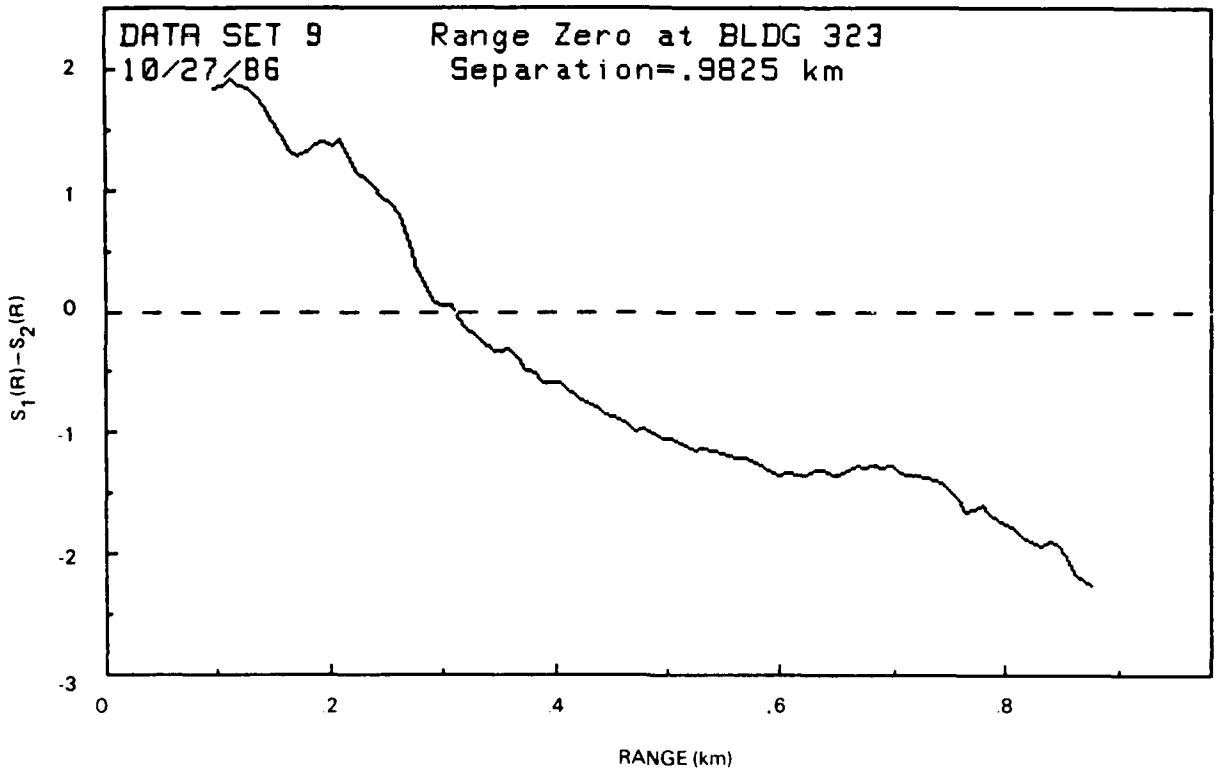
DATA SET 9
10/27/86
Range Zero at BLDG 323
Separation=.9825 km
$S_1(R)-S_2(R)$
RANGE (km)

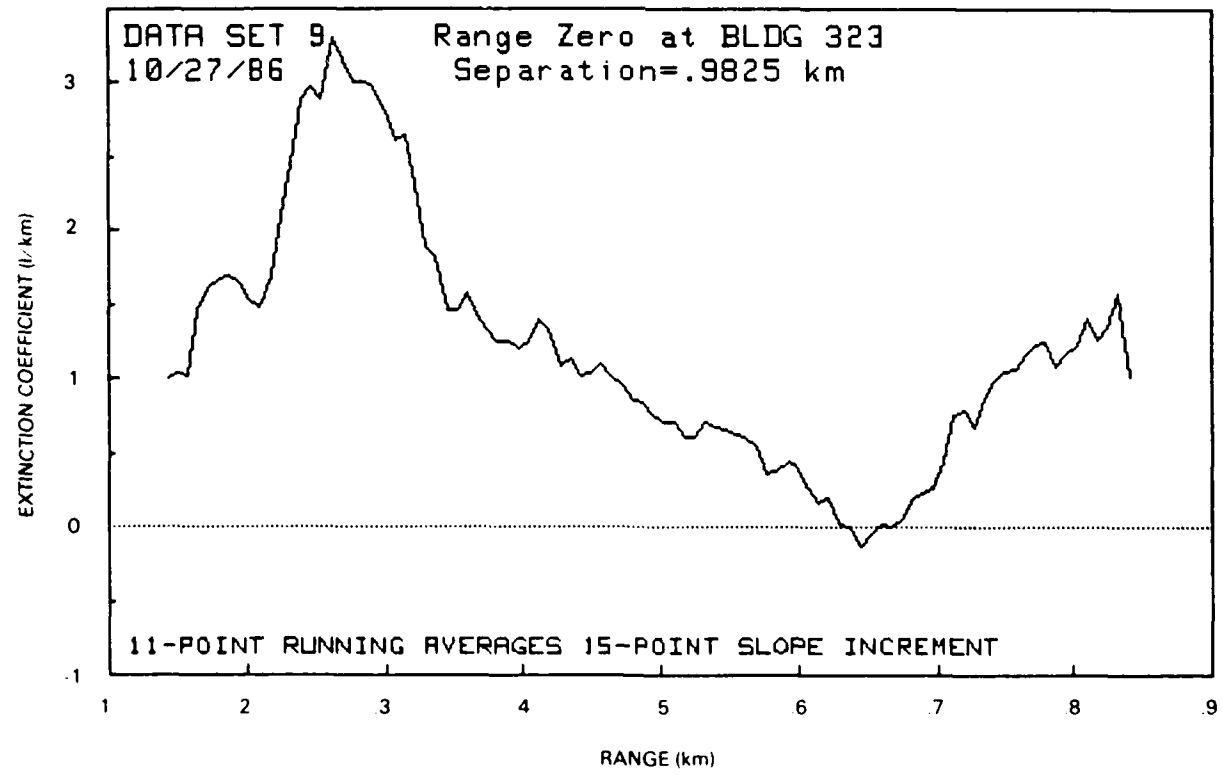
DATA SET 9
10/27/86
Range Zero at BLDG 323
Separation=.9825 km
EXTINCTION COEFFICIENT (l/ km)
11-POINT RUNNING AVERAGES 15-POINT SLOPE INCREMENT
RANGE (km)

Figure B-5.

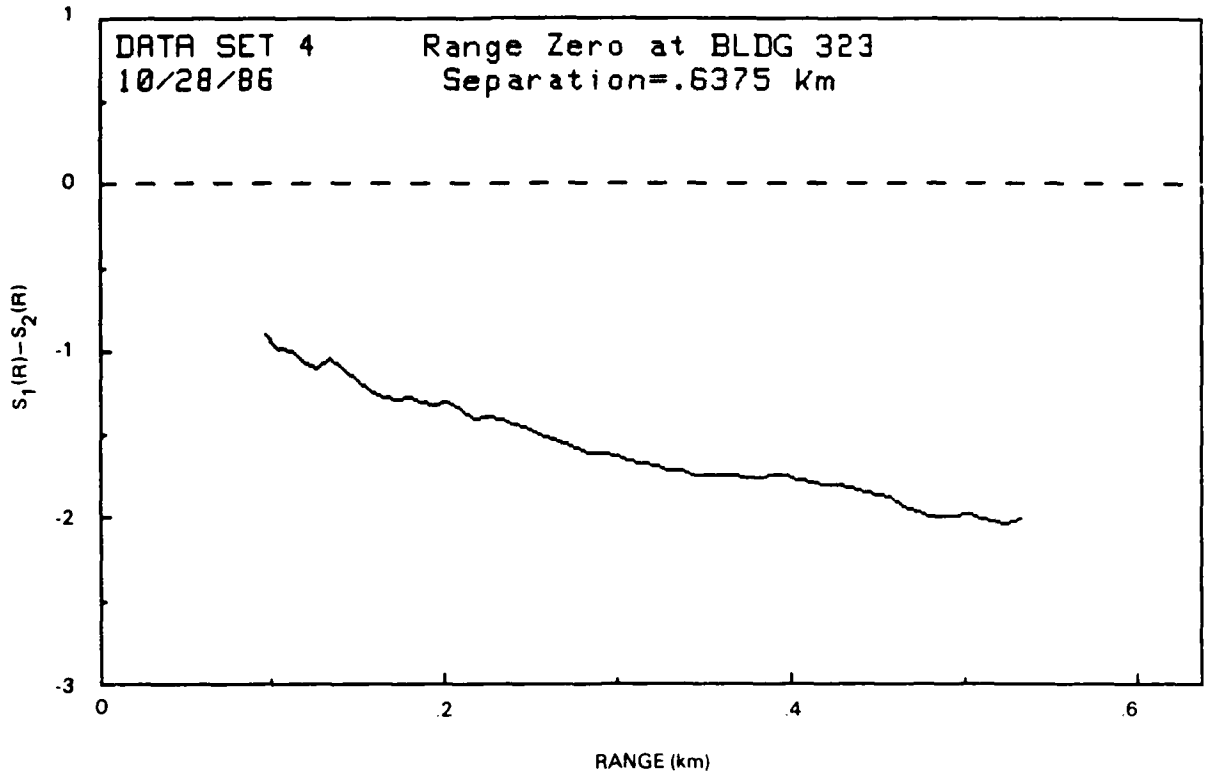
DATA SET 4
10/28/86
Range Zero at BLDG 323
Separation=.6375 km
1
0
-1
-2
-3
$S_1(R)-S_2(R)$
0
.2
.4
.6
RANGE (km)

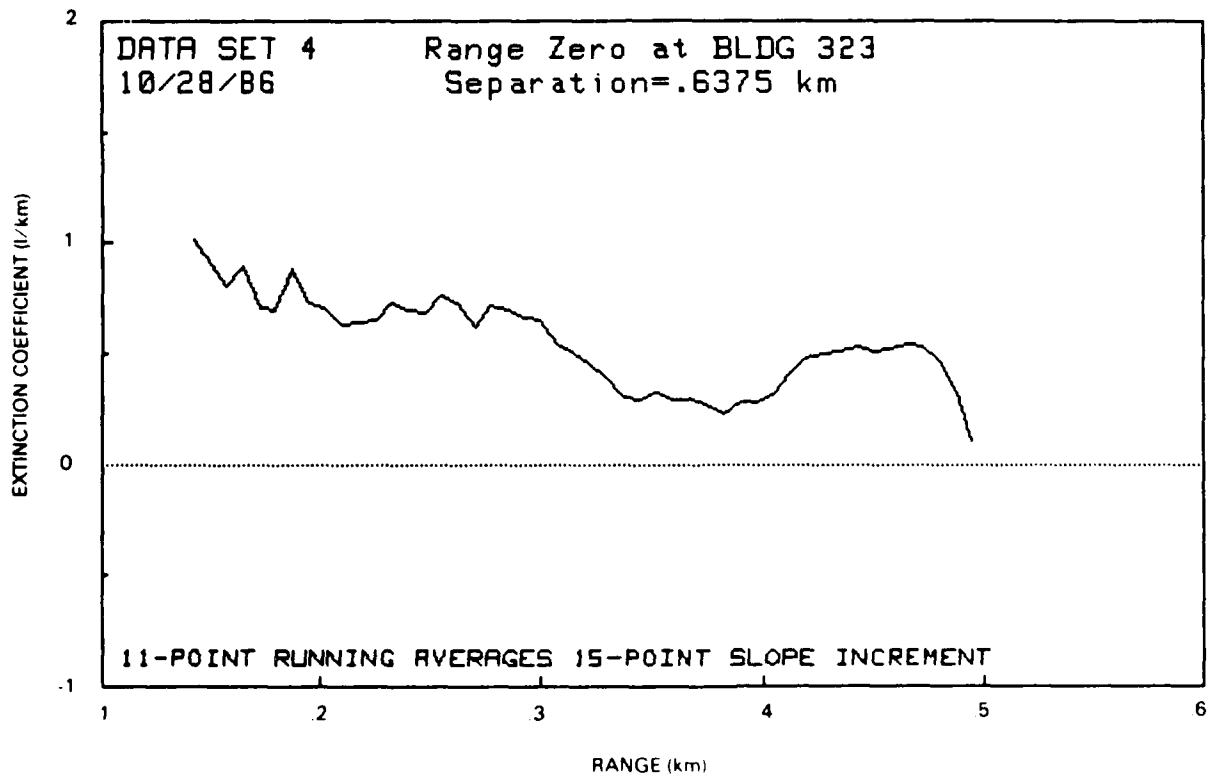
DATA SET 4
10/28/86
Range Zero at BLDG 323
Separation=.6375 km
2
1
0
-1
EXTINCTION COEFFICIENT (1/km)
11-POINT RUNNING AVERAGES 15-POINT SLOPE INCREMENT
1
.2
3
4
5
6
RANGE (km)

Figure B-6.

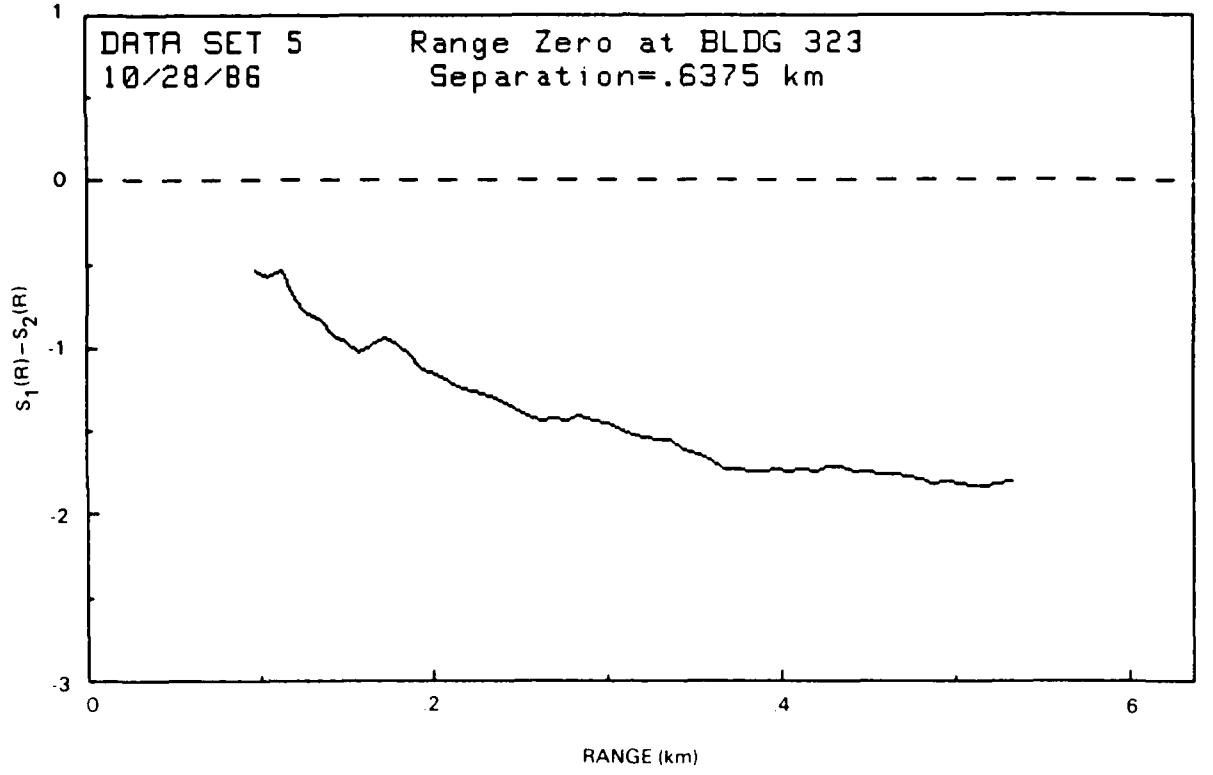
DATA SET 5
10/28/86
Range Zero at BLDG 323
Separation=.6375 km
1
0
-1
-2
-3
0
2
4
6
$S_1(R)-S_2(R)$
RANGE (km)

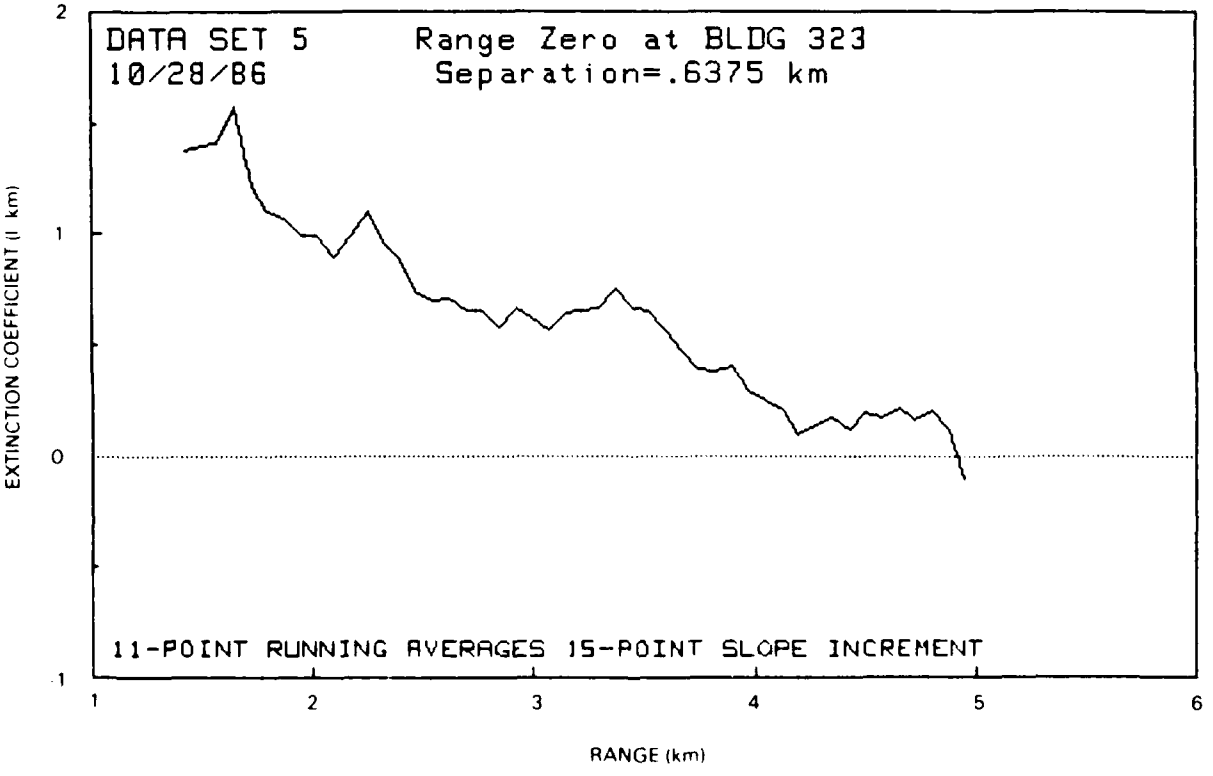
DATA SET 5
10/28/86
Range Zero at BLDG 323
Separation=.6375 km
11-POINT RUNNING AVERAGES 15-POINT SLOPE INCREMENT
2
1
0
-1
1
2
3
4
5
6
EXTINCTION COEFFICIENT (1 km)
RANGE (km)

Figure B-7

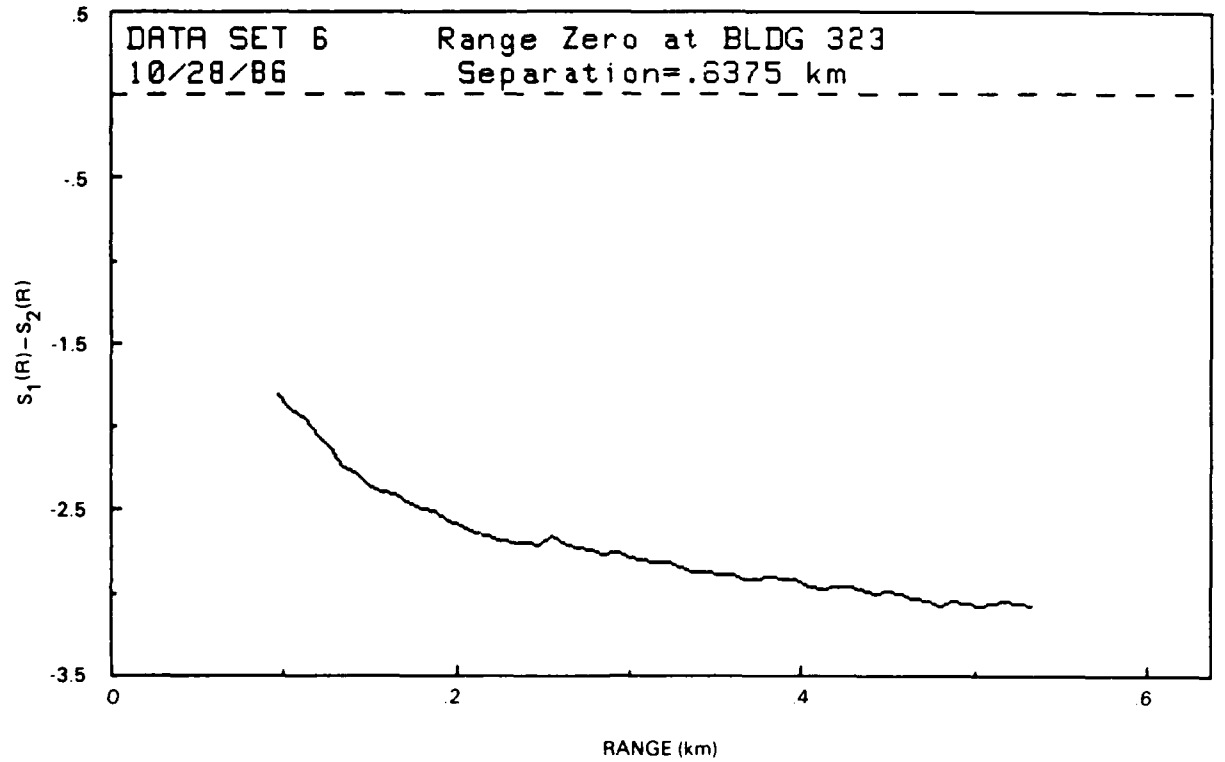
DATA SET 6
10/28/86
Range Zero at BLDG 323
Separation=.6375 km
.5
-.5
-1.5
-2.5
-3.5
$S_1(R)-S_2(R)$
0
.2
.4
.6
RANGE (km)

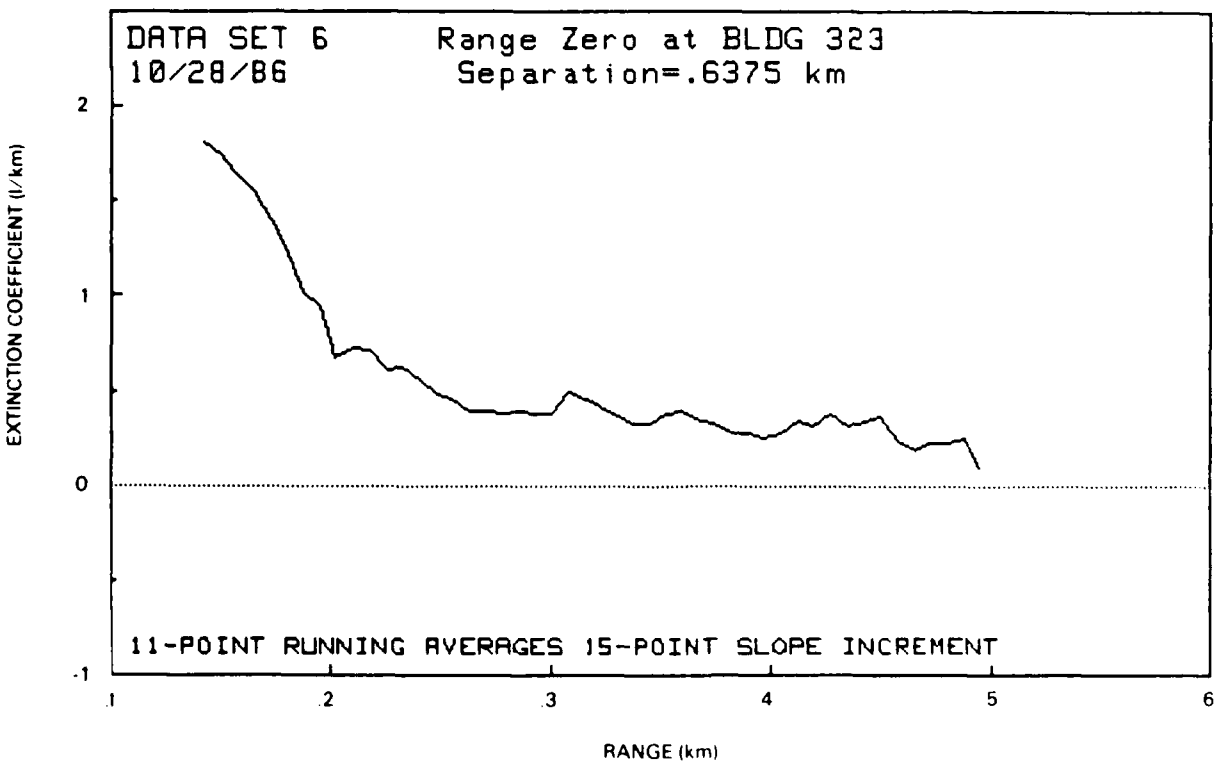
DATA SET 6
10/28/86
Range Zero at BLDG 323
Separation=.6375 km
2
1
0
-1
EXTINCTION COEFFICIENT (1/km)
11-POINT RUNNING AVERAGES 15-POINT SLOPE INCREMENT
.1
.2
.3
4
5
6
RANGE (km)

Figure B-8.

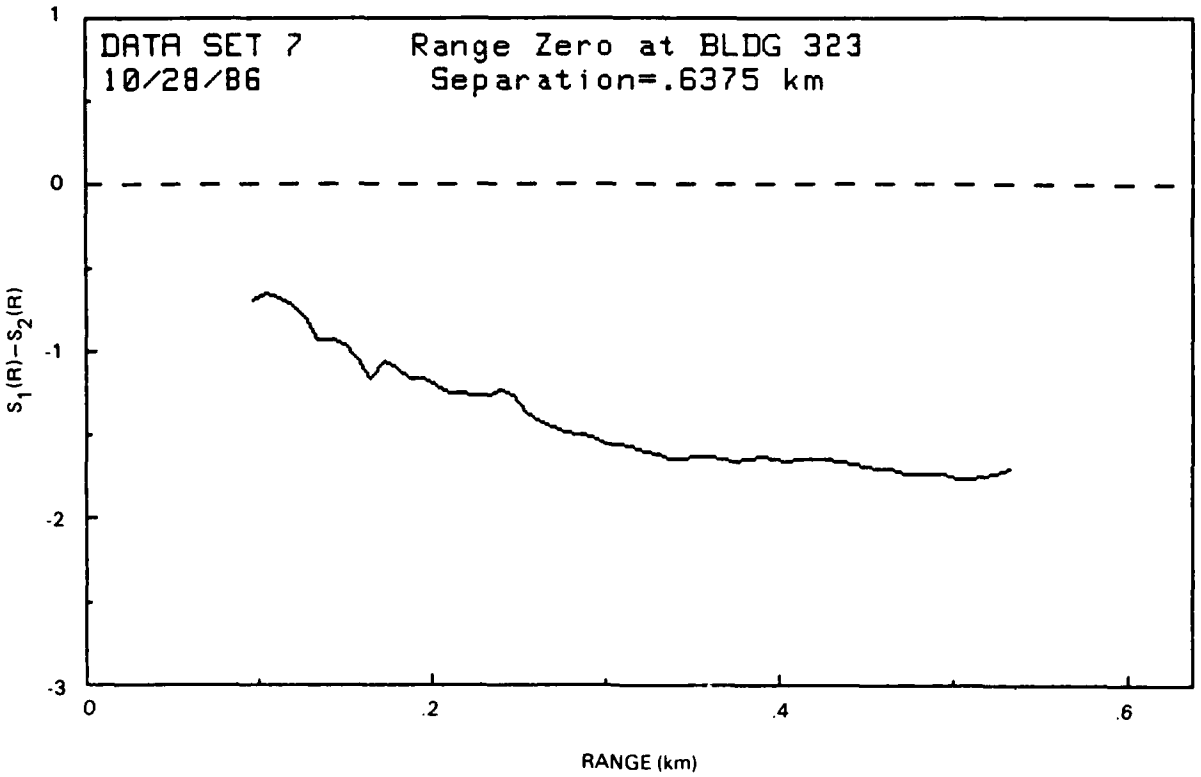
DATA SET 7
10/28/86
Range Zero at BLDG 323
Separation=.6375 km
1
0
-1
-2
-3
$S_1(R)-S_2(R)$
0
.2
.4
.6
RANGE (km)

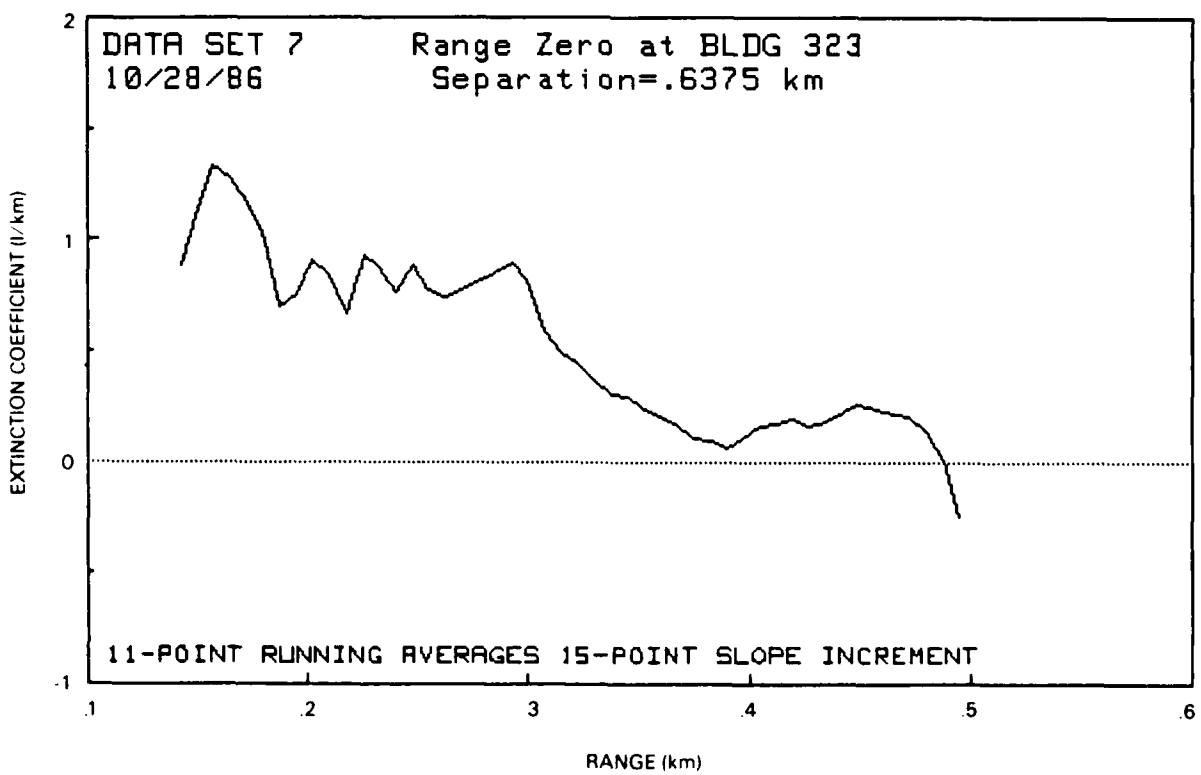
DATA SET 7
10/28/86
Range Zero at BLDG 323
Separation=.6375 km
2
1
0
-1
EXTINCTION COEFFICIENT (1/km)
11-POINT RUNNING AVERAGES 15-POINT SLOPE INCREMENT
.1
.2
3
.4
.5
.6
RANGE (km)

Figure B-9.

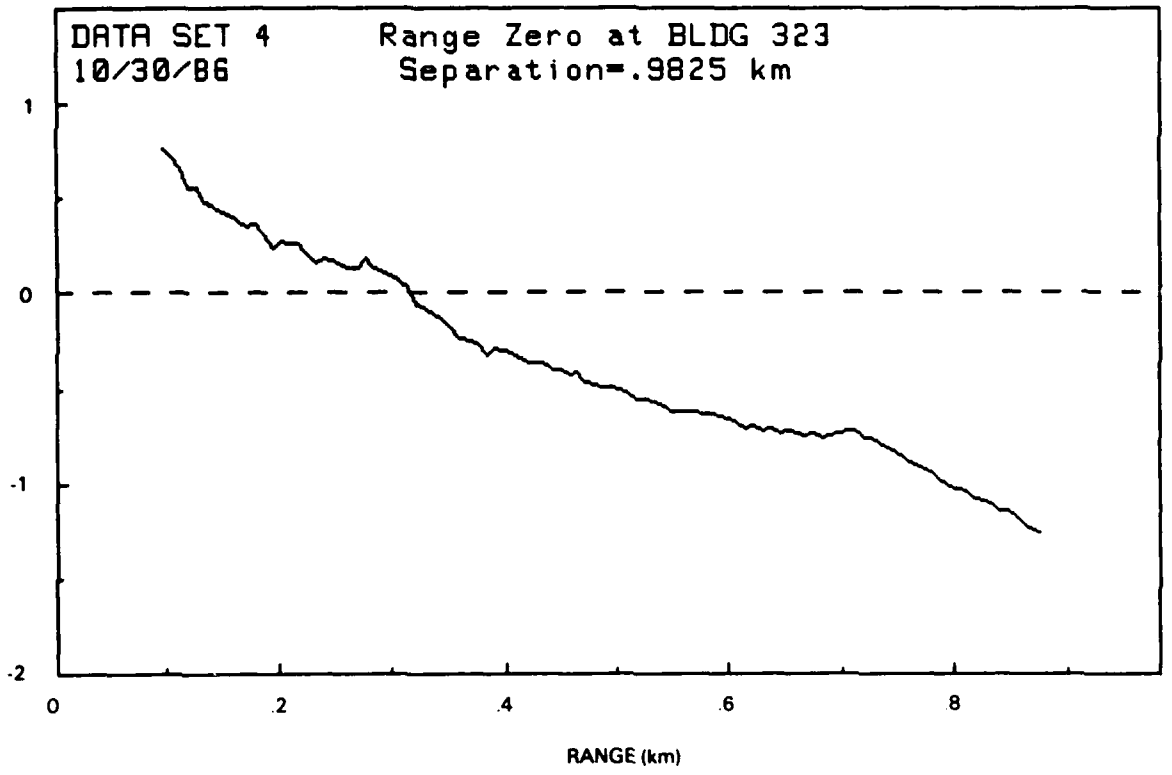
DATA SET 4
10/30/86
Range Zero at BLDG 323
Separation=.9825 km
1
0
-1
-2
0
.2
.4
.6
.8
RANGE (km)

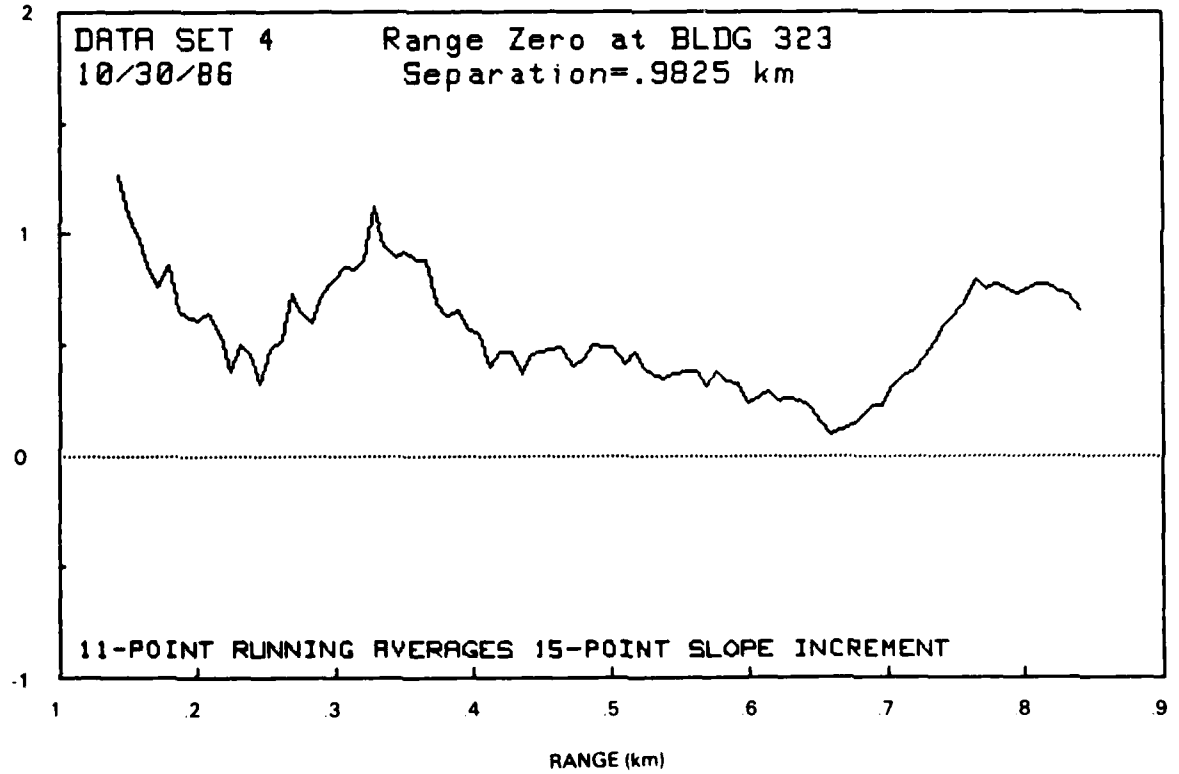
DATA SET 4
10/30/86
Range Zero at BLDG 323
Separation=.9825 km
2
1
0
-1
11-POINT RUNNING AVERAGES 15-POINT SLOPE INCREMENT
1
.2
.3
.4
.5
.6
.7
.8
.9
RANGE (km)

Figure B-10.

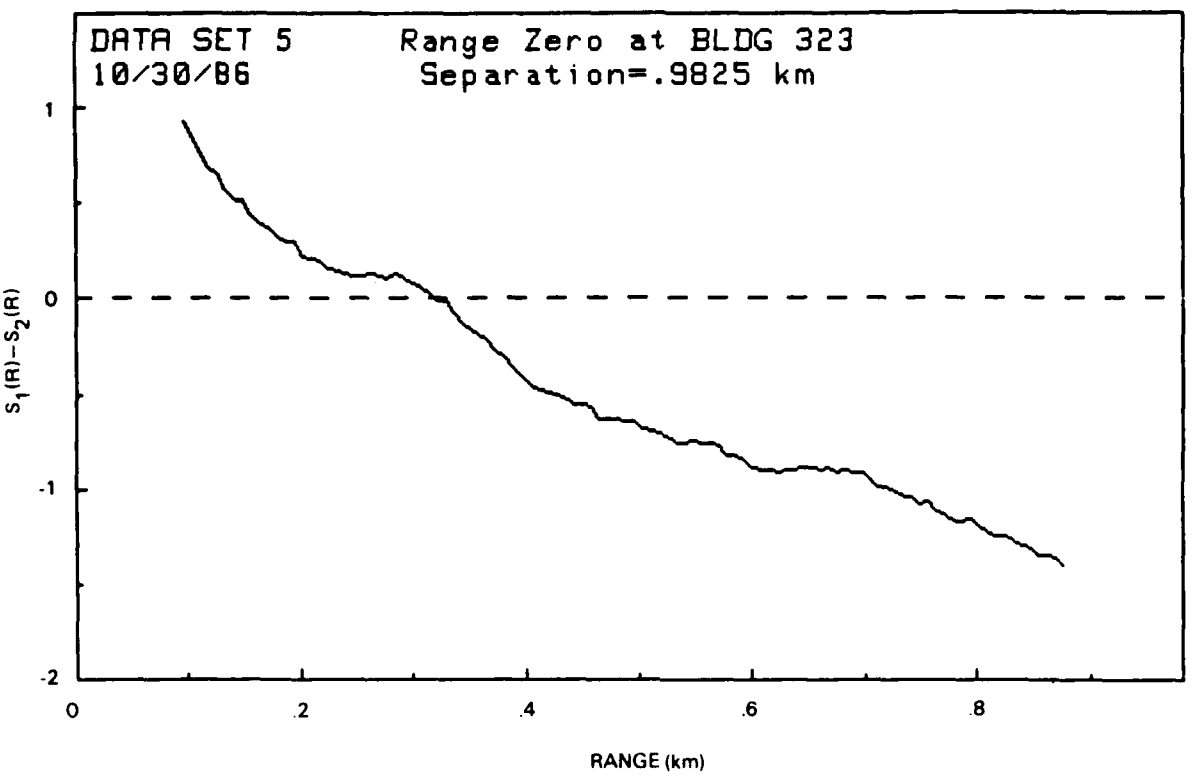
DATA SET 5
10/30/86
Range Zero at BLDG 323
Separation=.9825 km
1
0
-1
-2
$S_1(R)-S_2(R)$
0
.2
.4
.6
.8
RANGE (km)

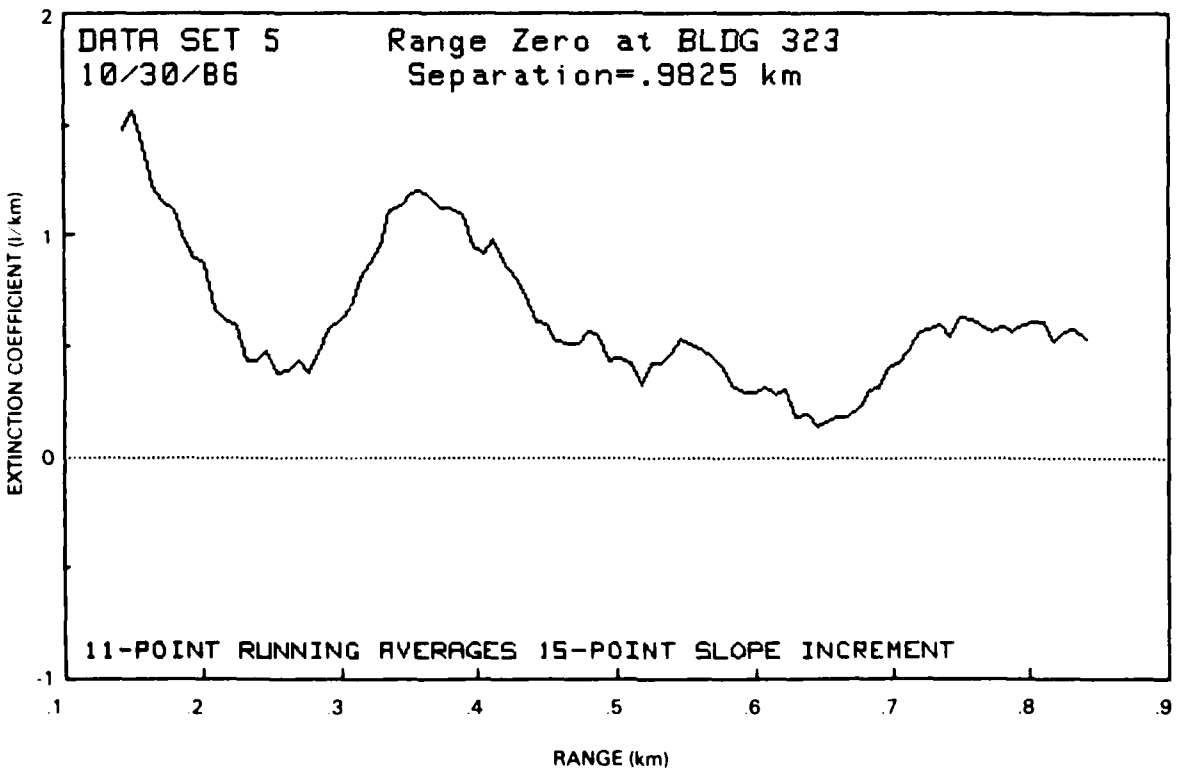
DATA SET 5
10/30/86
Range Zero at BLDG 323
Separation=.9825 km
2
1
0
-1
EXTINCTION COEFFICIENT (l/km)
11-POINT RUNNING AVERAGES 15-POINT SLOPE INCREMENT
.1
.2
.3
.4
.5
.6
.7
.8
.9
RANGE (km)

Figure B-11.

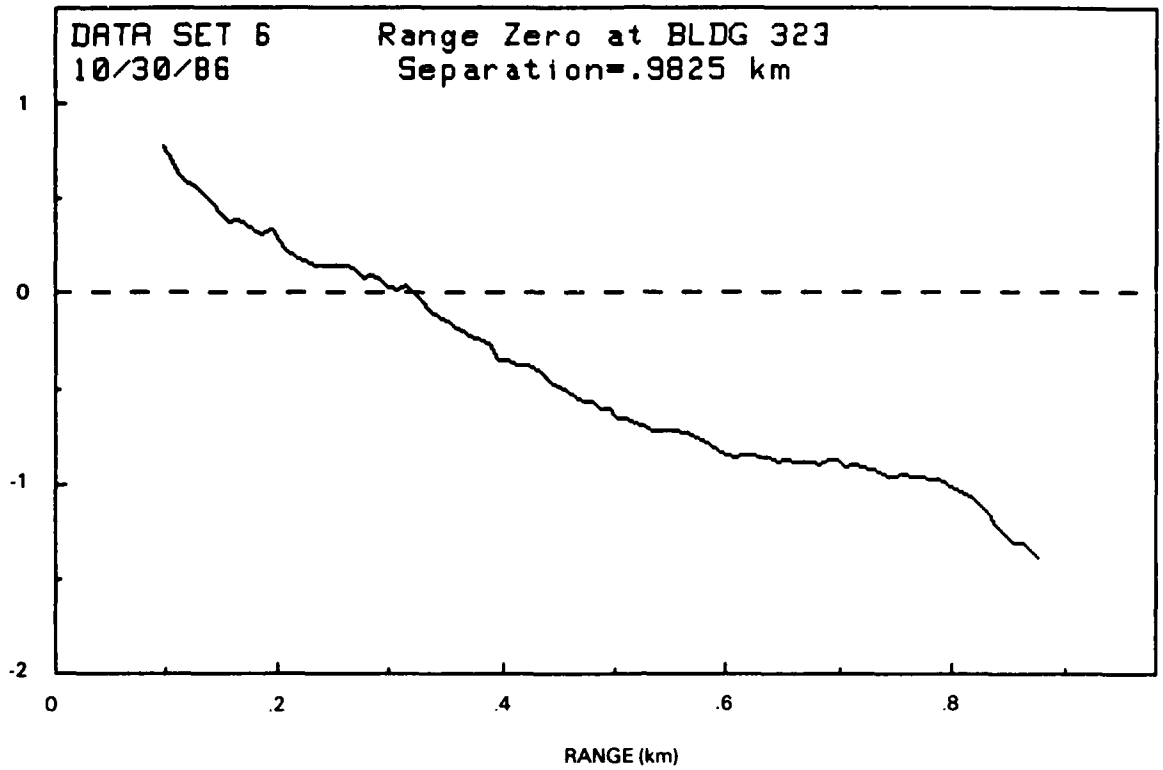
DATA SET 6
10/30/86
Range Zero at BLDG 323
Separation=.9825 km
1
0
-1
-2
0
.2
.4
.6
.8
RANGE (km)

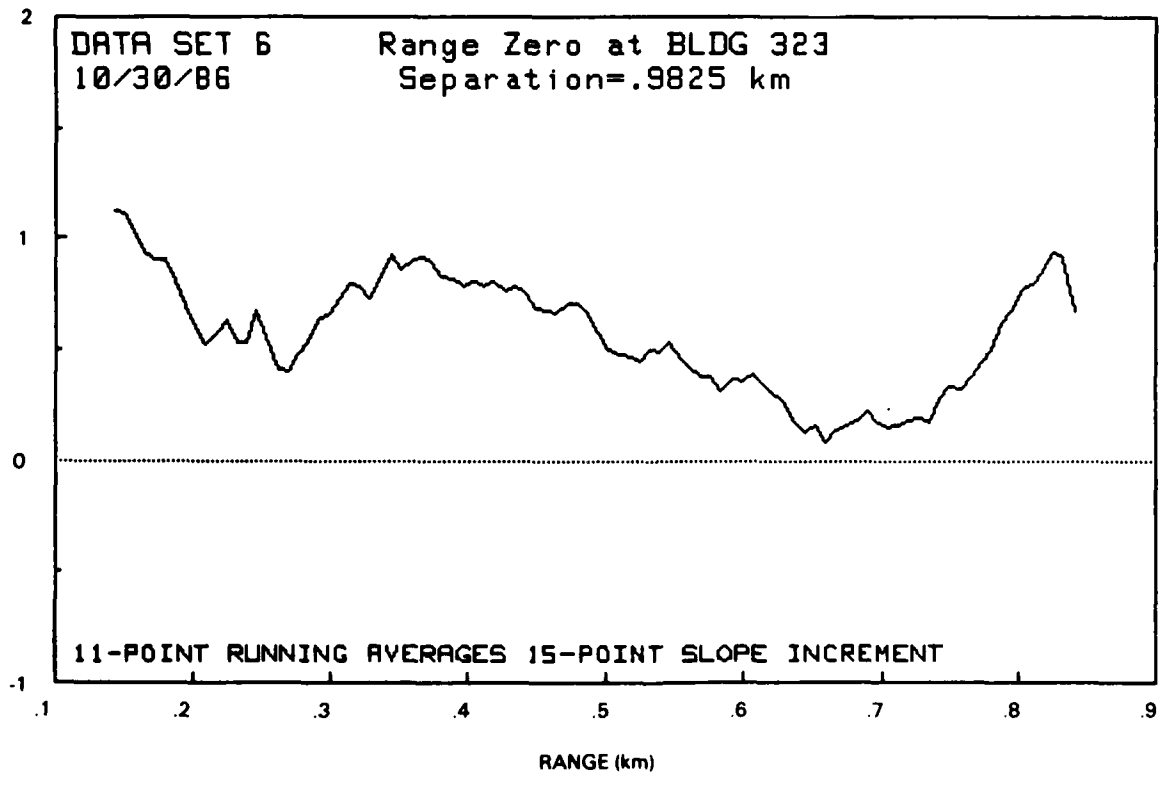
DATA SET 6
10/30/86
Range Zero at BLDG 323
Separation=.9825 km
2
1
0
-1
11-POINT RUNNING AVERAGES 15-POINT SLOPE INCREMENT
.1
.2
.3
.4
.5
.6
.7
.8
.9
RANGE (km)

Figure B-12.

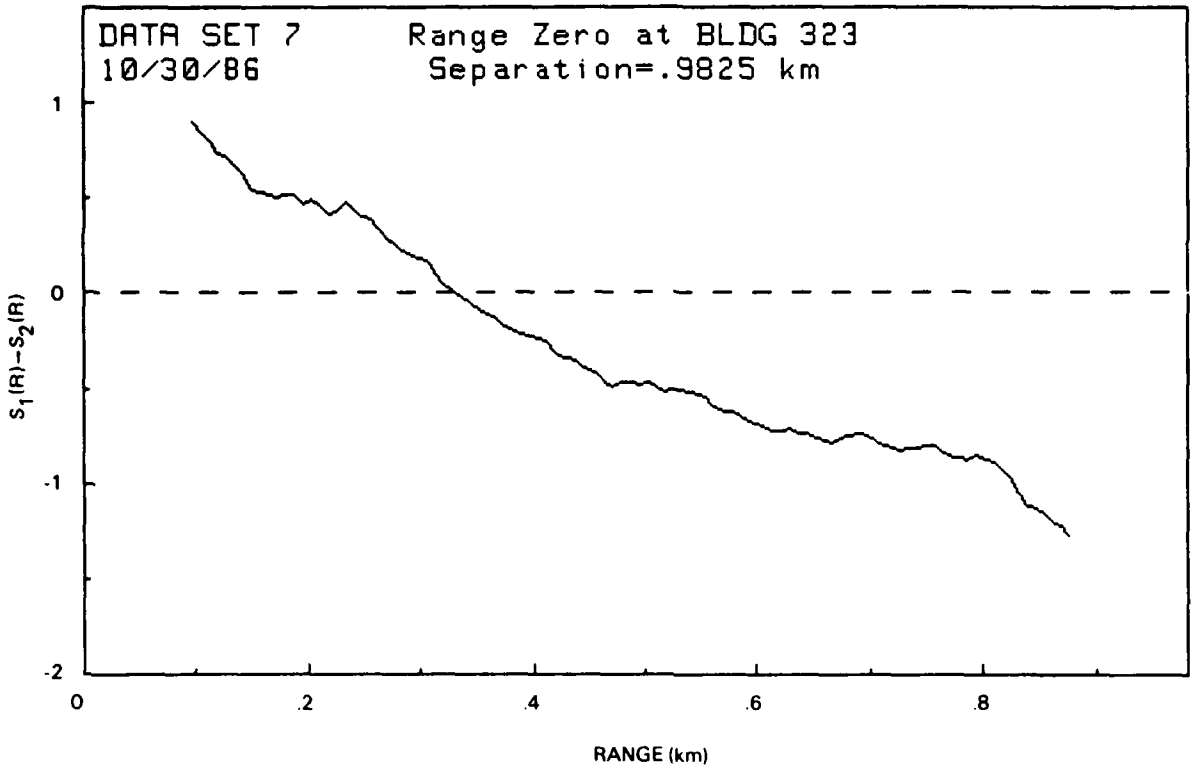
DATA SET 7
10/30/86
Range Zero at BLDG 323
Separation=.9825 km
1
0
-1
-2
0
.2
.4
.6
.8
$S_1(R)-S_2(R)$
RANGE (km)

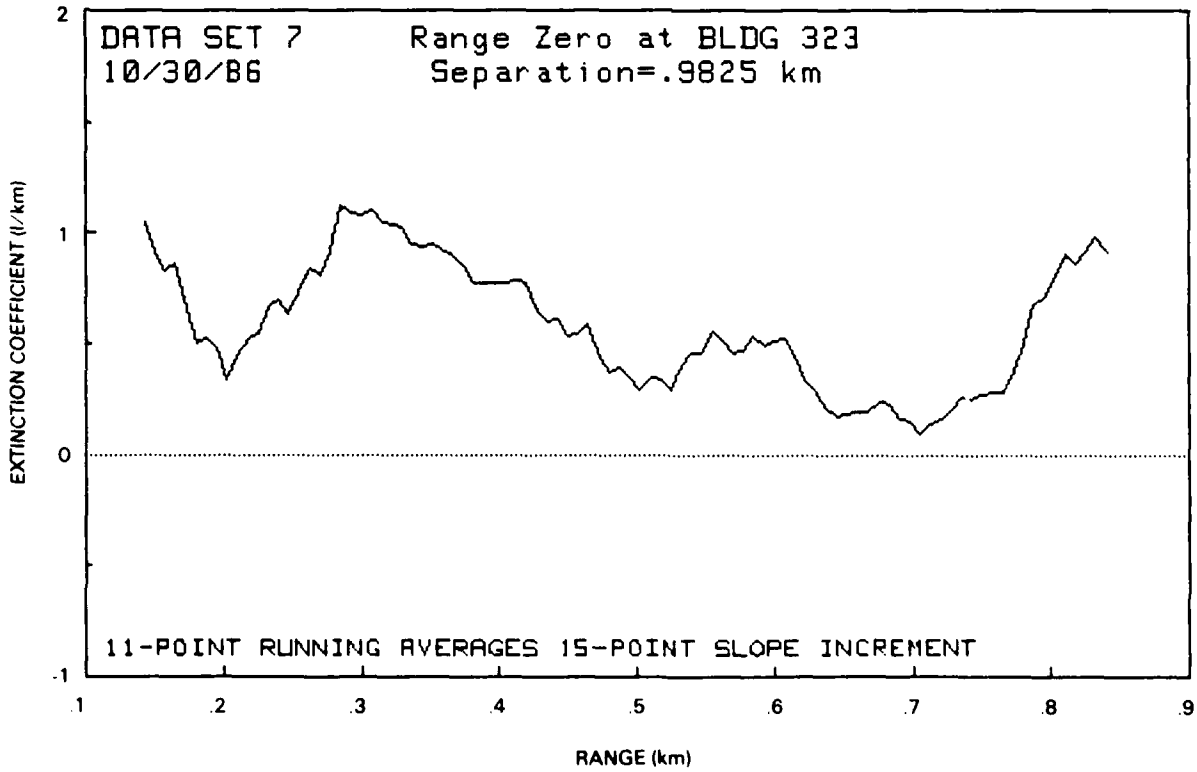
DATA SET 7
10/30/86
Range Zero at BLDG 323
Separation=.9825 km
2
1
0
-1
.1
.2
.3
.4
.5
.6
.7
.8
.9
11-POINT RUNNING AVERAGES 15-POINT SLOPE INCREMENT
EXTINCTION COEFFICIENT (1/km)
RANGE (km)

Figure B-13.

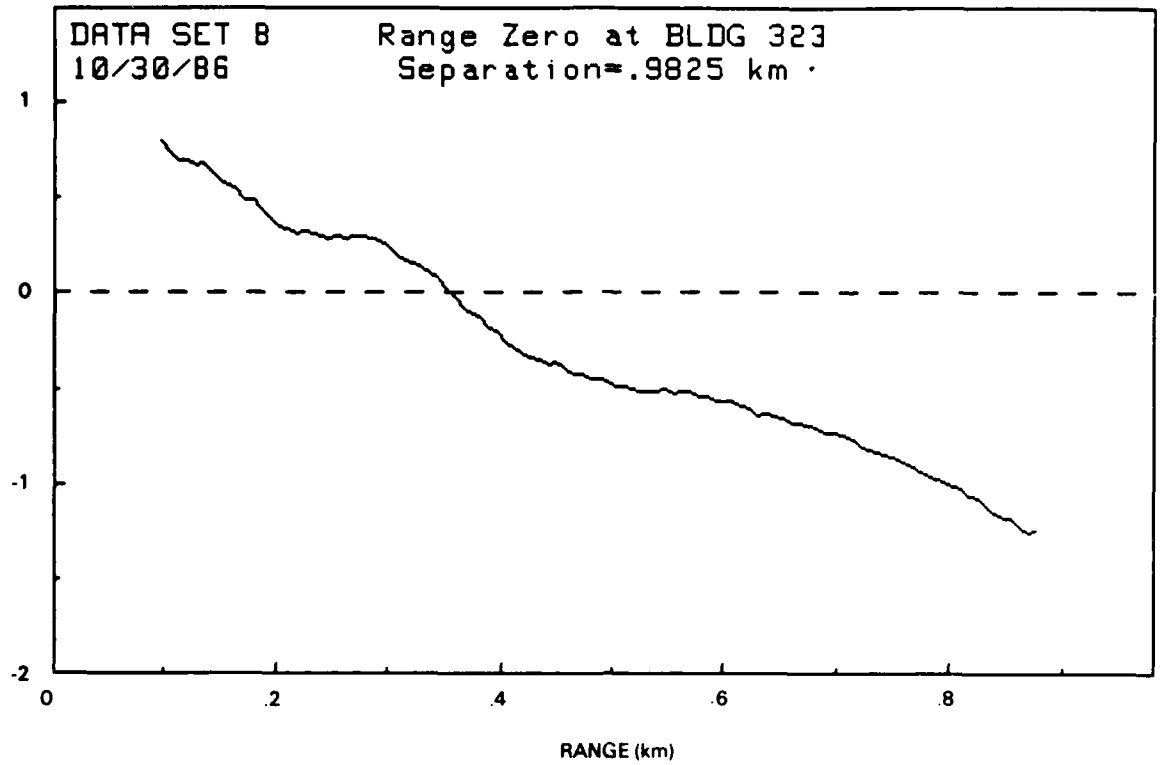
DATA SET 8
10/30/86
Range Zero at BLDG 323
Separation=.9825 km
1
0
-1
-2
0
.2
.4
.6
.8
RANGE (km)

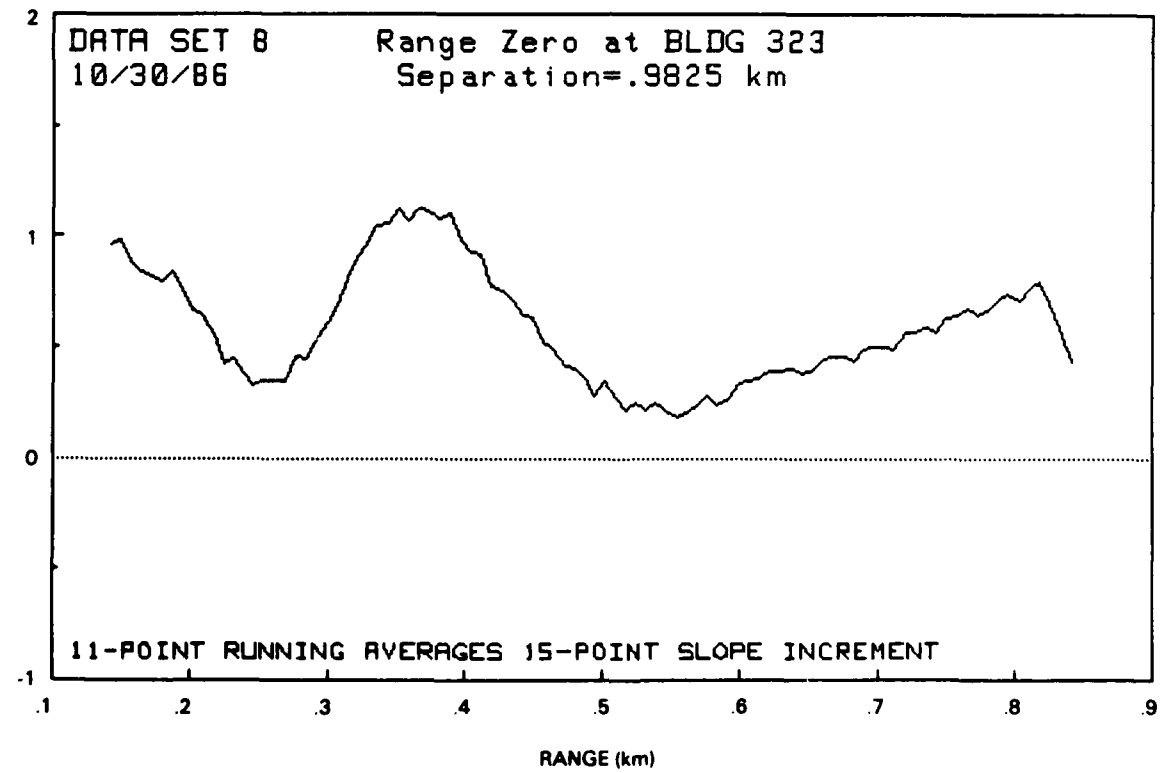
DATA SET 8
10/30/86
Range Zero at BLDG 323
Separation=.9825 km
2
1
0
-1
11-POINT RUNNING AVERAGES 15-POINT SLOPE INCREMENT
.1
.2
.3
.4
.5
.6
.7
.8
.9
RANGE (km)

Figure B-14.

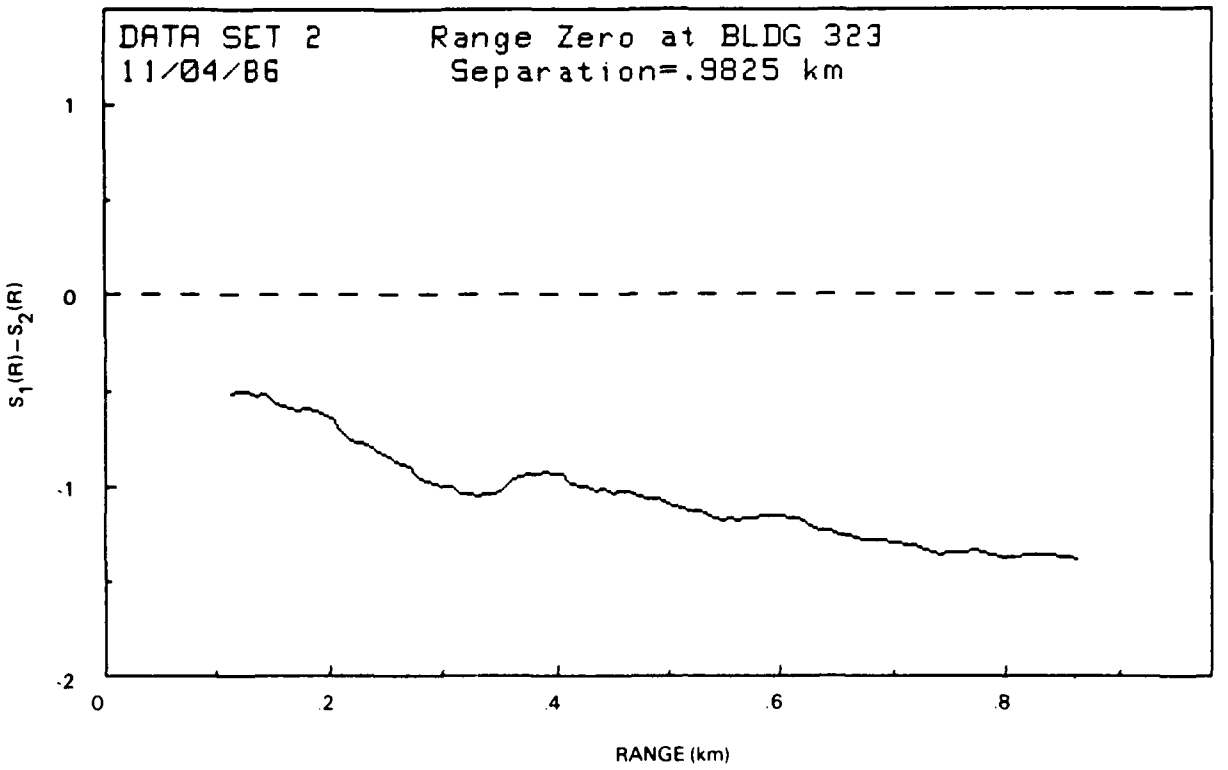
DATA SET 2
11/04/86
Range Zero at BLDG 323
Separation=.9825 km
1
0
-.1
-.2
$S_1(R)-S_2(R)$
0
.2
.4
.6
.8
RANGE (km)

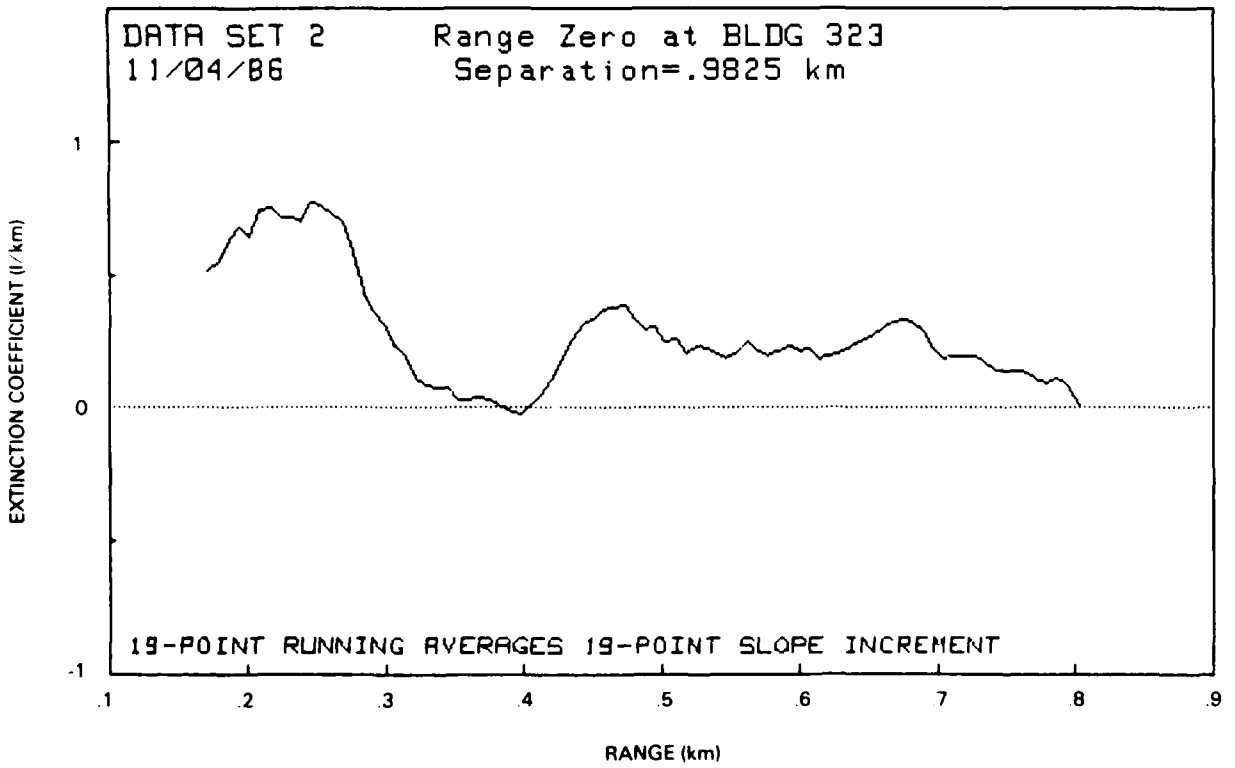
DATA SET 2
11/04/86
Range Zero at BLDG 323
Separation=.9825 km
1
0
-1
EXTINCTION COEFFICIENT (1/km)
19-POINT RUNNING AVERAGES 19-POINT SLOPE INCREMENT
.1
.2
.3
.4
.5
.6
.7
.8
.9
RANGE (km)

Figure B-15.

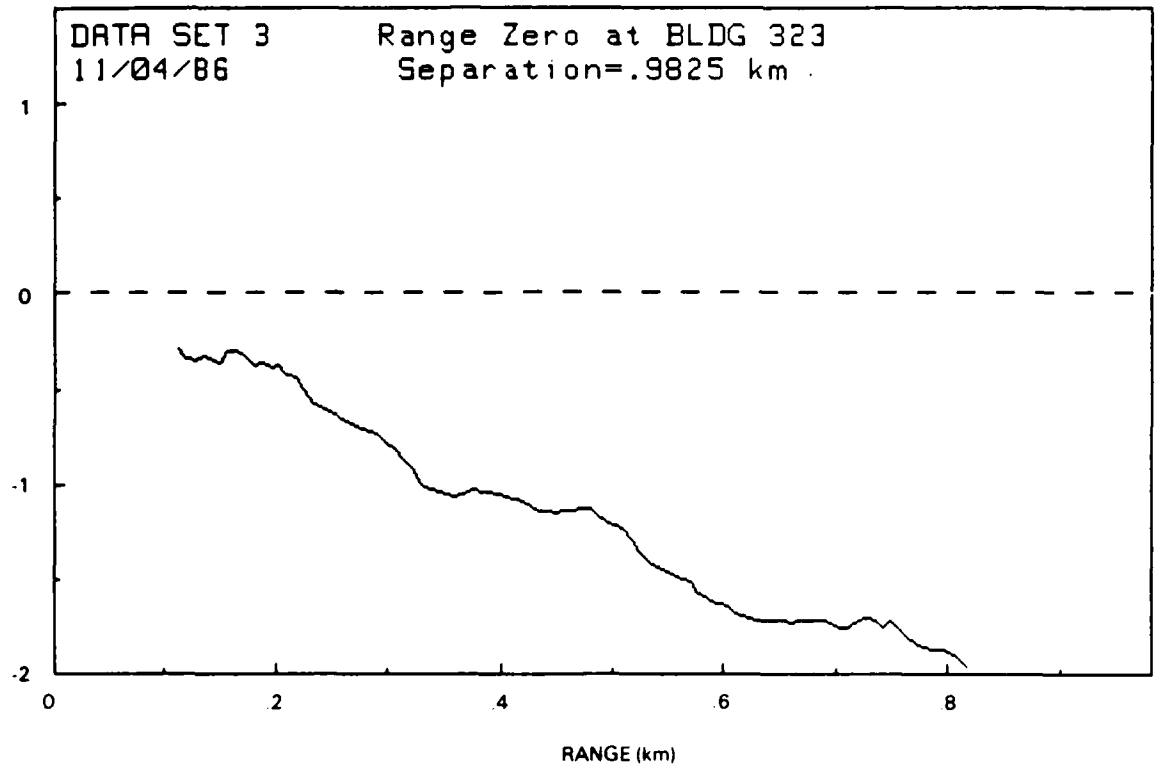
DATA SET 3
11/04/86
Range Zero at BLDG 323
Separation=.9825 km
1
0
-1
-2
0
.2
.4
.6
.8
RANGE (km)

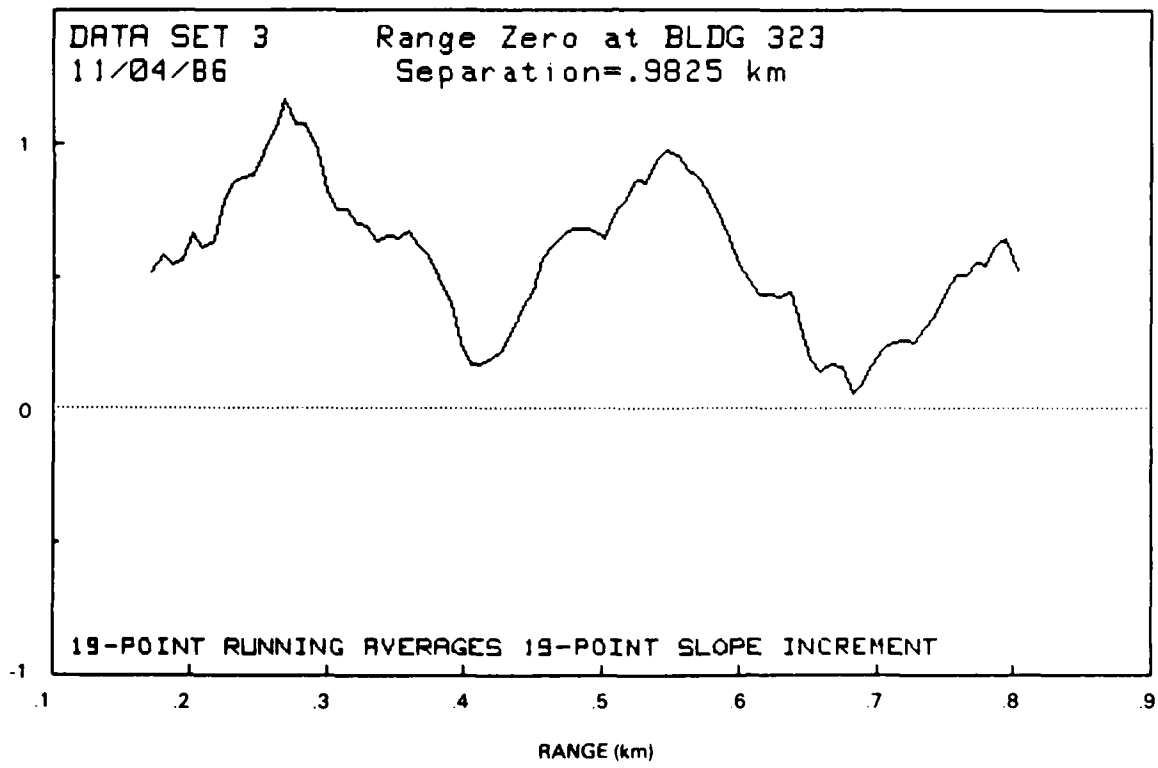
DATA SET 3
11/04/86
Range Zero at BLDG 323
Separation=.9825 km
1
0
-1
19-POINT RUNNING AVERAGES 19-POINT SLOPE INCREMENT
.1
.2
.3
.4
.5
.6
.7
.8
.9
RANGE (km)

Figure B-16.

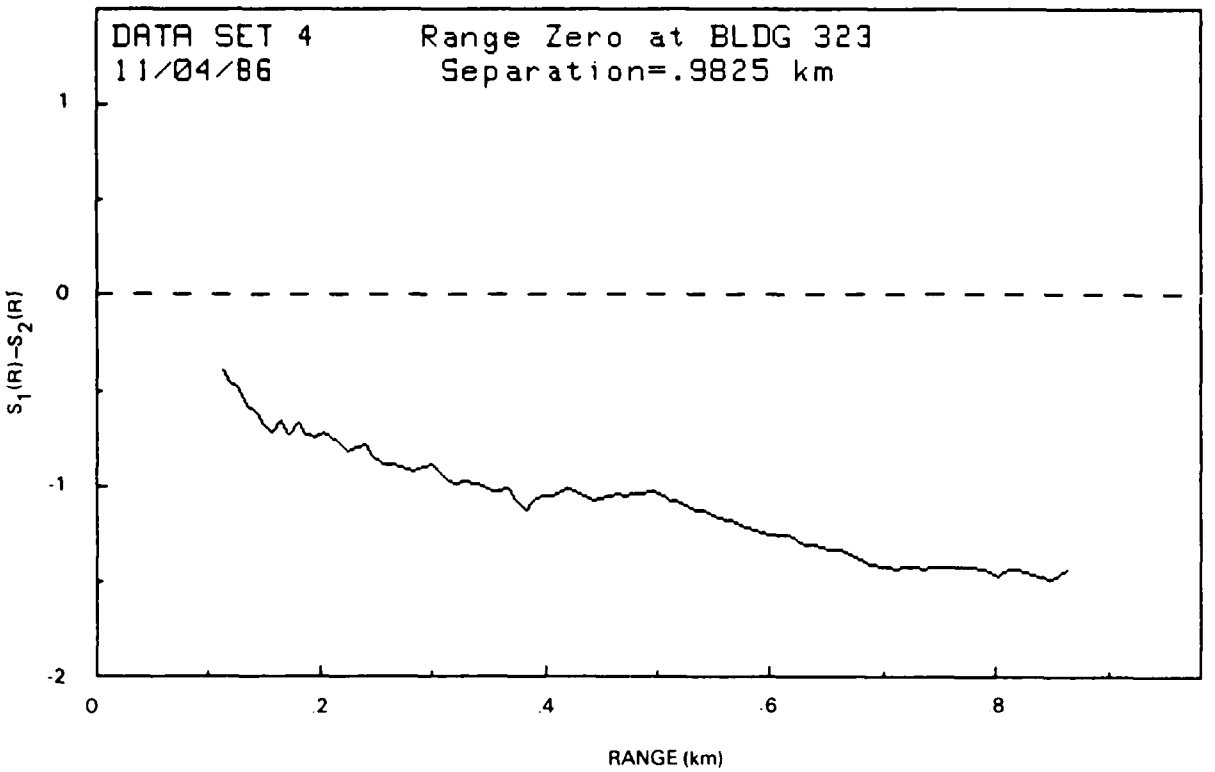
DATA SET 4
11/04/86
Range Zero at BLDG 323
Separation=.9825 km
1
0
-1
-2
$S_1(R)-S_2(R)$
0
.2
.4
.6
.8
RANGE (km)

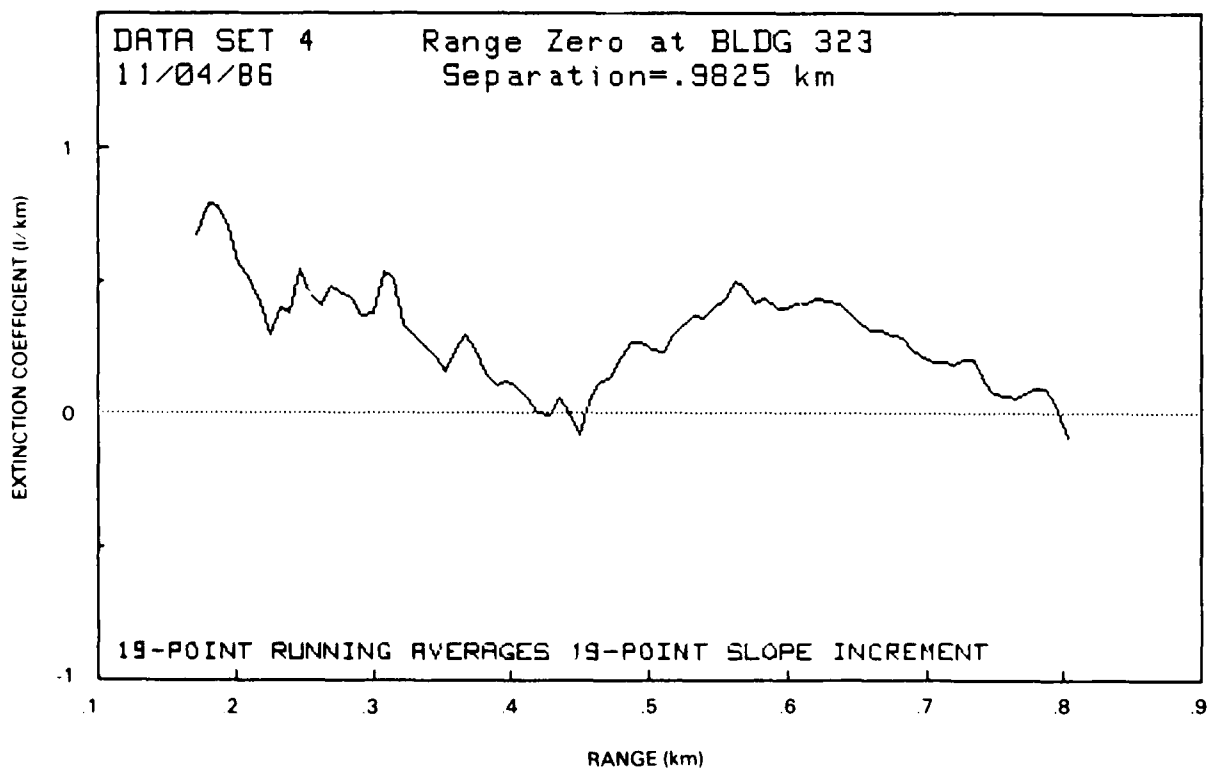
DATA SET 4
11/04/86
Range Zero at BLDG 323
Separation=.9825 km
1
0
-1
EXTINCTION COEFFICIENT (1/km)
19-POINT RUNNING AVERAGES 19-POINT SLOPE INCREMENT
.1
.2
.3
.4
.5
.6
.7
.8
.9
RANGE (km)

Figure B-17.

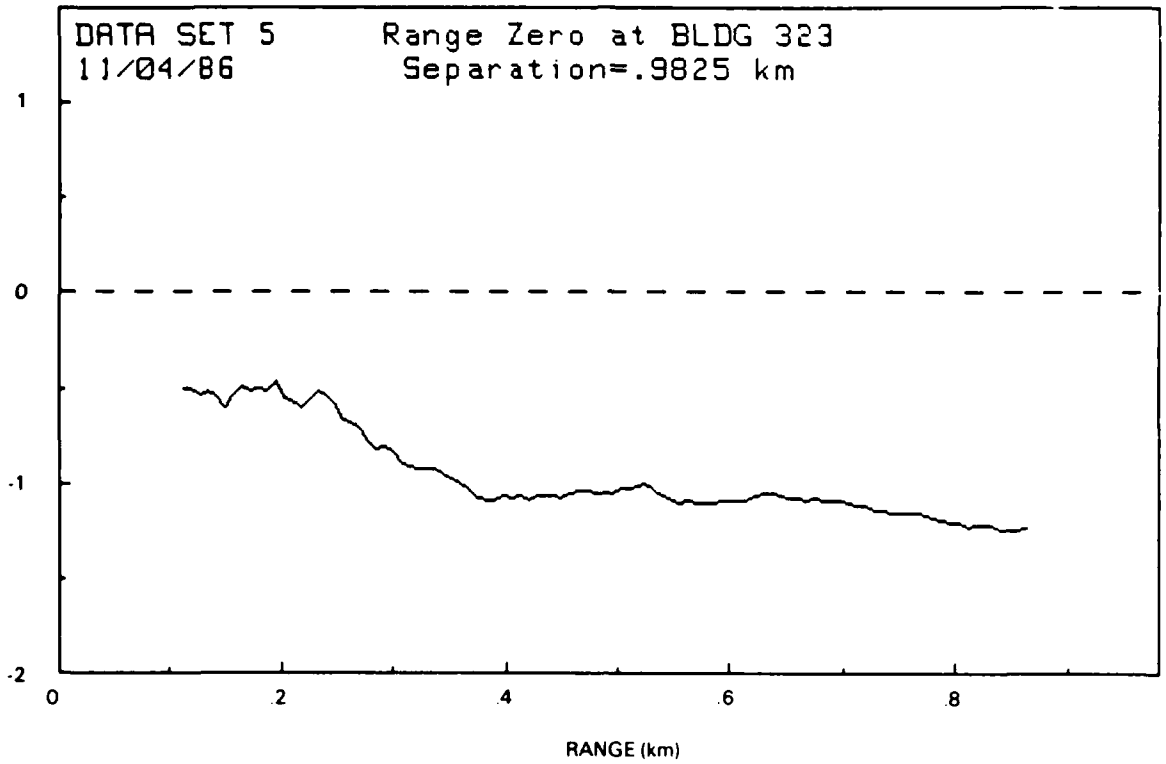
DATA SET 5
11/04/86
Range Zero at BLDG 323
Separation=.9825 km
1
0
-1
-2
0
.2
.4
.6
.8
RANGE (km)

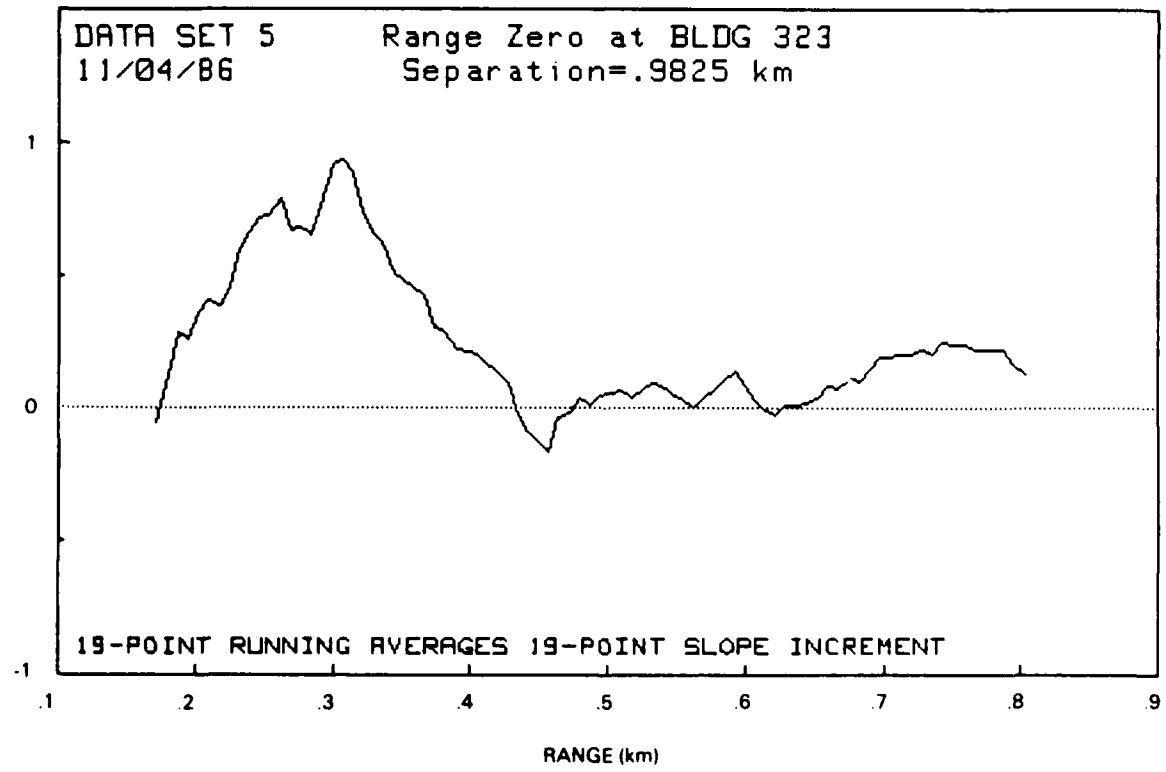
DATA SET 5
11/04/86
Range Zero at BLDG 323
Separation=.9825 km
1
0
-1
19-POINT RUNNING AVERAGES 19-POINT SLOPE INCREMENT
.1
.2
.3
.4
.5
.6
.7
.8
.9
RANGE (km)

Figure B-18.

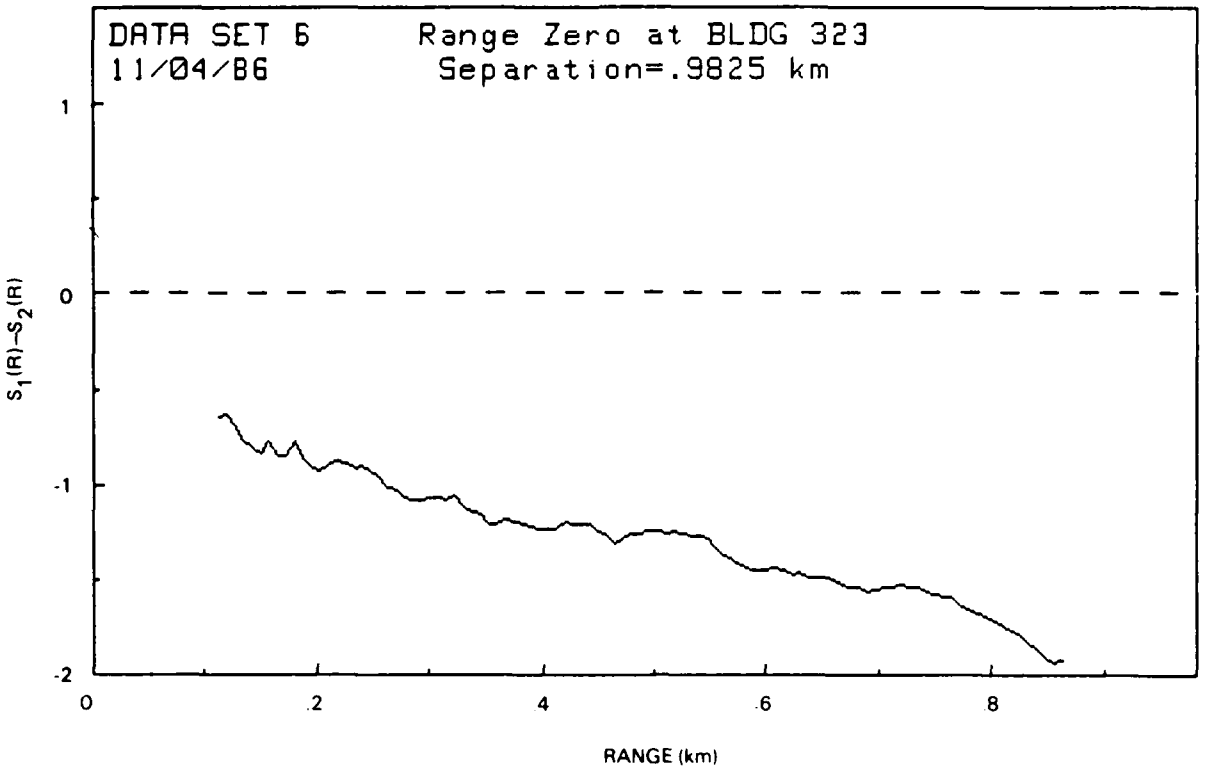
DATA SET 6
11/04/86
Range Zero at BLDG 323
Separation=.9825 km
1
0
-1
-2
$S_1(R)-S_2(R)$
0
.2
4
.6
8
RANGE (km)

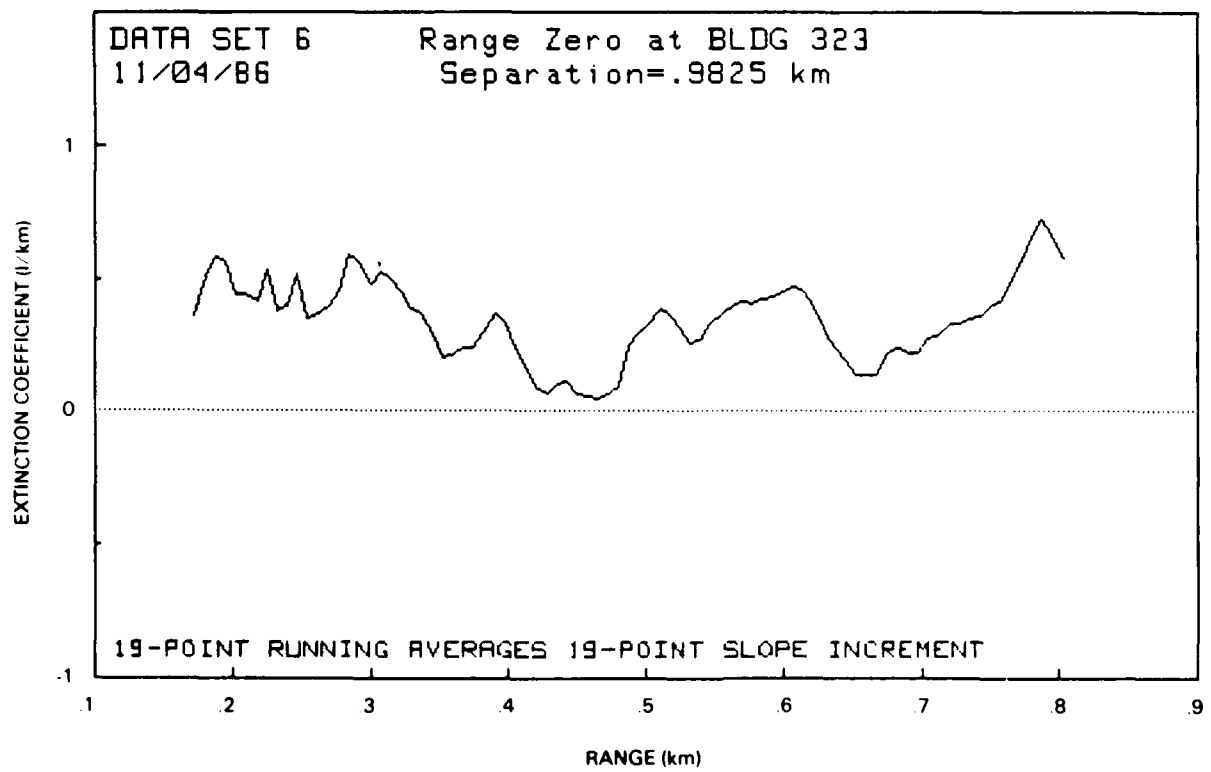
DATA SET 6
11/04/86
Range Zero at BLDG 323
Separation=.9825 km
1
0
-1
EXTINCTION COEFFICIENT (1/km)
19-POINT RUNNING AVERAGES 19-POINT SLOPE INCREMENT
.1
.2
3
.4
.5
.6
.7
.8
.9
RANGE (km)

Figure B-19.

END

9-87

DTIC